

Contract No:

This document was prepared in conjunction with work accomplished under Contract No. 89303321CEM000080 with the U.S. Department of Energy (DOE) Office of Environmental Management (EM).

Disclaimer:

This work was prepared under an agreement with and funded by the U.S. Government. Neither the U.S. Government or its employees, nor any of its contractors, subcontractors or their employees, makes any express or implied:

- 1) warranty or assumes any legal liability for the accuracy, completeness, or for the use or results of such use of any information, product, or process disclosed; or
- 2) representation that such use or results of such use would not infringe privately owned rights; or
- 3) endorsement or recommendation of any specifically identified commercial product, process, or service.

Any views and opinions of authors expressed in this work do not necessarily state or reflect those of the United States Government, or its contractors, or subcontractors.



Savannah River
National Laboratory®

A U.S. DEPARTMENT OF ENERGY NATIONAL LAB • SAVANNAH RIVER SITE • AIKEN, SC • USA

Composition-Based Density Model for High Level Waste Glasses

C. L. Trivelpiece

February 2022

SRNL-STI-2018-00599, Revision 1

SRNL.DOE.GOV

DISCLAIMER

This work was prepared under an agreement with and funded by the U.S. Government. Neither the U.S. Government or its employees, nor any of its contractors, subcontractors or their employees, makes any express or implied:

1. warranty or assumes any legal liability for the accuracy, completeness, or for the use or results of such use of any information, product, or process disclosed; or
2. representation that such use or results of such use would not infringe privately owned rights; or
3. endorsement or recommendation of any specifically identified commercial product, process, or service.

Any views and opinions of authors expressed in this work do not necessarily state or reflect those of the United States Government, or its contractors, or subcontractors.

Printed in the United States of America

**Prepared for
U.S. Department of Energy**

Keywords: *DWPF, glass, HLW, density*

Retention: *Permanent*

Composition-Based Density Model for High Level Waste Glasses

C. L. Trivelpiece

February 2022

Savannah River National Laboratory is operated by
Battelle Savannah River Alliance for the U.S. Department
of Energy under Contract No. 89303321CEM000080.



ACKNOWLEDGEMENTS

The authors thank Dr. Kevin M. Fox for his invaluable suggestions and contributions to the presentation of the information contained in the report. We would also like to thank Dr. Kimberly Crapse for her painstaking evaluation and verification of the glass composition data contained within the database. We would like to thank Dr. Fabienne C. Johnson for her valued review of the calculations and gravimetric data used in formulating the models presented in this work. Lastly, we would like to thank Dr. Carol Jantzen for establishing the THERMO database architecture upon which the density model was developed.

EXECUTIVE SUMMARY

In this report, the Savannah River National Laboratory (SRNL) provides a first-principles model capable of predicting the density of high-level waste (HLW) glass based on the glass composition. The model relies on the additivity of the specific volume of bound glass oxides to obtain a quantitative evaluation of the approximate glass density.

A database of glass densities and compositions was compiled from various sources including previous Defense Waste Processing Facility (DWPF) variability study glasses, HLW studies from other institutions, and literature references. There are a total of 1104 glass compositions in the database with densities ranging from 2.224 g/cm³ to 3.997 g/cm³. The breadth of the compositional coverage space is reported as well.

A predictive method was investigated in which the glass density was calculated as a function of the weighted partial molar volumes of the individual glass oxides and the molar mass of the glass. This method yielded a high correlation between the predicted density and the measured density. In addition, a linear regression of these predictions indicated that the predicted value was equal to the measured within the bounds of analytical uncertainty.

The following conclusions were drawn from the results of these analyses:

1. Measured glass density is highly correlated with glass composition ($R^2 \approx 0.95$).
2. The correlation between glass density and glass composition can be expressed as either:
 - a. A weighted sum of the individual oxide glass-component densities, or
 - b. A weighted sum of the individual oxide glass-component partial molar volumes.
3. A linear regression of the predicted density via partial molar volume method to the measured density yields a slope of 0.9975 and an intercept of -0.0007 – the uncertainty interval associated with these coefficients contain one and zero, respectively.
4. The fitted coefficients and associated uncertainty intervals of the linear regression of the predicted density via the partial molar volume method to the measured density suggest that the predicted theoretical density is, within analysis uncertainty, equal to the measured density of the glass.

It is recommended that glass density measurements included with the variability study for each sludge batch be discontinued. In their place, SRNL will calculate a bounding glass density value for the frit/sludge system using the model. It is also recommended that DWPF implement the density model as part of the fissile loading determination portion of the SME acceptability process. Details for implementation are provided in this report.

Revision 1 of this report updates the Functional Classification from Production Support to Safety Class. A reclassification of DWPF glass density occurred in 2021 after this task had already been completed. Revision bars are used to note the associated changes.

TABLE OF CONTENTS

LIST OF TABLES.....	viii
LIST OF FIGURES.....	ix
1.0 Introduction.....	1
2.0 Methods.....	1
2.1 Density Calculations.....	1
2.2 Database Development.....	3
2.3 Assumptions.....	4
2.4 Quality Assurance.....	5
3.0 Discussion and Results.....	6
3.1 Evaluation of Schumacher’s Method.....	6
3.2 Partial Molar Volume Method.....	7
3.3 Comparison to Variability Study Density Limits.....	11
3.4 Comparison to Other HLW Studies.....	12
4.0 Summary.....	13
5.0 Conclusions.....	13
6.0 Recommendations.....	13
6.1 Discontinue density measurements conducted with variability studies.....	13
6.2 Transition from a bounding density value to calculating the density of glass produced from each SME batch.....	14
7.0 References.....	15
Appendix A.....	A-1
Appendix B.....	B-1
Appendix C.....	C-1
Appendix D.....	D-1
Appendix E.....	E-1

LIST OF TABLES

Table 1: A re-creation of the data from Table 21-1 in Volf [11] with the addition of the calculated molar volume for a bound oxide, v_i	3
Table 2: Range of individual oxide concentrations included in the density database.....	4
Table 3. Determination of Fissile Loading in Recent SME Batches	14
Table 4: Select data from the density database used to develop the prediction model.....	A-1
Table 5: Partial molar volumes of the oxides used in the density predictions.....	C-1
Table 6: Frit 625 and SB9 Coupled with SWPF	E-2
Table 7: Operating Windows for Frits 625 and 803 with SB9 Coupled with Options from SWPF Additions	E-3

LIST OF FIGURES

Figure 3-1: Fit of predicted density using Schumacher's Method (additive density) versus the measured density of the glasses in the database.	6
Figure 3-2: A histogram of the residual density predictions establishing the over prediction of Schumacher's method.	7
Figure 3-3: The reciprocal of the measured density values versus calculated specific volume of the glass compositions.....	8
Figure 3-4: The upper and lower 95% confidence intervals associated with the fit determined via the partial molar volumes method projected through the origin.....	8
Figure 3-5: The predicted versus measured density shows a high degree of correlation in addition to an uncertainty interval that captures a slope of one and an intercept of zero.	9
Figure 3-6: Histogram and box plot showing the error in the predicted values versus the measured values	10
Figure 3-7: Density predictions for the five variability study glass groups included in the database are compared to the measured values.	11
Figure 3-8: The other HLW glass systems that were included in the database show a similar high degree of correlation between the predicted and measured values.....	12
Figure B-1: $X^T X$ and $(X^T X)^{-1}$ for the Density Model.....	B-2
Figure B-2: A comparison of the UTLs derived from theory and statistical approaches.	B-2
Figure D-1: The effect of varying Fe^{2+}/Fe^{3+} ratio on the HLW glass compositions.....	D-1
Figure E-1: Illustration of Use of PCCS Information to Determine a Bounding Density for the SME Glass Product and the Corresponding Fissile Loading (SB6 SME 565).....	E-6

LIST OF ABBREVIATIONS

%RSD	Percent Relative Standard Deviation
DWPF	Defense Waste Processing Facility
EA	Environmental Assessment (glass)
HLW	High Level Waste
PNNL	Pacific Northwest National Laboratory
REDOX	reduction/oxidation
RMSE	Root-mean-square Error
SB5	Sludge Batch 5
SB6	Sludge Batch 6
SB7a	Sludge Batch 7a
SB7b	Sludge Batch 7b
SB8	Sludge Batch 8
SB9	Sludge Batch 9
SME	Slurry Mix Evaporator
SRNL	Savannah River National Laboratory
UTL	Upper Tolerance Limit
VS	Variability Study
VSL	Vitreous State Laboratory
wt %	Weight Percent

1.0 Introduction

Per a directive from the Department of Energy – Savannah River, the fissile mass loading concentration must remain below 897 g/m³ in each high-level waste (HLW) glass canister produced by the Defense Waste Processing Facility (DWPF) [1]. In support of Sludge Batch 5 (SB5) processing, the Savannah River National Laboratory (SRNL) developed a technical basis and an associated Microsoft® Excel® spreadsheet for DWPF that facilitates the evaluation of the fissile mass loading of a glass product based on the iron (Fe) concentration in the glass as determined by the measurements from the Slurry Mix Evaporator (SME) acceptability analysis [2]. One of the primary inputs into the fissile mass loading spreadsheet includes an upper bound for the glass density, which SRNL has provided to DWPF for each sludge batch since SB5 [2-7].

For these previous efforts, density measurements were conducted for the variability study glasses associated with each sludge batch. A statistical evaluation of these measurements was performed to provide a bounding density value. This value was used as input to the Excel® spreadsheet employed by DWPF to maintain the fissile concentration in its glass waste form below 897 g/m³.

The purpose of this report is to provide the results of SRNL’s effort to develop a glass density-glass composition model.

Revision 1 of this report updates the Functional Classification from Production Support to Safety Class. A reclassification of DWPF glass density occurred in 2021 after this task had already been completed. Revision bars are used to note the associated changes.

2.0 Methods

2.1 Density Calculations

Several approaches to determining glass density based on composition were investigated. Initially, a method first employed at the Savannah River Site by R.F. Schumacher [8, 9] was investigated. Schumacher’s methodology treated the bulk density of a glass as an additive property of constituent glass oxides. The notion of additivity is demonstrated in Equation 1:

$$G = \sum x_i g_i \quad 1$$

where G is the bulk glass property, x_i is the molar fraction of glass component “i”, and g_i is the additive property of component “i”. As such, the approach employed by Schumacher is given in Equation 2:

$$\rho_{glass} = \sum x_i \rho_i \quad 2$$

where ρ_{glass} is the bulk glass density, x_i is the molar fraction of oxide “i”, and ρ_i is the density of the free oxide “i”. Thus, the right-hand side of Equation 2 is considered as the theoretical density, and a linear regression was utilized to assess the viability of this approach. In his original work [8], Schumacher reported the fitted model and coefficient of determination (R^2) that are given in Equation 3.

$$\rho_{actual} = 0.9548 + 0.6924\rho_{theoretical} \quad (R^2 = 0.99) \quad 3$$

While a high degree of correlation exists for the relationship developed in Equation 3, there is an offset and bias associated with directly using Equation 3 to calculate glass density: a non-zero intercept and a non-unity slope, respectively. This outcome provides a good demonstration of the non-additivity of oxide

density in calculating glass density. The intent of this effort was not to predict the glass density but to calculate it using Equation 2 (with some uncertainty, due to the ρ_{glass} and x_i quantities in the equation being measured). Once additional data were compiled to support this study, the Equation 2 approach was re-investigated for completeness, and the results are discussed in a later section.

The specific volume of a glass, which is the reciprocal of the glass density, can be determined by the summation of the partial molar volumes of the glass oxide constituents, and, thus, is an additive property of a glass system [10, 11]. This apparent contradiction between the non-additivity of density and the additivity of reciprocal density is reconciled by noting that partial molar volumes of the oxides are extensive properties in the context of a glass composition. The specific volume of a glass composition can be determined by Equation 4:

$$\frac{1}{\rho_T} = V_T = \frac{\sum x_i v_i}{M_{glass}} \quad 4$$

where ρ_T is the theoretical (calculated) glass density, V_T is the calculated specific volume of the glass, x_i is the mole fraction of oxide “i”, v_i is the partial molar volume of oxide “i”, and M_{glass} is the molar mass of the glass¹. This approach was used to predict the measured glass density of the compositions in the database compiled to support this study, and the results of this exercise are discussed in later sections.

In developing the database and the various parameters needed to calculate both the partial densities as well as the partial molar volumes, the idea of utilizing “bound molar volumes” and “bound oxide densities” was employed. As noted by Volf [11], “*the volume of melted glass is smaller than the sum of the volumes of free oxides.*” In this context, the phrase “free oxides” is referencing the stand-alone volume of a glass oxide component whereas “bound molar volume” or “bound oxide density” refers to the property of an oxide component when incorporated into a glass matrix.

Indeed, there is measured and reported variability between the free oxide and bound oxide densities and molar volumes for a number of major oxides contained in HLW glass formulations. Table 1 is replicated from [11] and data therein demonstrate this variability.

Inspection of Table 1 shows that some oxides have a greater density when bound in a glass matrix (e.g., B₂O₃ and Na₂O) while others (e.g., Al₂O₃ and MgO) are less dense. Unfortunately, there is no apparent correlation between the ratio ρ/ρ_v and any other property of the oxides listed in Table 1. Therefore, analytical methods could not be used, such as extrapolation or regression, to determine the bound oxide values for all the oxide components that are represented by glass compositions in the database. In instances where a bound density and molar volume were unavailable, the free oxide density or molar volume was used [12, 13]. The partial molar volumes of the oxides used in the density predictions are given in Appendix C.

¹ M_{glass} is the mass of one mole of the glass. For example, the molar mass of sodium disilicate glass ($\text{Na}_2\text{O} \cdot 2\text{SiO}_2 \rightarrow 0.33\text{Na}_2\text{O} \cdot 0.67\text{SiO}_2$) is $0.33 * M_{\text{Na}_2\text{O}} + 0.67 * M_{\text{SiO}_2} = 60.717 \text{ g/mol}$.

Table 1: A re-creation of the data from Table 21-1 in Volf [11] with the addition of the calculated molar volume for a bound oxide, v_i .

Oxide	Free Density, ρ_v (g/cm ³)	Bound Density, ρ_i (g/cm ³)	Molar Volume Bound Oxide, v_i (cm ³ /mol)	Ratio ρ_i/ρ_v
Al₂O₃	3.99	2.50	40.78	0.63
B₂O₃	1.85	2.80	24.87	1.51
BaO	5.72	7.00	21.91	1.22
BeO	3.02	3.20	7.82	1.06
Bi₂O₃	8.90	10.30	45.24	1.16
CaO	3.32	3.90	14.38	1.17
CdO	8.15	7.20	17.83	0.88
K₂O	2.32	2.80	33.64	1.21
Li₂O	2.43	2.70	11.07	1.11
MgO	3.65	3.30	12.22	0.90
Na₂O	2.27	3.10	20.00	1.37
PbO	9.53	10.00	22.32	1.05
Rb₂O	3.72	4.10	45.59	1.10
Sb₂O₃	5.20	6.20	47.02	1.19
SiO₂	2.20	2.28	26.36	1.04
SrO	4.70	5.90	17.56	1.26
TaO₂	8.74	8.50	25.05	0.97
ThO₂	9.69	8.30	31.81	0.86
TiO₂	3.84	3.80	21.02	0.99
Tl₂O	10.19	6.70	63.40	0.66
ZnO	5.49	5.60	14.53	1.02
ZrO₂	5.49	5.30	23.25	0.97

2.2 Database Development

The database to support this density study was compiled from multiple sources including:

- DWPF glass variability studies with experimental work done at SRNL or at the Vitreous State Laboratory at Catholic University of America (VSL) [3-7, 14-19]
- HLW studies from:
 - o Pacific Northwest National Laboratory (PNNL) [20]
- Various literature sources (references are provided in Table 4 of Appendix A)

The database contains 1104 unique glass compositions of which 340 are directly related to HLW glass. The remainder of the glass compositions and densities in the database were acquired from literature references [2, 8-10, 21-34]. Measured densities in the database range from 2.224 g/cm³ to 3.997 g/cm³. Table 2 shows the minimum and maximum oxide concentrations for the various glasses in the database.

Table 2: Range of individual oxide concentrations included in the density database.

Oxide	Min wt %	Max wt %	Oxide	Min wt %	Max wt %
Al ₂ O ₃	0	46.97	MoO ₃	0	2.84
As ₂ O ₃	0	0.33	Na ₂ O	0	49.79
B ₂ O ₃	0	40.05	Nd ₂ O ₃	0	3.23
BaO	0	57.75	NiO	0	2.97
Bi ₂ O ₃	0	0.65	P ₂ O ₅	0	1.99
CaO	0	50.08	PbO	0	45.30
Ce ₂ O ₃	0	1.97	Pr ₂ O ₃	0	0.95
CeO ₂	0	0.80	Rb ₂ O	0	29.14
CoO	0	0.19	RuO ₂	0	0.16
Cr ₂ O ₃	0	1.03	Sb ₂ O ₃	0	0.73
Cs ₂ O	0	41.94	Se	0	0.03
Cu ₂ O	0	0.54	SiO ₂	15.00	90.39
CuO	0	0.54	Sm ₂ O ₃	0	0.67
Fe ₂ O ₃	0	21.92	SO ₄	0	1.23
FeO	0	8.81	SrO	0	53.35
F	0	0.84	Ta ₂ O ₅	0	21.18
Gd ₂ O ₃	0	4.17	TeO ₂	0	0.34
K ₂ O	0	45.99	ThO ₂	0	1.12
La ₂ O ₃	0	22.79	TiO ₂	0	54.95
Li ₂ O	0	20.49	U ₃ O ₈	0	6.24
MgO	0	38.11	Y ₂ O ₃	0	0.44
MnO	0	4.20	ZnO	0	42.02
MnO ₂	0	2.21	ZrO ₂	0	20.58

The glasses taken from literature sources represent simple binary compositions to glasses that rival the complexity of HLW compositions. Selected data from the database for every composition are given in Table A-1 in Appendix A.

2.3 Assumptions

The following assumptions were used in the development of the density prediction model via the partial molar volume method:

1. The composition of the glasses in the database may be up to ± 0.1 wt % or ± 0.001 mole fraction different from the value listed in the respective reference. This difference is due to rounding uncertainty and normalization that occurs during the calculation of the composition from elemental weight percent to weight percent or mole fraction.

An investigation into the uncertainty in the measurements demonstrated that a simultaneous error of up to ± 0.1 oxide wt % in all glass components does not affect the conclusions about the applicability of the density prediction model. It should be noted that this is a worst-case scenario where every component of every glass composition is inaccurate by ± 0.1 wt %.

Measured (not measured-normalized) compositions were used in every case they were available; however, targeted values were used for certain glass compositions when no measured data were available. Target compositions account for <10% of the glasses in the database, and their inclusion or exclusion does not affect the conclusions of the model's applicability or efficacy.

2. Many of the HLW compositions and some of the other glasses in the database contain some form of sulfur (usually given as a concentration of SO_4 or SO_3). It was assumed that any sulfur species present in the glass were incorporated into the glass structure as Na_2SO_4 [35]. This assumption has no effect on the conclusions about the applicability of the density prediction model for sulfate concentrations of less than 2 wt % SO_4 .

If the concentration of sulfate is expected to be greater than this value, the model could be reevaluated; however, it should be noted that 2 wt % is near the maximum amount of SO_4 that can be incorporated into glass matrices [36, 37] and is well over the maximum allowable sulfate limits in place for DWPF processing [38].

Similarly, a small subset of glasses from one referenced source contain elemental F and Se [33]. In these instances, it was assumed that F behaves as being loosely bonded to SiO_4 and AlO_4 tetrahedra [39-43], and subsequently only slightly adds to the molar volume of the glass especially in the very small quantities found in the database glasses. The effect of variations in the partial molar volume of fluorine in glass was tested over a range of 5 – 20 cm^3/mol , and the results indicated immeasurable impacts to the density predictions. It was assumed that Se behavior in the silicate network closely resembles that of SeO_3^{2-} [44, 45].

3. Concentrations of uranium were partitioned between UO_2 and UO_3 as suggested in Volf [12]. Uranium takes on two oxidation states in glass matrices depending on the reduction/oxidation (REDOX) environment of the melt as well as the coordination of other glass matrix constituents. Per the suggestion, any given U_3O_8 concentration was divided accordingly: $\text{U}_3\text{O}_8 = \text{UO}_2 \cdot 2\text{UO}_3$. This assumption was tested by using the concentration of U_3O_8 to predict the glass density as opposed to the more structurally accurate partitioning between UO_2 and UO_3 . The result of the test did not affect the methodology of density prediction presented in this work.
4. The effect of glass REDOX on density was assumed to be negligible. This assumption was validated by the results of a paper study presented in Appendix D.
5. The effect of thermal history on glass density was assumed to be negligible and was therefore not considered.
6. It was assumed that the density prediction model would only be applied to homogeneous glasses (i.e., glasses that are not partially devitrified).

2.4 Quality Assurance

Requirements for performing reviews of technical reports and the extent of review are established in Savannah River Site Manual E7, Procedure 2.60 [46]. This document, including calculations, was reviewed by a Design Verification. SRNL documents the Design Verification using the SRNL Technical Report Design Checklist contained in WSRC-IM-2002-00011, Rev. 2 [47]. This work was performed as specified in Revision 0 of the Technical Task Request: "Sludge Batch 10 Frit Evaluation and Measurement

Acceptance Region Assessment – Task 3, Deliverable 2” and Revision 1 of the Task Technical Quality Assurance Plan: “Task Technical and Quality Assurance Plan for Sludge Batch 10 Frit Evaluation and Measurement Acceptance Region Assessments.” Per Revision 4 of both the Technical Task Request and Task Technical and Quality Assurance Plan [48,49], the Functional Classification of this work has been changed to Safety Class. Glass density is waste form affecting and needs to follow the quality assurance requirements of DOE/RW-0333P. This work was supported using JMP Pro Version 11.2.1 [50], which is covered by Software Classification Document Number B-SWCD-W-00023, Rev. 0. Glass density calculations performed with JMP were independently verified with Microsoft Excel.

3.0 Discussion and Results

3.1 Evaluation of Schumacher’s Method

The method employed by Schumacher was applied to the density database compiled for the present work. A density was calculated for each glass composition in the database using the bound oxide densities and the mole fractions of the respective oxide components using Equation 2. The calculated versus measured density are shown in Figure 3-1 along with a linear fit of the data.

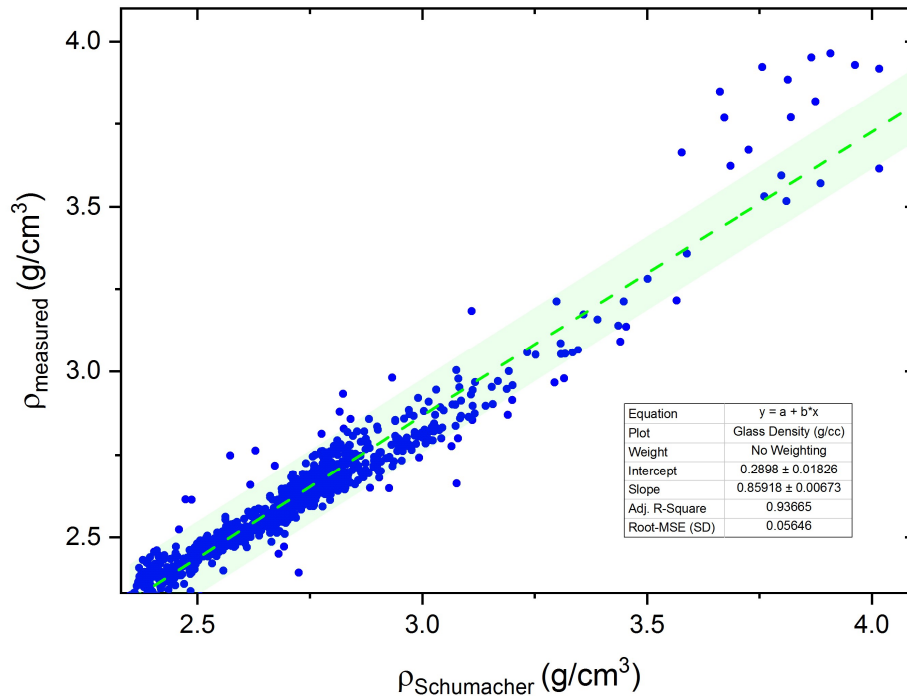


Figure 3-1: Fit of predicted density using Schumacher’s Method (additive density) versus the measured density of the glasses in the database. The adjusted R^2 value is 0.94; however, the slope and intercept are 0.86 and 0.29, respectively, demonstrating that the bulk density is not additive. The green shaded region represents the 95% confidence interval associated with the prediction.

The linear fit to the predicted density in Figure 3-1 has a slope that is less than one, which suggests that Schumacher’s methodology overpredicts density. The overprediction is more clearly demonstrated by examining the distribution of residual data from a linear fit to Schumacher’s method with a constrained slope ($b=1$) and intercept ($a=0$) in Figure 3-2. The overpredicting tendency of Schumacher’s method implies that a phenomenological factor is not accounted for by the model – not surprising given the assertion that density is a non-additive property of glass.

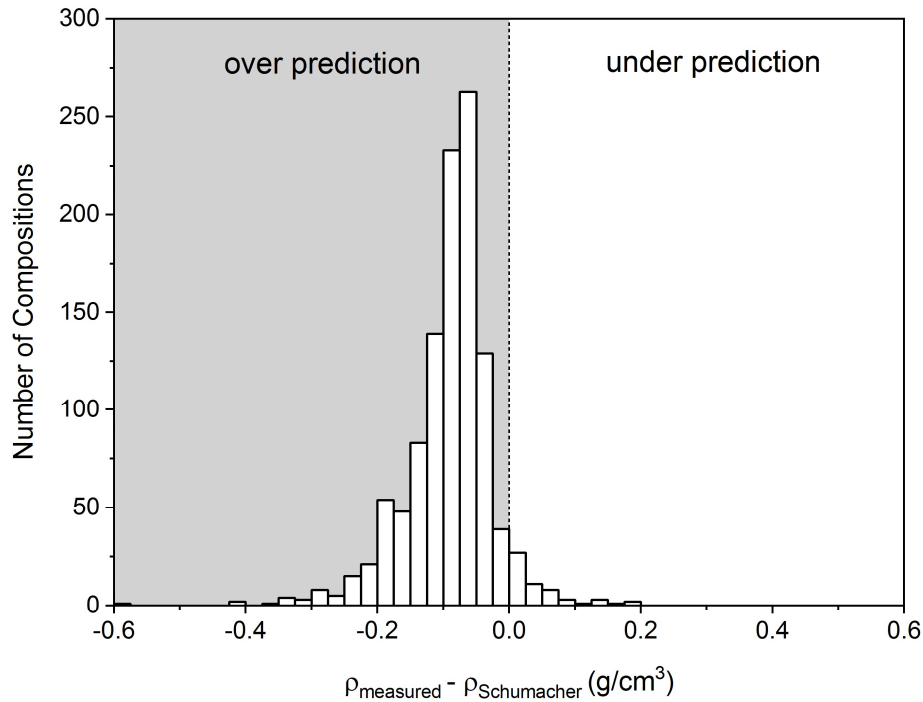


Figure 3-2: A histogram of the residual density predictions establishing the over prediction of Schumacher’s method.

3.2 Partial Molar Volume Method

In parallel to efforts utilizing the additive density method of Schumacher, a method using the bound partial molar volumes of the glass systems’ oxide components was investigated. As previously mentioned, the specific volume is an extensive, additive property of glass systems. Data from Table 2 [11] above and Table 5 in Appendix C [12] were inputted into the model described by Equation 4. The results, a predicted specific volume for a glass composition versus the reciprocal of the measured density, are shown in Figure 3-3.

A high degree of correlation exists between the predicted and measured specific volumes as evidenced by the fit’s R^2 value of 0.943. More importantly, a slope of one and an intercept of zero are captured with the 95% upper and lower confidence intervals of the fit as illustrated in Figure 3-4. By inverting the predicted specific volume (i.e., $\sum x_i v_i / M_g$) and $1/\rho_{\text{measured}}$ terms, the predicted and measured densities were compared. Again, a high correlation coefficient ($R^2 = 0.950$) was obtained as shown in Figure 3-5.

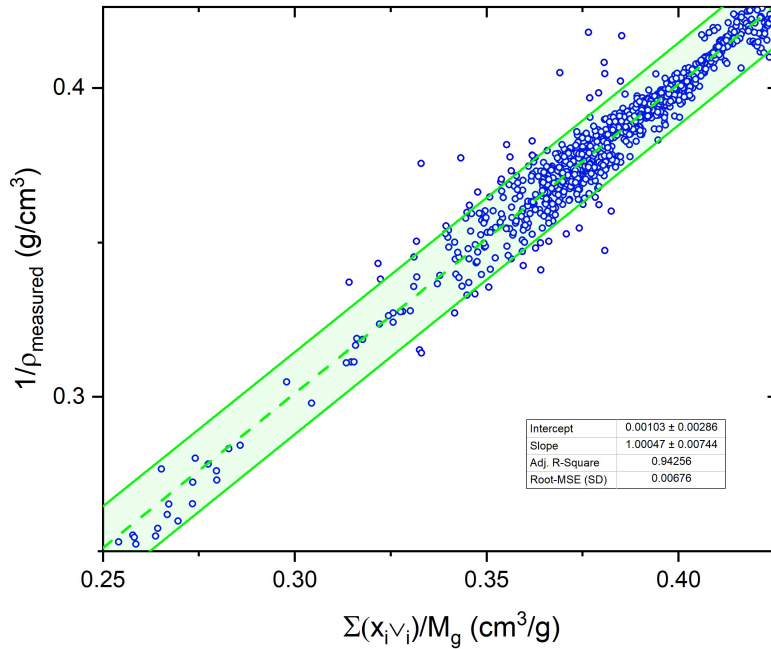


Figure 3-3: The reciprocal of the measured density values versus calculated specific volume of the glass compositions in the density database. The green shaded region is enclosed by the upper and lower 95% confidence limits.

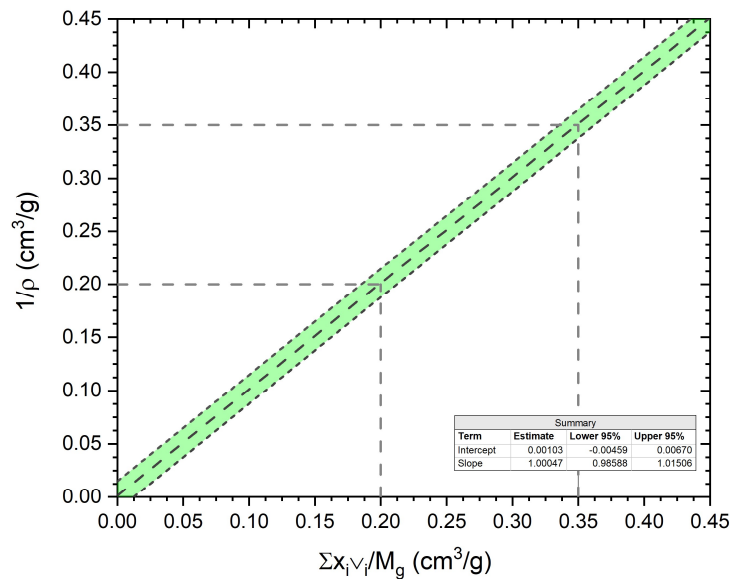


Figure 3-4: The upper and lower 95% confidence intervals associated with the fit determined via the partial molar volumes method projected through the origin. The green shaded region is enclosed by the upper and lower 95% confidence limits.

Similar to the specific volume, the slope and intercept of the linear regression on the measured versus predicted density, shown in Figure 3-5, are approximately one and zero, respectively. As was the case with

the regression shown in Figure 3-3, the upper and lower 95% confidence intervals for the estimated parameters encapsulate a slope of one and an intercept of zero.

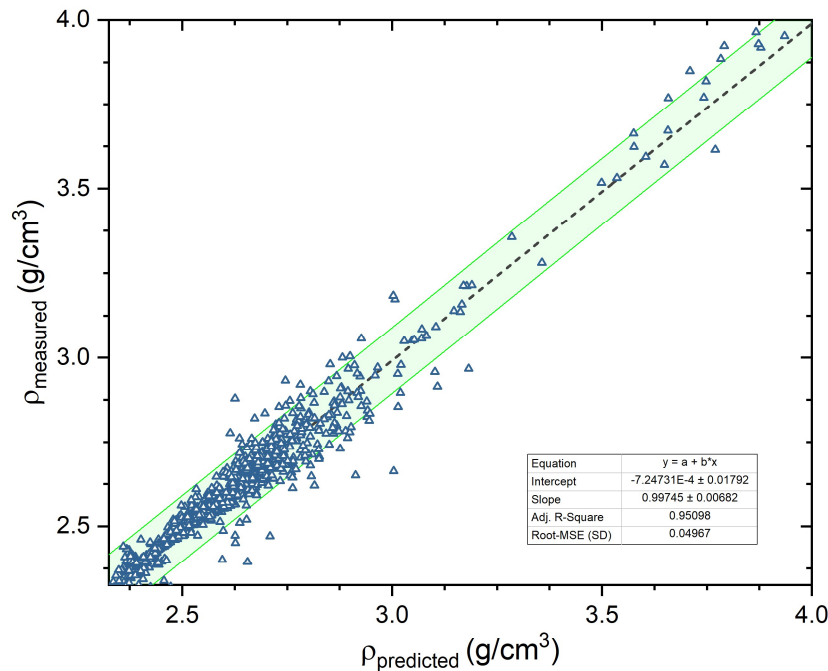


Figure 3-5: The predicted versus measured density shows a high degree of correlation in addition to an uncertainty interval that captures a slope of one and an intercept of zero. The green shaded region is enclosed by the upper and lower 95% confidence limits.

Furthermore, if the slope and the intercept are constrained to one and zero such that the predicted density is compared directly to the measured density, the resulting root-mean-square error (RMSE, the uncertainty of an individual prediction) is similar to that of the unconstrained fit in Figure 3-5 ($\text{RMSE}_{\text{unconstrained}} = 0.050$; $\text{RMSE}_{\text{constrained}} = 0.050$). This similarity indicates that the theoretical prediction produced by the partial molar volume method is within the uncertainty of the empirical regression of the data. The theory is accurately predicting the measured density for individual glass compositions and regression of the theoretical data is not necessary to develop a model with which density can be predicted.

Thus, the model to estimate the density of an HLW glass based upon its composition is given by:

$$\rho = \left(\frac{1}{V_T} \right) + \epsilon = \frac{M_g}{\sum x_i v_i} + \epsilon \quad 5$$

where ρ is the density of the glass, V_T , $\sum x_i v_i$, and M_g are as defined above, and ϵ is the error term associated with this model, which reflects the fact that this evaluation relies upon measurements with intrinsic uncertainties. Figure 3-6 provides the descriptive statistics associated with the error term, ϵ , for the results from the density database. There is a slightly high bias in using $M_g/\sum x_i v_i$ to estimate the glass density. Also, with the assumption that the errors, ϵ , are normally distributed (but, conservatively, not accounting for the high bias), an upper tolerance limit (UTL) can be computed for the errors associated with Equation 5. The equation for a bound covering 99% of the possible errors at a confidence interval of 99% is given by:

$$U_{TL,99/99} = k_{99/99,n-1} \times s = 2.4671 \times 0.04965 = 0.123$$

6

where n is the sample size (1104 in this case), $k_{99/99,n-1} = k_{99/99,1103}$ is the term (based upon the normal probability distribution) that provides the 99% coverage and 99% confidence desired, and s is the standard deviation of the sample (provided in Figure 3-6). Thus, for a given HLW glass, adding the value of 0.123 to the value for $M_g/\sum X_i V_i$ computed from the measured glass composition would provide a bound on the density for that glass. This bound holds for any glass composition at a given $M_g/\sum X_i V_i$ value. In other words, there is an infinite number of compositions that are bounded by the UTL determined for that specific ratio.

A review of the errors, ϵ , seen in Figure 3-6, finds that only 14 out of the 1104 glasses have errors between the ρ and $M_g/\sum X_i V_i$ terms that are greater than 0.123, about 1.3%. This is in line with the 99% coverage at 99% confidence desired.

An additional method for determining an upper 99% tolerance limit is given in Appendix B. This method is based purely on the model fit of Figure 3-5 rather than the theoretical approach discussed above. These two independent methods yield UTLs in the density region of interest for HLW glass that are nearly identical as demonstrated in Appendix B.

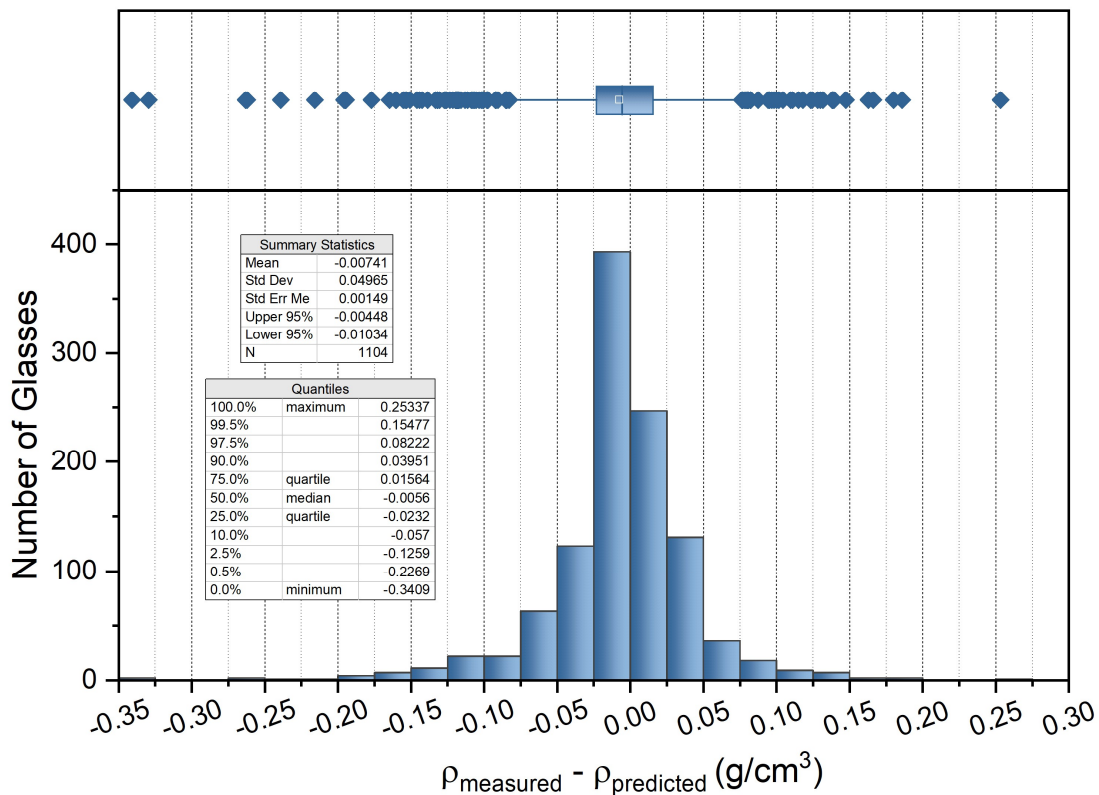


Figure 3-6: Histogram and box plot showing the error in the predicted values versus the measured values including quantiles.

3.3 Comparison to Variability Study Density Limits

As mentioned earlier, the database contains several groups of HLW compositions from DWPF variability studies conducted for past sludge batches. During these studies, a density bound was determined to control the fissile loading of the waste product. The density model developed in this work was used to predict densities for the variability study glasses included in the database, and the results of the individual group predictions and uncertainties for the various sludge batches were compared to the density bound developed during the original variability study. The predictions, density bound determined during the variability studies for the highest waste loading, upper 99% confidence band, lower 95% confidence band, and measured densities for the five groups of glasses are shown in Figure 3-7.

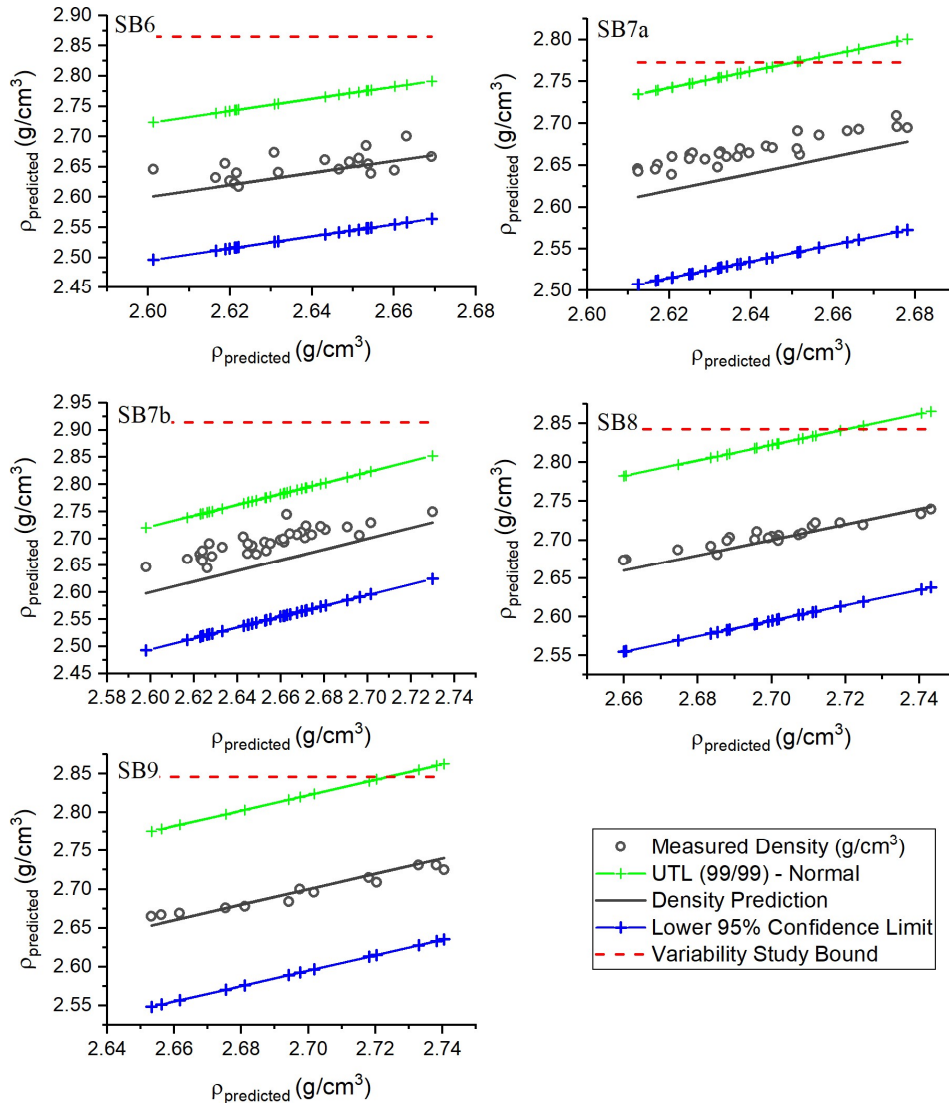


Figure 3-7: Density predictions for the five variability study glass groups included in the database are compared to the measured values. The density bound imposed by the variability study is shown by the dashed red line, while the upper 99% confidence band for the individual density predictions is given with the green line.

The various sub-plots in Figure 3-7 show that the measured densities for the various HLW glasses are within the uncertainty interval of the prediction. In some instances, the upper 99% confidence for the individual predictions yields a value that is less conservative than the bound imposed by the respective variability study (underpredicted) – such a condition is present for SB6 and SB7b glasses. For the other VS subsets, the upper 99% confidence band is more conservative than the imposed bound from the variability study for the top 20-30% of the range of densities examined in the VS. Given the similarity in composition between these glasses and all the other variability study glasses relative to the composition-space covered by the entire database, this underprediction is likely indicative of analytical errors associated with input data collection (e.g., compositional errors) rather than a calculational shortcoming.

3.4 Comparison to Other HLW Studies

In addition to the DWPF variability study glasses, the predicted densities of the other HLW glasses in the database were also examined within their respective groupings. These comparisons are shown in Figure 3-8; however, only the upper 99% and lower 95% confidence intervals on the predictions are shown since these glass systems do not have associated density bounds.

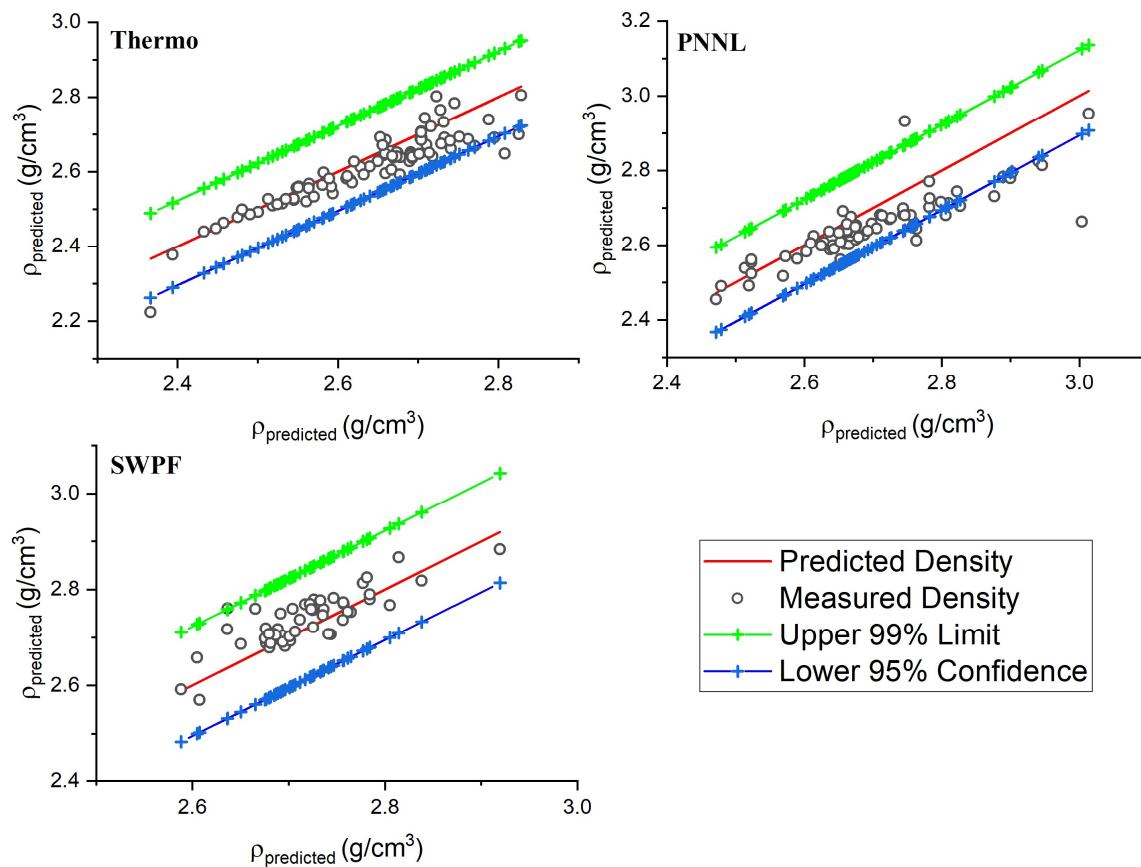


Figure 3-8: The other HLW glass systems that were included in the database show a similar high degree of correlation between the predicted and measured values when compared to the variability study glasses. In total, only two compositions were measured to have higher measured densities than the conservative upper 99% confidence bound.

4.0 Summary

As stated earlier, the density of HLW glass plays a role in DWPF's process of controlling the fissile loading of its waste form product. Currently, DWPF utilizes a bounding value for the density of the glass system as it processes a sludge batch with a corresponding selected frit. This bounding density is determined by SRNL, and this determination relies on measured densities of the associated variability study glasses.

A previous effort to predict the density of glasses was reviewed and compared to the newer model, which predicts glass density based on the additive property of partial molar volumes as opposed to the non-additive individual oxide densities. While both methods lead to predicted density values that are highly correlated with the measured densities, the method utilizing the non-additive oxide densities tended to overpredict. In contrast, the partial molar volume method yielded predicted values that were essentially equal to the measured values within the uncertainty of the prediction thereby negating the need to "fit" the data. In other words, the first-principles approach used to predict the density values provides an estimate of measured glass density ($\rho_{\text{predicted}} \approx \rho_{\text{measured}}$).

The availability of the model developed in this work provides DWPF with options for supporting the control of fissile loading in its waste form product. As a point of comparison, Figure 3-7 demonstrated the efficacy of the partial molar volume method of calculating density with respect to the bounding values established during previous variability studies.

5.0 Conclusions

The following conclusions are supported by the information presented in this work as well as the references presented in this report.

1. Measured glass density is correlated with glass composition.
2. The correlation between glass density and glass composition can be expressed as either:
 - a. a weighted sum of the individual oxide glass-component densities, or
 - b. a weighted sum of the individual oxide glass-component partial molar volumes.
3. A linear regression of the predicted density via partial molar volume method to the measured density yields a slope of 0.9974 ± 0.0068 ($1-\sigma$) and an intercept of -0.0007 ± 0.0180 ($1-\sigma$) – the uncertainty interval associated with these coefficients contain one and zero, respectively.
4. The fitted coefficients and associated uncertainty intervals of the linear regression of the predicted density via the partial molar volume method to the measured density suggest that the predicted theoretical density is, within analysis uncertainty, equal to the measured density of the glass.

6.0 Recommendations

Two ways to utilize the glass density model are outlined in this section: one that SRNL will pursue as part of frit development efforts and one that SRNL recommends for implementation by DWPF Engineering. It is anticipated that having density predictions available as part of the information included in frit recommendation efforts will allow DWPF to make preliminary determinations regarding potential fissile loadings of its future glass product. Implementing the density model into the calculations that are conducted as part of evaluation of each SME batch will allow for the ongoing monitoring of the fissile loading during processing. More information and related examples of these two uses for the density model are provided in Appendix E.

6.1 Discontinue density measurements conducted with variability studies

For the last several sludge batches processed at DWPF, the supporting variability studies have included experimental determinations of glass density (e.g., Reference [7]). The measured values are used to calculate a single, bounding glass density for each sludge batch [2]. It is recommended that the measurement

process can now be omitted from variability studies, and SRNL will instead use the glass density model to develop a bounding density value for the frit/sludge glass system. Examples are provided in Appendix E.

6.2 Transition from a bounding density value to calculating the density of glass produced from each SME batch

For determining the acceptability of each SME batch, there is the potential to reduce conservatism in the process of ensuring that the fissile loading constraint is met by using the model to calculate glass density based on the measured SME composition rather than using a bounding density value. Individual SME evaluations from a few recent sludge batches were reviewed to determine the degree of influence the glass density model would have on the fissile loading calculation. The results of these comparisons are shown in Table 3. As shown in the bottom row of the table, using the glass density model in place of the bounding density value provides a reduction in conservatism associated with the fissile loading determination for a SME batch. It is recommended that DWPF implement the glass density model as part of its process of demonstrating the acceptability of each SME batch, following the detail provided in Appendix E.

Table 3. Determination of Fissile Loading in Recent SME Batches Using Model Predicted and Bounding Glass Density Values

Sludge Batch	SB6	SB7a	SB9		
SME Batch	SME 565	SME 600	SME 787	SME 788	SME 789
Avg. Corrected SME Iron Concentration (wt %)*	6.43	6.55	7.00	6.84	7.86
Glass Density Used by DWPF (g/cm³)	2.85	2.85	2.846	2.846	2.846
Glass Density, Model Prediction (g/cm³)	2.785	2.79	2.756	2.768	2.800
Fissile Loading Using Variability Study Bounding Glass Density (g/m³)	750	724	576	563	646
Fissile Loading Using Model Predicted Glass Density (g/m³)	733	708	557	547	636
Difference (g/m³)	17	16	19	16	10

*Data sourced from the DWPF wg09\chmgrp network folder

7.0 References

- [1] Olson, L, Fissile Isotope Glass Concentration in Defense Waste Processing Facility (DWPF) Canisters, LWO-EVP-2008-00043, (2008).
- [2] Edwards, T and D Peeler, Estimation of Fissile Mass Loadings from Iron Concentrations in SB5 Glasses, SRNL-TR-2009-00258, Rev.0, (2009).
- [3] Edwards, T, D Peeler, W Kot, H Gan and I Pegg, Evaluation of Glass Density to Support the Estimation of Fissile Mass Loadings from Iron Concentrations in SB8 Glasses, SRNL-STI-2013-00212, Rev. 0, (2013).
- [4] Edwards, T and D Peeler, Evaluation of Glass Density to Support the Estimation of Fissile Mass Loadings from Iron Concentrations in SB7b Glasses, SRNL-STI-2012-00007, Rev. 0, (2012).
- [5] Edwards, T and D Peeler, Evaluation of Glass Density to Support the Estimation of Fissile Mass Loadings from Iron Concentrations in SB7a Glasses, SRNL-STI-2011-00512, Rev. 0, (2011).
- [6] Edwards, T and D Peeler, Evaluation of Glass Density to Support the Estimation of Fissile Mass Loadings from Iron Concentrations in SB6 Glasses, SRNL-STI-2010-00757, Rev. 0, (2010).
- [7] Edwards, T, F Johnson, W Kot, H Gan and I Pegg, Evaluation of Glass Density to Support the Estimation of Fissile Mass Loadings from Iron Concentrations in SB9 Glasses, SRNL-TR-2016-00071, Rev. 0, (2016).
- [8] Schumacher, R, DWPF Batch 1, Waste Glass Investigations, WSRC-MS-90-348, (1990).
- [9] Schumacher, R, Basic Data Report: Simulated New Batch 1 Glasses, WSRC-RP-95-0539, Rev. 0, (1998).
- [10] Morey, G, *Properties of Glass*, Reinhold Publishing Corporation: New York, NY, 1938; 221-262.
- [11] Volf, M, *Mathematical Approach to Glass*, Elsevier Science Publishing Company, Inc.: Amsterdam 1988; 107-114.
- [12] Volf, M, *Chemical Approach to Glass*, Elsevier Science Publishing Company, Inc: Amsterdam, 1984; 379-385.
- [13] Handbook of Chemistry and Physics, 2018, Accessed: February 26, 2019, [^http://hbcponline.com/faces/contents/InteractiveTable.xhtml?search=true&tableId=15](http://hbcponline.com/faces/contents/InteractiveTable.xhtml?search=true&tableId=15).
- [14] Kot, W, I Pegg, F Johnson and T Edwards, Final Report Sludge Batch 9 Variability Study with Frit 803, VSL-16R3370-1, Rev. 0, (2016).
- [15] Kot, W, I Pegg, D Peeler and T Edwards, Final Report Sludge Batch 8 Variability Study with Frit 803, VSL-13R2580-1, Rev. 0, (2013).
- [16] Johnson, F and T Edwards, Sludge Batch 7b Glass Variability Study, SRNL-STI-2011-00440, Rev. 0, (2011).
- [17] Peeler, D and T Edwards, The Sludge Batch 7a Glass Variability Study with Frit 418 and Frit 702, SRNL-STI-2011-00063, Rev. 0, (2011).
- [18] Johnson, F and T Edwards, Sludge Batch 6 Variability Study with Frit 418, SRNL-STI-2010-00242, Rev. 0, (2010).
- [19] Kot, W and I Pegg, Measurements of Glass Density and Melt Viscosity to Support Salt Waste Processing Facility (SWPF) Gap Analysis Study, VSL-15L3500-2, Rev. 1, (2016).
- [20] Vienna, J, P Hrma, A Jiricka, D Smith, T Lorier, I Reamer and R Schulz, Hanford Immobilized LAW Product Acceptance Testing: Tanks Focus Area Results, PNNL-13744, (2001).
- [21] Standard Reference Material 1830, Soda-Lime Float Glass, National Institute of Standards and Technology, Gaithersburg, MD, July 12, 2017.
- [22] Standard Reference Material 1826a, Soda-Lime Glass Mass Density Standard, National Institute of Standards and Technology, Gaithersburg, MD, February 27, 1996.
- [23] Standard Reference Material 1827a, Lead Silica Glass Mass Density Standard, National Institute of Standards and Technology, Gaithersburg, MD, February 26, 1997.
- [24] Bansal, N and R Doremus, *Handbook of Glass Properties*, Academic Press, Inc.: Orlando, FL, 1986; 50-100.

- [25] Jantzen, C, J Pickett, K Brown, T Edwards and D Beam, Process/Product Models for the Defense Waste Processing Facility (DWPF): Part I. Predicting Glass Durability from Composition Using a Thermodynamic Hydration Energy Reaction Model (THERMO), WSRC-TR-93-672, Rev. 1, (1995).
- [26] Johnson, F, T Edwards and K Fox, The User Guide for the ComPro™ Database, SRNL-STI-2009-00093, Rev. 1, (2013).
- [27] Johnson, F, T Edwards and K Fox, Data Qualification Report: SRNL Glass Composition - Properties (ComPro™) Database, SRNL-STI-2009-00094, Rev. 1, (2013).
- [28] Knoche, R, D Dingwell and S Webb, Melt densities for leucogranites and granitic pegmatites: Partial molar volumes for SiO₂, Al₂O₃, Na₂O, K₂O, Li₂O, Rb₂O, Cs₂O, MgO, CaO, SrO, BaO, B₂O₃, P₂O₅, F₂O₋₁, TiO₂, Nb₂O₅, Ta₂O₅, and WO₃, *Geochimica et Cosmochimica Acta* **1995**, 59 (22), 4645-4652.
- [29] McClane, D, J Amoroso, K Fox and A Kruger, Nepheline crystallization behavior in simulated high-level waste glasses, *Journal of Non-Crystalline Solids* **2019**, 505 (1), 215-224.
- [30] Morey, G and H Merwin, The relation between the composition and the density and optical properties of glass. I. The soda-lime-silica glasses, *Journal of the Optical Society of America* **1932**, 22 (11), 632-662.
- [31] Parkinson, B, D Holland, M Smith, A Howes and C Scales, The effect of Cs₂O additions on HLW wastefrom glasses, *Journal of Non-Crystalline Solids* **2005**, 351 (30-32), 2425-2432.
- [32] Rao, B, Influence of TiO₂ on properties of glasses in the system K₂O–PbO–SiO₂–TiO₂ and its relation to structure, *Journal of the American Ceramic Society* **1963**, 46 (3), 107-114.
- [33] Shelby, J, Appendix I, In *High Temperature Glass Melt Property Database for Process Modelling*; T. Seward III and T. Vascott, Eds., The American Ceramic Society: Westerville, OH, 2005, 261-274.
- [34] Trivelpiece, C, C Jantzen and C Crawford, Accelerated Leach Testing of GLASS: ALTGLASS Version 3.0, SRNL-STI-2016-00527, Rev. 0, (2016).
- [35] Tsujimura, T, X Xue, M Kanzaki and M Walter, Sulfur speciation and network structural changes in sodium silicate glasses: Constraints from NMR and Raman spectroscopy, *Geochimica et Cosmochimica Acta* **2004**, 68 (24), 5081-5101.
- [36] Skidmore, C, J Vienna, T Jin, D Kim, B Stanfill, K Fox and A Kruger, Sulfur Solubility in Low Activity Waste Glass and its Correlation to Melter Tolerance, *International Journal of Applied Glass Science* **2019**, 00 1-11. <https://doi.org/10.1111/ijag.13272>.
- [37] Bingham, P, S Vaishnav, S Forder, A Scrimshire, B Jaganathan, J Rohini, J Marra, K Fox, E Pierce, P Workman and J Vienna, Modelling the sulfate capacity of simulated radioactive waste borosilicate glasses, *Journal of Alloys and Compounds* **2017**, 695 656-667.
- [38] Johnson, F, Recommendation for the Sludge Batch 9 Sulfate Solubility Limit, SRNL-L3100-2016-00044, Rev. 0, (2016).
- [39] Mysen, B, G Cody and A Smith, Solubility mechanisms of fluorine in peralkaline and meta-aluminous silicate glasses and in melts to magmatic temperatures, *Geochimica et Cosmochimica Acta* **2004**, 68 (12), 2745-2769.
- [40] Baasner, A, B Schmidt, R Dupree and S Webb, Fluorine speciation as a function of composition in peralkaline and peraluminous Na₂O–CaO–Al₂O₃–SiO₂ glasses: A multinuclear NMR study, *Geochimica et Cosmochimica Acta* **2014**, 132 151-169.
- [41] Hill, R, D Wood and M Thomas, Trimethylsilylation analysis of the silicate structure of fluoro-alumino-silicate glasses and the structural role of fluorine, *Journal of Materials Science* **1999**, 34 (8), 1767-1774.
- [42] Dingwell, D, R Knoche and S Webb, The effect of F on the density of haplogranite melt, *American Mineralogist* **1993**, 78 (3-4), 325-330.
- [43] Hanifi, A, A Genson, M Pomeroy and S Hampshire, Independent but additive effects of fluorine and nitrogen substitution on properties of a calcium aluminosilicate glass, *Journal of the American Ceramic Society* **2012**, 95 (2), 600-606.

- [44] Ramos, A, C Levelut and J Petiau, Local environment of selenium in silicate glasses, Journal of Non-Crystalline Solids **1992**, 151 (1-2), 13-22.
- [45] Bingham, P, A Connelly, N Cassingham and N Hyatt, Oxidation state and local environment of selenium in alkali borosilicate glasses for radioactive waste immobilisation, Journal of Non-Crystalline Solids **2011**, 357 (14), 2726-2734.
- [46] Conduct of Engineering - Technical Reviews, Savannah River Site, 2021, Manual E7 - Procedure 2.60, Rev. 20.
- [47] Savannah River National Laboratory Technical Report Design Check Guidelines, Savannah River National Laboratory, 2004, WSRC-IM-2002-00011, Rev.2.
- [48] Russell, K, Sludge Batch 10 Frit Evaluation and Measurement Acceptance Region Assessment, X-TTR-S-00064, Rev. 4, (2021).
- [49] Johnson, F, Task Technical and Quality Assurance Plan for Sludge Batch 10 Frit Evaluation and Measurement Acceptance Region Assessments, SRNL-RP-2017-00384, Rev. 4, (2021).
- [50] SAS Institute, Inc., JMP Pro Version 11.2.1, Cary, North Carolina, (1989-2014).
- [51] Vienna, J D, P R Hrma, A Jiricka, D E Smith, T H Lorier, I A Reamer and R L Schulz, Hanford Immobilized LAW Product Acceptance Testing: Tanks Focus Area Results, PNNL-13744, (2000).
- [52] Miller, R, *Simultaneous Statistical Inference*, Springer-Verlag: New York, NY, 1989; 124.
- [53] Jantzen, C, M Williams, T Edwards, C Trivelpiece and W Ramsey, Nitric-Glycolic Flowsheet REDuction/OXidation (REDOX) Model for the Defense Waste Processing Facility (DWPF), SRNL-STI-2017-00005, Rev. 0, (2017).
- [54] Johnson, F and T Edwards, Frit Recommendation for Sludge Batch 9 Coupled Operation with the Salt Waste Processing Facility, SRNL-STI-2019-00004, Rev.0, (2019).
- [55] Elder, H, Control of Fissile Concentration in Sludge Batch 8 Glass, X-ESR-S-00134, Rev.1, (2013).
- [56] Jamison, L, Control of Fissile Concentration in Sludge Batch 9 Glass X-ESR-S-00280, Rev.0, (2016).

Appendix A

Table 4: Select data from the density database used to develop the prediction model.

Glass ID	ρ_{measured} (g/cm ³)	$\rho_{\text{predicted}}$ (g/cm ³)	$1/\rho_{\text{measured}}$ (cm ³ /g)	$\Sigma V_i/M_g$ (cm ³ /g)	V_{glass} (cm ³ /mol)	M_g	Reference
+2Al	2.321	2.355	0.431	0.425	27.961	64.900	[28]
+5Al	2.333	2.361	0.429	0.424	28.085	65.508	[28]
-2Al	2.317	2.350	0.432	0.425	27.643	64.044	[28]
-5Al	2.313	2.348	0.432	0.426	27.406	63.401	[28]
AH 131AL	2.576	2.616	0.388	0.382	25.000	64.399	[25]
AH 131AV	2.685	2.660	0.372	0.376	24.071	64.632	[25]
AH 131FE	2.765	2.728	0.362	0.367	22.906	63.335	[25]
AH 165AL	2.568	2.564	0.389	0.390	24.954	64.081	[25]
AH 165AV	2.692	2.653	0.371	0.377	23.769	63.987	[25]
AH 165FE	2.802	2.723	0.357	0.367	22.688	63.572	[25]
AH 168AL	2.515	2.530	0.398	0.395	24.224	60.924	[25]
AH 168AV	2.655	2.666	0.377	0.375	24.430	64.862	[25]
AH 168FE	2.733	2.732	0.366	0.366	23.457	64.107	[25]
AH 200AL	2.542	2.594	0.393	0.386	25.918	65.885	[25]
AH 200AV	2.651	2.691	0.377	0.372	25.199	66.803	[25]
AH 200FE	2.784	2.745	0.359	0.364	23.637	65.805	[25]
AH 202AL	2.520	2.560	0.397	0.391	25.637	64.606	[25]
AH 202AV	2.644	2.657	0.378	0.376	24.666	65.217	[25]
AH 202FE	2.744	2.708	0.364	0.369	23.323	64.000	[25]
AH-10	2.628	2.650	0.381	0.377	24.715	64.951	[25]
AH-13	2.721	2.716	0.367	0.368	24.819	67.538	[25]
AH-16	2.687	2.703	0.372	0.370	24.798	66.636	[25]
AH-5	2.648	2.659	0.378	0.376	24.823	65.723	[25]
AH-8	2.645	2.691	0.378	0.372	25.145	66.502	[25]
AH-9	2.650	2.674	0.377	0.374	25.066	66.431	[25]
B05	2.299	2.370	0.435	0.422	28.114	64.620	[28]
B10	2.269	2.388	0.441	0.419	28.649	65.016	[28]
Ba05	2.408	2.433	0.415	0.411	27.556	66.349	[28]
Ba10	2.491	2.509	0.401	0.399	27.375	68.182	[28]
Ba20	2.737	2.703	0.365	0.370	26.453	72.396	[28]
Ca05	2.383	2.403	0.420	0.416	26.890	64.081	[28]
Ca10	2.442	2.449	0.410	0.408	26.074	63.661	[28]
Ca20	2.598	2.561	0.385	0.390	23.993	62.333	[28]
Cleek and Babcock - 1973 - Ba-La-Si - 1	3.663	3.575	0.273	0.280	25.888	94.828	[24]
Cleek and Babcock - 1973 - Ba-La-Si - 11	3.819	3.748	0.262	0.267	24.940	95.246	[24]

Glass ID	ρ_{measured} (g/cm ³)	$\rho_{\text{predicted}}$ (g/cm ³)	$1/\rho_{\text{measured}}$ (cm ³ /g)	$\Sigma V_i/M_g$ (cm ³ /g)	V_{glass} (cm ³ /mol)	M_g	Reference
Cleek and Babcock - 1973 - Ba-La-Si - 13	3.918	3.878	0.255	0.258	25.022	98.037	[24]
Cleek and Babcock - 1973 - Ba-La-Si - 17	3.997	4.010	0.250	0.249	25.228	100.836	[24]
Cleek and Babcock - 1973 - Ba-La-Si - 2	3.849	3.710	0.260	0.270	26.019	100.148	[24]
Cleek and Babcock - 1973 - Ba-La-Si - 4	3.768	3.658	0.265	0.273	25.662	96.694	[24]
Cleek and Babcock - 1973 - Ba-La-Si - 5	3.923	3.791	0.255	0.264	26.003	102.012	[24]
Cleek and Babcock - 1973 - Ba-La-Si - 7	3.623	3.576	0.276	0.280	25.258	91.510	[24]
Cleek and Babcock - 1973 - Ba-La-Si - 8	3.885	3.783	0.257	0.264	25.611	99.497	[24]
Cleek and Babcock - 1973 - Ba-La-Si - 9	3.964	3.867	0.252	0.259	25.570	101.358	[24]
Cleek and Babcock - Ba-Ta-Si-1	3.952	3.935	0.253	0.254	26.409	104.367	[24]
Cleek and Babcock - Ba-Ta-Si-2	3.672	3.657	0.272	0.273	25.556	93.841	[24]
Cleek and Babcock - Ba-Ta-Si-3	3.770	3.743	0.265	0.267	25.385	95.700	[24]
Cleek and Babcock - Ba-Ta-Si-6	3.929	3.873	0.255	0.258	25.073	98.512	[24]
Co 00	2.520	2.478	0.397	0.403	23.916	60.269	[33]
Co 01	2.405	2.422	0.416	0.413	25.081	60.320	[33]
Co 02	2.503	2.486	0.400	0.402	24.243	60.680	[33]
Co 03	2.534	2.526	0.395	0.396	23.636	59.895	[33]
Co 04	2.487	2.486	0.402	0.402	24.050	59.811	[33]
Co 05	2.494	2.482	0.401	0.403	23.819	59.406	[33]
Co 06	2.545	2.527	0.393	0.396	23.294	59.284	[33]
Co 07	2.477	2.470	0.404	0.405	24.881	61.630	[33]
Co 08	2.444	2.450	0.409	0.408	24.951	60.981	[33]
Co 09	2.554	2.522	0.392	0.396	23.547	60.138	[33]
Co 10	2.477	2.464	0.404	0.406	24.036	59.538	[33]
Co 11	2.559	2.548	0.391	0.392	23.566	60.307	[33]
Co 12	2.520	2.507	0.397	0.399	23.769	59.899	[33]
Co 13	2.497	2.466	0.400	0.406	24.282	60.632	[33]
Co 14	2.430	2.431	0.412	0.411	24.677	59.965	[33]
Co 15	2.536	2.519	0.394	0.397	23.925	60.673	[33]
Co 16	2.470	2.458	0.405	0.407	24.314	60.056	[33]
Co 17	2.556	2.533	0.391	0.395	23.201	59.302	[33]
Co 18	2.538	2.516	0.394	0.397	23.119	58.675	[33]
Co 19	2.461	2.458	0.406	0.407	24.812	61.063	[33]
Co 20	2.517	2.495	0.397	0.401	24.172	60.840	[33]
Co 21	2.514	2.487	0.398	0.402	24.061	60.489	[33]
Co 22	2.469	2.465	0.405	0.406	24.479	60.440	[33]
Co 23	2.502	2.486	0.400	0.402	23.788	59.516	[33]
Co 24	2.590	2.559	0.386	0.391	23.164	59.994	[33]
Cs05	2.392	2.400	0.418	0.417	27.802	66.508	[28]
Cs10	2.456	2.456	0.407	0.407	28.225	69.330	[28]

Glass ID	ρ_{measured} (g/cm ³)	$\rho_{\text{predicted}}$ (g/cm ³)	$1/\rho_{\text{measured}}$ (cm ³ /g)	$\Sigma V_i/M_g$ (cm ³ /g)	V_{glass} (cm ³ /mol)	M_g	Reference
Cs20	2.614	2.588	0.383	0.386	28.813	75.309	[28]
Dubrovo - Kasimova - 1964 - 9	2.595	2.602	0.385	0.384	24.908	64.636	[24]
Dubrovo - Kasimova - 1964 - 1	2.718	2.718	0.368	0.368	23.886	64.921	[24]
Dubrovo - Kasimova - 1964 - 10	3.356	3.285	0.298	0.304	22.476	75.430	[24]
Dubrovo - Kasimova - 1964 - 11	3.212	3.178	0.311	0.315	22.835	73.347	[24]
Dubrovo - Kasimova - 1964 - 12	3.085	3.071	0.324	0.326	23.100	71.264	[24]
Dubrovo - Kasimova - 1964 - 13	3.050	3.029	0.328	0.330	23.092	70.431	[24]
Dubrovo - Kasimova - 1964 - 14	2.971	2.966	0.337	0.337	23.286	69.181	[24]
Dubrovo - Kasimova - 1964 - 15	2.944	2.924	0.340	0.342	23.216	68.348	[24]
Dubrovo - Kasimova - 1964 - 16	2.901	2.895	0.345	0.345	23.359	67.765	[24]
Dubrovo - Kasimova - 1964 - 17	2.883	2.876	0.347	0.348	23.375	67.390	[24]
Dubrovo - Kasimova - 1964 - 18	2.870	2.861	0.348	0.349	23.379	67.099	[24]
Dubrovo - Kasimova - 1964 - 19	2.474	2.506	0.404	0.399	25.284	62.553	[24]
Dubrovo - Kasimova - 1964 - 2	3.158	3.166	0.317	0.316	22.626	71.454	[24]
Dubrovo - Kasimova - 1964 - 20	2.776	2.843	0.360	0.352	23.489	65.206	[24]
Dubrovo - Kasimova - 1964 - 21	2.757	2.738	0.363	0.365	24.234	66.814	[24]
Dubrovo - Kasimova - 1964 - 3	2.698	2.689	0.371	0.372	24.378	65.773	[24]
Dubrovo - Kasimova - 1964 - 4	2.537	2.542	0.394	0.393	24.694	62.648	[24]
Dubrovo - Kasimova - 1964 - 5	2.912	2.879	0.343	0.347	23.692	68.992	[24]
Dubrovo - Kasimova - 1964 - 6	2.800	2.778	0.357	0.360	23.896	66.909	[24]
Dubrovo - Kasimova - 1964 - 7	2.689	2.678	0.372	0.373	24.108	64.826	[24]
Dubrovo - Kasimova - 1964 - 8	2.576	2.579	0.388	0.388	24.357	62.743	[24]
DWPF STARTUP FRIT	2.692	2.733	0.372	0.366	24.934	67.114	[25]
E 00	2.620	2.582	0.382	0.387	23.777	62.295	[33]
E 01	2.500	2.477	0.400	0.404	24.961	62.404	[33]
E 02	2.558	2.506	0.391	0.399	24.649	63.052	[33]
E 03	2.734	2.655	0.366	0.377	22.238	60.798	[33]
E 04	2.572	2.523	0.389	0.396	24.434	62.845	[33]
E 05	2.671	2.607	0.374	0.384	23.527	62.841	[33]
E 06	2.743	2.643	0.365	0.378	22.117	60.667	[33]
E 07	2.518	2.544	0.397	0.393	24.839	62.545	[33]
E 09	2.682	2.639	0.373	0.379	22.814	61.187	[33]
E 10	2.662	2.621	0.376	0.382	23.870	63.541	[33]
E 11	2.593	2.608	0.386	0.383	24.250	62.880	[33]
E 12	2.583	2.586	0.387	0.387	24.325	62.831	[33]
E 13	2.660	2.598	0.376	0.385	23.033	61.267	[33]
E 14	2.647	2.582	0.378	0.387	23.109	61.170	[33]
E 15	2.586	2.540	0.387	0.394	23.854	61.687	[33]
E 16	2.561	2.498	0.390	0.400	24.501	62.747	[33]

Glass ID	ρ_{measured} (g/cm ³)	$\rho_{\text{predicted}}$ (g/cm ³)	$1/\rho_{\text{measured}}$ (cm ³ /g)	$\Sigma V_i/M_g$ (cm ³ /g)	V_{glass} (cm ³ /mol)	M_g	Reference
E 17	2.610	2.533	0.383	0.395	23.410	61.099	[33]
E 18	2.721	2.639	0.368	0.379	22.523	61.286	[33]
E 19	2.517	2.508	0.397	0.399	24.904	62.684	[33]
E 21	2.677	2.633	0.374	0.380	22.959	61.461	[33]
E 22	2.513	2.535	0.398	0.395	25.215	63.366	[33]
E 23	2.665	2.641	0.375	0.379	24.105	64.240	[33]
E 24	2.730	2.705	0.366	0.370	22.838	62.348	[33]
EA Glass	2.648	2.684	0.378	0.373	23.708	62.773	[24, 25]
Faick - Na-Al-Si - 1	2.401	2.418	0.416	0.414	25.289	60.719	[24]
Faick - Na-Al-Si - 10	2.440	2.449	0.410	0.408	24.925	60.817	[24]
Faick - Na-Al-Si - 11	2.421	2.425	0.413	0.412	25.970	62.873	[24]
Faick - Na-Al-Si - 12	2.434	2.440	0.411	0.410	25.545	62.178	[24]
Faick - Na-Al-Si - 13	2.451	2.457	0.408	0.407	25.011	61.302	[24]
Faick - Na-Al-Si - 14	2.443	2.449	0.409	0.408	25.297	61.801	[24]
Faick - Na-Al-Si - 15	2.445	2.451	0.409	0.408	25.273	61.793	[24]
Faick - Na-Al-Si - 16	2.457	2.466	0.407	0.406	24.876	61.121	[24]
Faick - Na-Al-Si - 17	2.461	2.472	0.406	0.405	24.736	60.874	[24]
Faick - Na-Al-Si - 18	2.453	2.458	0.408	0.407	25.293	62.043	[24]
Faick - Na-Al-Si - 19	2.454	2.458	0.407	0.407	25.386	62.296	[24]
Faick - Na-Al-Si - 2	2.412	2.424	0.415	0.413	25.377	61.210	[24]
Faick - Na-Al-Si - 20	2.468	2.478	0.405	0.404	24.872	61.385	[24]
Faick - Na-Al-Si - 21	2.465	2.475	0.406	0.404	25.053	61.754	[24]
Faick - Na-Al-Si - 22	2.481	2.493	0.403	0.401	24.665	61.193	[24]
Faick - Na-Al-Si - 23	2.481	2.494	0.403	0.401	24.704	61.291	[24]
Faick - Na-Al-Si - 24	2.483	2.492	0.403	0.401	24.729	61.401	[24]
Faick - Na-Al-Si - 25	2.458	2.461	0.407	0.406	25.633	63.006	[24]
Faick - Na-Al-Si - 26	2.475	2.484	0.404	0.403	24.992	61.856	[24]
Faick - Na-Al-Si - 27	2.462	2.464	0.406	0.406	25.652	63.155	[24]
Faick - Na-Al-Si - 28	2.492	2.509	0.401	0.399	24.472	60.985	[24]
Faick - Na-Al-Si - 29	2.498	2.510	0.400	0.398	24.977	62.393	[24]
Faick - Na-Al-Si - 3	2.402	2.416	0.416	0.414	25.680	61.683	[24]
Faick - Na-Al-Si - 30	2.489	2.496	0.402	0.401	25.371	63.147	[24]
Faick - Na-Al-Si - 31	2.517	2.538	0.397	0.394	24.266	61.077	[24]
Faick - Na-Al-Si - 32	2.511	2.530	0.398	0.395	24.488	61.488	[24]
Faick - Na-Al-Si - 33	2.503	2.520	0.400	0.397	24.763	61.981	[24]
Faick - Na-Al-Si - 34	2.490	2.498	0.402	0.400	25.389	63.219	[24]
Faick - Na-Al-Si - 35	2.530	2.556	0.395	0.391	24.532	62.067	[24]
Faick - Na-Al-Si - 36	2.536	2.567	0.394	0.390	24.290	61.598	[24]
Faick - Na-Al-Si - 37	2.516	2.534	0.397	0.395	25.150	63.276	[24]

Glass ID	ρ_{measured} (g/cm ³)	$\rho_{\text{predicted}}$ (g/cm ³)	$1/\rho_{\text{measured}}$ (cm ³ /g)	$\Sigma V_i/M_g$ (cm ³ /g)	V_{glass} (cm ³ /mol)	M_g	Reference
Faick - Na-Al-Si - 38	2.526	2.548	0.396	0.392	24.779	62.592	[24]
Faick - Na-Al-Si - 39	2.518	2.536	0.397	0.394	25.148	63.323	[24]
Faick - Na-Al-Si - 4	2.403	2.416	0.416	0.414	25.701	61.760	[24]
Faick - Na-Al-Si - 40	2.553	2.594	0.392	0.386	24.355	62.177	[24]
Faick - Na-Al-Si - 41	2.541	2.570	0.394	0.389	24.930	63.346	[24]
Faick - Na-Al-Si - 42	2.548	2.585	0.392	0.387	24.580	62.629	[24]
Faick - Na-Al-Si - 43	2.550	2.586	0.392	0.387	24.591	62.707	[24]
Faick - Na-Al-Si - 44	2.561	2.609	0.390	0.383	24.092	61.700	[24]
Faick - Na-Al-Si - 5	2.419	2.432	0.413	0.411	25.226	61.022	[24]
Faick - Na-Al-Si - 6	2.423	2.436	0.413	0.410	25.095	60.804	[24]
Faick - Na-Al-Si - 7	2.416	2.428	0.414	0.412	25.356	61.260	[24]
Faick - Na-Al-Si - 8	2.428	2.438	0.412	0.410	25.036	60.787	[24]
Faick - Na-Al-Si - 9	2.418	2.428	0.414	0.412	25.510	61.684	[24]
FL 00	2.530	2.494	0.395	0.401	23.295	58.936	[33]
FL 01	2.462	2.466	0.406	0.406	24.298	59.821	[33]
FL 02	2.524	2.503	0.396	0.400	23.835	60.159	[33]
FL 03	2.492	2.489	0.401	0.402	23.961	59.710	[33]
FL 04	2.529	2.520	0.395	0.397	23.631	59.763	[33]
FL 05	2.520	2.517	0.397	0.397	23.539	59.317	[33]
FL 06	2.586	2.531	0.387	0.395	23.236	60.089	[33]
FL 07	2.526	2.518	0.396	0.397	23.888	60.342	[33]
FL 08	2.536	2.538	0.394	0.394	23.655	59.989	[33]
FL 09	2.513	2.511	0.398	0.398	24.102	60.569	[33]
FL 10	2.548	2.541	0.392	0.394	23.717	60.431	[33]
FL 11	2.533	2.531	0.395	0.395	23.725	60.096	[33]
FL 12	2.522	2.507	0.397	0.399	23.871	60.203	[33]
FL 13	2.530	2.531	0.395	0.395	23.603	59.715	[33]
FL 14	2.490	2.496	0.402	0.401	23.929	59.583	[33]
FL 15	2.471	2.502	0.405	0.400	24.690	61.010	[33]
FL 16	2.515	2.511	0.398	0.398	23.894	60.094	[33]
FL 17	2.505	2.502	0.399	0.400	23.601	59.119	[33]
FL 18	2.511	2.501	0.398	0.400	23.768	59.680	[33]
FL 19	2.484	2.491	0.403	0.401	24.418	60.654	[33]
FL 20	2.554	2.538	0.392	0.394	23.509	60.042	[33]
FL 21	2.489	2.489	0.402	0.402	23.965	59.648	[33]
FL 22	2.514	2.499	0.398	0.400	23.858	59.978	[33]
FL 23	2.474	2.487	0.404	0.402	24.072	59.555	[33]
FL 24	2.443	2.456	0.409	0.407	24.281	59.318	[33]
G.Morey-1932-1	2.310	2.360	0.433	0.424	25.938	59.917	[30]

Glass ID	ρ_{measured} (g/cm ³)	$\rho_{\text{predicted}}$ (g/cm ³)	$1/\rho_{\text{measured}}$ (cm ³ /g)	$\Sigma V_i/M_g$ (cm ³ /g)	V_{glass} (cm ³ /mol)	M_g	Reference
G.Morey-1932-10	2.497	2.494	0.400	0.401	23.874	59.613	[30]
G.Morey-1932-100	2.719	2.739	0.368	0.365	21.868	59.460	[30]
G.Morey-1932-11	2.485	2.477	0.402	0.404	24.086	59.854	[30]
G.Morey-1932-12	2.455	2.453	0.407	0.408	24.531	60.223	[30]
G.Morey-1932-13	2.505	2.508	0.399	0.399	23.728	59.439	[30]
G.Morey-1932-14	2.468	2.460	0.405	0.407	24.387	60.186	[30]
G.Morey-1932-15	2.535	2.521	0.394	0.397	23.398	59.313	[30]
G.Morey-1932-16	2.475	2.470	0.404	0.405	24.276	60.084	[30]
G.Morey-1932-17	2.477	2.471	0.404	0.405	24.259	60.090	[30]
G.Morey-1932-18	2.489	2.481	0.402	0.403	24.081	59.939	[30]
G.Morey-1932-19	2.495	2.488	0.401	0.402	23.983	59.838	[30]
G.Morey-1932-2	2.311	2.356	0.433	0.424	25.975	60.029	[30]
G.Morey-1932-20	2.506	2.502	0.399	0.400	23.797	59.636	[30]
G.Morey-1932-21	2.489	2.484	0.402	0.403	24.080	59.936	[30]
G.Morey-1932-22	2.492	2.484	0.401	0.403	24.053	59.941	[30]
G.Morey-1932-23	2.532	2.528	0.395	0.396	23.431	59.328	[30]
G.Morey-1932-24	2.536	2.529	0.394	0.395	23.395	59.330	[30]
G.Morey-1932-25	2.522	2.528	0.397	0.396	23.531	59.344	[30]
G.Morey-1932-26	2.641	2.674	0.379	0.374	22.824	60.278	[30]
G.Morey-1932-27	2.761	2.772	0.362	0.361	21.395	59.072	[30]
G.Morey-1932-28	2.820	2.815	0.355	0.355	20.781	58.601	[30]
G.Morey-1932-29	2.741	2.755	0.365	0.363	21.633	59.296	[30]
G.Morey-1932-3	2.345	2.378	0.426	0.421	25.655	60.161	[30]
G.Morey-1932-30	2.670	2.698	0.375	0.371	22.479	60.020	[30]
G.Morey-1932-31	2.696	2.722	0.371	0.367	22.171	59.773	[30]
G.Morey-1932-32	2.663	2.700	0.376	0.370	22.552	60.056	[30]
G.Morey-1932-33	2.710	2.743	0.369	0.365	21.984	59.575	[30]
G.Morey-1932-34	2.867	2.860	0.349	0.350	20.331	58.290	[30]
G.Morey-1932-35	2.717	2.742	0.368	0.365	21.955	59.651	[30]
G.Morey-1932-36	2.697	2.735	0.371	0.366	22.151	59.742	[30]
G.Morey-1932-37	2.859	2.863	0.350	0.349	20.417	58.373	[30]
G.Morey-1932-38	2.794	2.823	0.358	0.354	21.081	58.899	[30]
G.Morey-1932-39	2.654	2.711	0.377	0.369	22.725	60.312	[30]
G.Morey-1932-4	2.355	2.392	0.425	0.418	25.468	59.977	[30]
G.Morey-1932-40	2.863	2.881	0.349	0.347	20.380	58.348	[30]
G.Morey-1932-41	2.681	2.741	0.373	0.365	22.387	60.020	[30]
G.Morey-1932-42	2.630	2.701	0.380	0.370	23.015	60.529	[30]
G.Morey-1932-43	2.640	2.713	0.379	0.369	22.909	60.481	[30]
G.Morey-1932-44	2.874	2.897	0.348	0.345	20.307	58.362	[30]

Glass ID	ρ_{measured} (g/cm ³)	$\rho_{\text{predicted}}$ (g/cm ³)	$1/\rho_{\text{measured}}$ (cm ³ /g)	$\Sigma V_i/M_g$ (cm ³ /g)	V_{glass} (cm ³ /mol)	M_g	Reference
G.Morey-1932-45	2.837	2.869	0.352	0.349	20.677	58.662	[30]
G.Morey-1932-46	2.902	2.925	0.345	0.342	20.019	58.095	[30]
G.Morey-1932-47	2.703	2.765	0.370	0.362	22.151	59.873	[30]
G.Morey-1932-48	2.784	2.826	0.359	0.354	21.234	59.115	[30]
G.Morey-1932-49	2.800	2.868	0.357	0.349	21.147	59.212	[30]
G.Morey-1932-5	2.389	2.415	0.419	0.414	25.088	59.934	[30]
G.Morey-1932-50	2.742	2.851	0.365	0.351	21.809	59.801	[30]
G.Morey-1932-51	2.557	2.537	0.391	0.394	23.355	59.720	[30]
G.Morey-1932-52	2.504	2.501	0.399	0.400	24.057	60.239	[30]
G.Morey-1932-53	2.499	2.495	0.400	0.401	24.144	60.337	[30]
G.Morey-1932-54	2.548	2.535	0.392	0.395	23.461	59.780	[30]
G.Morey-1932-55	2.496	2.498	0.401	0.400	24.166	60.318	[30]
G.Morey-1932-56	2.503	2.496	0.400	0.401	24.117	60.364	[30]
G.Morey-1932-57	2.540	2.532	0.394	0.395	23.563	59.850	[30]
G.Morey-1932-58	2.504	2.502	0.399	0.400	24.102	60.351	[30]
G.Morey-1932-59	2.609	2.591	0.383	0.386	22.659	59.117	[30]
G.Morey-1932-6	2.421	2.440	0.413	0.410	24.664	59.712	[30]
G.Morey-1932-60	2.544	2.530	0.393	0.395	23.587	60.005	[30]
G.Morey-1932-61	2.543	2.534	0.393	0.395	23.598	60.009	[30]
G.Morey-1932-62	2.586	2.566	0.387	0.390	23.037	59.574	[30]
G.Morey-1932-63	2.520	2.519	0.397	0.397	23.908	60.249	[30]
G.Morey-1932-64	2.543	2.535	0.393	0.395	23.618	60.061	[30]
G.Morey-1932-65	2.561	2.550	0.390	0.392	23.386	59.892	[30]
G.Morey-1932-66	2.655	2.621	0.377	0.382	22.201	58.944	[30]
G.Morey-1932-67	2.582	2.564	0.387	0.390	23.139	59.744	[30]
G.Morey-1932-68	2.654	2.617	0.377	0.382	22.249	59.048	[30]
G.Morey-1932-69	2.613	2.588	0.383	0.386	22.745	59.433	[30]
G.Morey-1932-7	2.432	2.440	0.411	0.410	24.748	60.188	[30]
G.Morey-1932-70	2.547	2.544	0.393	0.393	23.592	60.089	[30]
G.Morey-1932-71	2.581	2.565	0.387	0.390	23.167	59.795	[30]
G.Morey-1932-72	2.591	2.572	0.386	0.389	23.053	59.731	[30]
G.Morey-1932-73	2.584	2.569	0.387	0.389	23.140	59.793	[30]
G.Morey-1932-74	2.586	2.570	0.387	0.389	23.124	59.799	[30]
G.Morey-1932-75	2.656	2.617	0.377	0.382	22.283	59.184	[30]
G.Morey-1932-76	2.683	2.682	0.373	0.373	22.221	59.618	[30]
G.Morey-1932-77	2.773	2.749	0.361	0.364	21.208	58.809	[30]
G.Morey-1932-78	2.733	2.717	0.366	0.368	21.657	59.189	[30]
G.Morey-1932-79	2.610	2.635	0.383	0.380	23.083	60.247	[30]
G.Morey-1932-8	2.455	2.460	0.407	0.407	24.392	59.882	[30]

Glass ID	ρ_{measured} (g/cm ³)	$\rho_{\text{predicted}}$ (g/cm ³)	$1/\rho_{\text{measured}}$ (cm ³ /g)	$\Sigma V_i/M_g$ (cm ³ /g)	V_{glass} (cm ³ /mol)	M_g	Reference
G.Morey-1932-80	2.808	2.771	0.356	0.361	20.861	58.577	[30]
G.Morey-1932-81	2.816	2.780	0.355	0.360	20.767	58.481	[30]
G.Morey-1932-82	2.568	2.605	0.389	0.384	23.647	60.726	[30]
G.Morey-1932-83	2.587	2.624	0.387	0.381	23.382	60.489	[30]
G.Morey-1932-84	2.630	2.663	0.380	0.375	22.827	60.035	[30]
G.Morey-1932-85	2.705	2.712	0.370	0.369	21.964	59.413	[30]
G.Morey-1932-86	2.838	2.802	0.352	0.357	20.583	58.413	[30]
G.Morey-1932-87	2.832	2.801	0.353	0.357	20.638	58.448	[30]
G.Morey-1932-88	2.664	2.686	0.375	0.372	22.458	59.829	[30]
G.Morey-1932-89	2.601	2.641	0.384	0.379	23.262	60.505	[30]
G.Morey-1932-9	2.456	2.459	0.407	0.407	24.438	60.021	[30]
G.Morey-1932-90	2.730	2.739	0.366	0.365	21.728	59.319	[30]
G.Morey-1932-91	2.665	2.685	0.375	0.372	22.509	59.986	[30]
G.Morey-1932-92	2.807	2.797	0.356	0.358	20.905	58.680	[30]
G.Morey-1932-93	2.802	2.795	0.357	0.358	20.950	58.701	[30]
G.Morey-1932-94	2.712	2.733	0.369	0.366	21.924	59.457	[30]
G.Morey-1932-95	2.761	2.763	0.362	0.362	21.413	59.120	[30]
G.Morey-1932-96	2.777	2.782	0.360	0.359	21.216	58.917	[30]
G.Morey-1932-97	2.821	2.809	0.354	0.356	20.784	58.631	[30]
G.Morey-1932-98	2.764	2.772	0.362	0.361	21.370	59.068	[30]
G.Morey-1932-99	2.648	2.678	0.378	0.373	22.740	60.216	[30]
HB-1	3.517	3.499	0.284	0.286	22.091	77.693	[24]
HB-2	2.332	2.370	0.429	0.422	26.158	61.000	[24]
HLP-01	2.649	2.673	0.377	0.374	25.254	66.906	[51]
HLP-02	2.702	2.782	0.370	0.359	25.346	68.489	[51]
HLP-03	2.636	2.636	0.379	0.379	25.097	66.166	[51]
HLP-04	2.683	2.744	0.373	0.364	25.306	67.892	[51]
HLP-05	2.676	2.667	0.374	0.375	24.610	65.848	[51]
HLP-06	2.561	2.653	0.390	0.377	26.486	67.828	[51]
HLP-07	2.603	2.658	0.384	0.376	25.771	67.074	[51]
HLP-08	2.692	2.656	0.372	0.376	24.689	66.450	[51]
HLP-09	2.601	2.665	0.384	0.375	25.616	66.638	[51]
HLP-10	2.623	2.659	0.381	0.376	25.360	66.517	[51]
HLP-11	2.563	2.589	0.390	0.386	25.122	64.389	[51]
HLP-12	2.682	2.710	0.373	0.369	25.376	68.057	[51]
HLP-13	2.607	2.629	0.384	0.380	25.147	65.567	[51]
HLP-14	2.588	2.638	0.386	0.379	25.598	66.249	[51]
HLP-15	2.628	2.687	0.381	0.372	25.472	66.928	[51]
HLP-16	2.592	2.641	0.386	0.379	25.618	66.400	[51]

Glass ID	ρ_{measured} (g/cm ³)	$\rho_{\text{predicted}}$ (g/cm ³)	$1/\rho_{\text{measured}}$ (cm ³ /g)	$\Sigma V_i/M_g$ (cm ³ /g)	V_{glass} (cm ³ /mol)	M_g	Reference
HLP-17	2.657	2.698	0.376	0.371	25.171	66.889	[51]
HLP-18	2.600	2.642	0.385	0.379	25.433	66.118	[51]
HLP-19	2.669	2.724	0.375	0.367	25.481	68.013	[51]
HLP-20	2.626	2.654	0.381	0.377	25.613	67.254	[51]
HLP-21	2.615	2.675	0.382	0.374	25.046	65.491	[51]
HLP-22	2.590	2.643	0.386	0.378	25.788	66.791	[51]
HLP-23	2.629	2.677	0.380	0.374	25.271	66.425	[51]
HLP-24	2.609	2.652	0.383	0.377	25.564	66.689	[51]
HLP-25	2.641	2.662	0.379	0.376	25.214	66.587	[51]
HLP-26	2.642	2.662	0.379	0.376	25.205	66.587	[51]
HLP-27	2.491	2.519	0.401	0.397	26.096	65.017	[51]
HLP-28	2.517	2.569	0.397	0.389	26.489	66.659	[51]
HLP-29	2.569	2.572	0.389	0.389	25.669	65.945	[51]
HLP-30	2.599	2.624	0.385	0.381	26.026	67.640	[51]
HLP-31	2.624	2.613	0.381	0.383	24.655	64.704	[51]
HLP-32	2.625	2.666	0.381	0.375	25.269	66.329	[51]
HLP-33	2.635	2.670	0.379	0.374	24.903	65.621	[51]
HLP-34	2.673	2.726	0.374	0.367	25.177	67.296	[51]
HLP-35	2.644	2.763	0.378	0.362	26.203	69.274	[51]
HLP-36	2.744	2.822	0.364	0.354	25.928	71.138	[51]
HLP-37	2.706	2.827	0.370	0.354	25.995	70.333	[51]
HLP-38	2.783	2.889	0.359	0.346	25.964	72.253	[51]
HLP-39	2.730	2.876	0.366	0.348	25.242	68.921	[51]
HLP-40	2.825	2.941	0.354	0.340	25.046	70.755	[51]
HLP-41	2.814	2.946	0.355	0.339	24.862	69.961	[51]
HLP-42	2.952	3.014	0.339	0.332	24.345	71.866	[51]
HLP-43	2.635	2.662	0.379	0.376	25.266	66.587	[51]
HLP-44	2.639	2.662	0.379	0.376	25.231	66.587	[51]
HLP-45	2.657	2.662	0.376	0.376	25.059	66.587	[51]
HLP-46	2.539	2.514	0.394	0.398	25.411	64.516	[51]
HLP-47	2.523	2.523	0.396	0.396	25.895	65.341	[51]
HLP-48	2.659	2.760	0.376	0.362	26.177	69.613	[51]
HLP-49	2.771	2.782	0.361	0.359	23.176	64.225	[51]
HLP-51	2.698	2.743	0.371	0.365	25.794	69.603	[51]
HLP-52	2.654	2.676	0.377	0.374	25.328	67.218	[51]
HLP-53	2.726	2.782	0.367	0.359	24.508	66.803	[51]
HLP-54	2.490	2.479	0.402	0.403	26.175	65.169	[51]
HLP-55	2.455	2.472	0.407	0.405	26.198	64.303	[51]
HLP-56	2.681	2.755	0.373	0.363	25.117	67.332	[51]

Glass ID	ρ_{measured} (g/cm ³)	$\rho_{\text{predicted}}$ (g/cm ³)	$1/\rho_{\text{measured}}$ (cm ³ /g)	$\Sigma V_i/M_g$ (cm ³ /g)	V_{glass} (cm ³ /mol)	M_g	Reference
HLP-58	2.622	2.679	0.381	0.373	25.302	66.334	[51]
HLP-59	2.645	2.705	0.378	0.370	24.942	65.976	[51]
HLP-60	2.932	2.746	0.341	0.364	23.476	68.831	[51]
HLP-61	2.649	2.757	0.377	0.363	24.286	64.343	[51]
HLP-62	2.680	2.713	0.373	0.369	24.639	66.020	[51]
HLP-63	2.780	2.899	0.360	0.345	24.827	69.015	[51]
HLP-64	2.633	2.650	0.380	0.377	24.832	65.384	[51]
HLP-65	2.649	2.674	0.377	0.374	24.657	65.327	[51]
HLP-66	2.583	2.603	0.387	0.384	25.222	65.139	[51]
HLP-67	2.712	2.810	0.369	0.356	25.827	70.047	[51]
HLP-68	2.795	2.902	0.358	0.345	26.821	74.959	[51]
HLP-69	2.605	2.610	0.384	0.383	25.604	66.694	[51]
HLP-70	2.638	2.692	0.379	0.371	25.702	67.812	[51]
HLP-71	2.716	2.799	0.368	0.357	24.249	65.858	[51]
HLP-72	2.663	3.004	0.376	0.333	28.409	75.651	[51]
HLP-73	2.612	2.763	0.383	0.362	27.217	71.099	[51]
HLP-74	2.680	2.806	0.373	0.356	26.811	71.855	[51]
HLP-75	2.681	2.746	0.373	0.364	25.366	67.996	[51]
HLP-76	2.554	2.523	0.392	0.396	25.587	65.341	[51]
HLP-77	2.561	2.523	0.390	0.396	25.511	65.341	[51]
HPG8	2.326	2.353	0.430	0.425	27.722	64.478	[28]
Hurt - 1970 - 1	3.215	3.190	0.311	0.313	21.098	67.830	[24]
Hurt - 1970 - 10	2.818	2.773	0.355	0.361	22.626	63.761	[24]
Hurt - 1970 - 11	2.717	2.699	0.368	0.371	23.110	62.791	[24]
Hurt - 1970 - 12	2.624	2.626	0.381	0.381	23.560	61.820	[24]
Hurt - 1970 - 13	3.000	2.882	0.333	0.347	21.869	65.606	[24]
Hurt - 1970 - 14	2.901	2.806	0.345	0.356	22.281	64.636	[24]
Hurt - 1970 - 15	2.796	2.731	0.358	0.366	22.770	63.666	[24]
Hurt - 1970 - 16	2.694	2.658	0.371	0.376	23.272	62.696	[24]
Hurt - 1970 - 17	2.591	2.587	0.386	0.387	23.823	61.725	[24]
Hurt - 1970 - 18	2.836	2.763	0.353	0.362	22.758	64.541	[24]
Hurt - 1970 - 19	2.748	2.690	0.364	0.372	23.133	63.571	[24]
Hurt - 1970 - 2	3.091	3.104	0.324	0.322	21.631	66.860	[24]
Hurt - 1970 - 20	2.634	2.619	0.380	0.382	23.766	62.601	[24]
Hurt - 1970 - 21	2.561	2.549	0.390	0.392	24.065	61.630	[24]
Hurt - 1970 - 22	2.705	2.651	0.370	0.377	23.466	63.476	[24]
Hurt - 1970 - 23	2.657	2.615	0.376	0.382	23.707	62.991	[24]
Hurt - 1970 - 24	2.597	2.581	0.385	0.388	24.068	62.506	[24]
Hurt - 1970 - 25	2.507	2.512	0.399	0.398	24.545	61.535	[24]

Glass ID	ρ_{measured} (g/cm ³)	$\rho_{\text{predicted}}$ (g/cm ³)	$1/\rho_{\text{measured}}$ (cm ³ /g)	$\Sigma V_i/M_g$ (cm ³ /g)	V_{glass} (cm ³ /mol)	M_g	Reference
Hurt - 1970 - 3	2.979	3.021	0.336	0.331	22.118	65.890	[24]
Hurt - 1970 - 4	2.870	2.940	0.348	0.340	22.620	64.921	[24]
Hurt - 1970 - 5	2.776	2.860	0.360	0.350	23.037	63.951	[24]
Hurt - 1970 - 6	2.851	2.783	0.351	0.359	22.091	62.980	[24]
Hurt - 1970 - 7	3.173	3.007	0.315	0.333	21.012	66.671	[24]
Hurt - 1970 - 8	3.057	2.927	0.327	0.342	21.492	65.701	[24]
Hurt - 1970 - 9	2.930	2.849	0.341	0.351	22.092	64.731	[24]
K05	2.365	2.372	0.423	0.421	27.718	65.540	[28]
K10	2.390	2.391	0.418	0.418	27.804	66.459	[28]
K20	2.448	2.425	0.409	0.412	27.949	68.406	[28]
Karapetyan Li-Al-Si - 1	2.452	2.423	0.408	0.413	26.542	65.081	[24]
Karapetyan Li-Al-Si - 10	2.376	2.367	0.421	0.422	22.097	52.502	[24]
Karapetyan Li-Al-Si - 11	2.430	2.373	0.412	0.421	26.903	65.373	[24]
Karapetyan Li-Al-Si - 12	2.423	2.372	0.413	0.422	26.382	63.924	[24]
Karapetyan Li-Al-Si - 13	2.398	2.371	0.417	0.422	26.057	62.485	[24]
Karapetyan Li-Al-Si - 14	2.400	2.371	0.417	0.422	25.886	62.127	[24]
Karapetyan Li-Al-Si - 15	2.393	2.370	0.418	0.422	25.511	61.048	[24]
Karapetyan Li-Al-Si - 16	2.399	2.368	0.417	0.422	24.846	59.606	[24]
Karapetyan Li-Al-Si - 17	2.392	2.367	0.418	0.422	24.315	58.162	[24]
Karapetyan Li-Al-Si - 18	2.385	2.366	0.419	0.423	23.781	56.719	[24]
Karapetyan Li-Al-Si - 19	2.381	2.364	0.420	0.423	23.213	55.269	[24]
Karapetyan Li-Al-Si - 2	2.363	2.410	0.423	0.415	26.660	62.997	[24]
Karapetyan Li-Al-Si - 20	2.372	2.362	0.422	0.423	22.695	53.833	[24]
Karapetyan Li-Al-Si - 21	2.368	2.361	0.422	0.424	22.124	52.389	[24]
Karapetyan Li-Al-Si - 22	2.361	2.359	0.424	0.424	21.578	50.945	[24]
Karapetyan Li-Al-Si - 23	2.350	2.371	0.426	0.422	27.639	64.953	[24]
Karapetyan Li-Al-Si - 24	2.381	2.362	0.420	0.423	23.643	56.293	[24]
Karapetyan Li-Al-Si - 25	2.432	2.368	0.411	0.422	26.534	64.532	[24]
Karapetyan Li-Al-Si - 26	2.396	2.367	0.417	0.423	26.333	63.095	[24]
Karapetyan Li-Al-Si - 27	2.408	2.363	0.415	0.423	27.048	65.131	[24]
Karapetyan Li-Al-Si - 28	2.377	2.361	0.421	0.424	26.187	62.247	[24]
Karapetyan Li-Al-Si - 29	2.369	2.358	0.422	0.424	26.100	61.831	[24]
Karapetyan Li-Al-Si - 3	2.410	2.389	0.415	0.419	23.723	57.172	[24]
Karapetyan Li-Al-Si - 30	2.369	2.356	0.422	0.424	25.492	60.391	[24]
Karapetyan Li-Al-Si - 31	2.363	2.351	0.423	0.425	23.724	56.060	[24]
Karapetyan Li-Al-Si - 32	2.355	2.349	0.425	0.426	23.194	54.621	[24]
Karapetyan Li-Al-Si - 33	2.369	2.349	0.422	0.426	25.570	60.575	[24]
Karapetyan Li-Al-Si - 34	2.353	2.342	0.425	0.427	25.388	59.738	[24]
Karapetyan Li-Al-Si - 35	2.334	2.336	0.428	0.428	25.234	58.897	[24]

Glass ID	ρ_{measured} (g/cm ³)	$\rho_{\text{predicted}}$ (g/cm ³)	$1/\rho_{\text{measured}}$ (cm ³ /g)	$\Sigma V_i/M_g$ (cm ³ /g)	V_{glass} (cm ³ /mol)	M_g	Reference
Karapetyan Li-Al-Si - 36	2.317	2.329	0.432	0.429	25.059	58.061	[24]
Karapetyan Li-Al-Si - 37	2.299	2.323	0.435	0.431	24.893	57.228	[24]
Karapetyan Li-Al-Si - 4	2.410	2.384	0.415	0.419	25.898	62.415	[24]
Karapetyan Li-Al-Si - 5	2.414	2.381	0.414	0.420	25.980	62.715	[24]
Karapetyan Li-Al-Si - 6	2.395	2.375	0.418	0.421	22.873	54.781	[24]
Karapetyan Li-Al-Si - 7	2.414	2.380	0.414	0.420	26.401	63.733	[24]
Karapetyan Li-Al-Si - 8	2.419	2.378	0.413	0.421	26.771	64.759	[24]
Karapetyan Li-Al-Si - 9	2.411	2.377	0.415	0.421	26.262	63.318	[24]
Larsen - Mg-Ca-Si - 1	2.899	2.838	0.345	0.352	19.884	57.644	[24]
Larsen - Mg-Ca-Si - 10	2.920	2.781	0.342	0.360	18.045	52.692	[24]
Larsen - Mg-Ca-Si - 11	2.820	2.673	0.355	0.374	18.558	52.334	[24]
Larsen - Mg-Ca-Si - 12	2.879	2.626	0.347	0.381	17.680	50.900	[24]
Larsen - Mg-Ca-Si - 13	2.777	2.614	0.360	0.383	18.204	50.553	[24]
Larsen - Mg-Ca-Si - 2	2.953	2.917	0.339	0.343	19.330	57.080	[24]
Larsen - Mg-Ca-Si - 3	2.892	2.812	0.346	0.356	19.627	56.761	[24]
Larsen - Mg-Ca-Si - 4	2.881	2.783	0.347	0.359	19.374	55.816	[24]
Larsen - Mg-Ca-Si - 5	2.872	2.757	0.348	0.363	19.144	54.981	[24]
Larsen - Mg-Ca-Si - 6	2.967	2.895	0.337	0.345	18.375	54.518	[24]
Larsen - Mg-Ca-Si - 7	2.858	2.747	0.350	0.364	19.127	54.666	[24]
Larsen - Mg-Ca-Si - 8	2.854	2.731	0.350	0.366	18.972	54.146	[24]
Larsen - Mg-Ca-Si - 9	2.835	2.697	0.353	0.371	18.727	53.090	[24]
Li05	2.367	2.371	0.423	0.422	25.926	61.358	[28]
Li10	2.393	2.382	0.418	0.420	24.367	58.315	[28]
Li20	2.415	2.414	0.414	0.414	21.542	52.015	[28]
LO 00	2.235	2.365	0.447	0.423	27.651	61.799	[33]
LO 01	2.250	2.351	0.444	0.425	27.357	61.554	[33]
LO 02	2.342	2.407	0.427	0.416	26.589	62.272	[33]
LO 03	2.405	2.413	0.416	0.414	25.879	62.240	[33]
LO 04	2.280	2.377	0.439	0.421	27.869	63.540	[33]
LO 05	2.385	2.444	0.419	0.409	27.079	64.584	[33]
LO 06	2.394	2.451	0.418	0.408	26.607	63.696	[33]
LO 07	2.319	2.424	0.431	0.412	27.385	63.506	[33]
LO 08	2.385	2.438	0.419	0.410	26.362	62.873	[33]
LO 09	2.420	2.434	0.413	0.411	25.884	62.640	[33]
LO 10	2.295	2.412	0.436	0.415	27.631	63.413	[33]
LO 11	2.338	2.457	0.428	0.407	27.723	64.816	[33]
LO 12	2.245	2.410	0.445	0.415	28.167	63.234	[33]
LO 14	2.353	2.378	0.425	0.421	26.185	61.613	[33]
LO 15	2.376	2.422	0.421	0.413	26.498	62.958	[33]

Glass ID	ρ_{measured} (g/cm ³)	$\rho_{\text{predicted}}$ (g/cm ³)	$1/\rho_{\text{measured}}$ (cm ³ /g)	$\Sigma V_i/M_g$ (cm ³ /g)	V_{glass} (cm ³ /mol)	M_g	Reference
LO 17	2.304	2.396	0.434	0.417	27.558	63.493	[33]
LO 18	2.360	2.413	0.424	0.414	26.642	62.875	[33]
LO 19	2.272	2.390	0.440	0.418	27.605	62.719	[33]
LO 20	2.256	2.394	0.443	0.418	27.459	61.948	[33]
LO 21	2.404	2.458	0.416	0.407	26.114	62.778	[33]
LO 23	2.398	2.463	0.417	0.406	27.073	64.922	[33]
Mg05	2.370	2.386	0.422	0.419	26.433	62.641	[28]
Mg10	2.416	2.419	0.414	0.413	25.303	61.120	[28]
Mg20	2.533	2.497	0.395	0.401	22.664	57.407	[28]
Morey - X.3.123	2.452	2.458	0.408	0.407	24.849	60.930	[10]
Morey - X.3.124	2.468	2.479	0.405	0.403	24.839	61.290	[10]
Morey - X.3.125	2.482	2.488	0.403	0.402	24.771	61.475	[10]
Morey - X.3.126	2.505	2.504	0.399	0.399	24.630	61.699	[10]
Morey - X.3.127	2.487	2.496	0.402	0.401	24.830	61.751	[10]
Morey - X.3.128	2.525	2.544	0.396	0.393	24.646	62.224	[10]
Morey - X.3.129	2.543	2.558	0.393	0.391	24.537	62.394	[10]
Morey - X.3.130	2.550	2.559	0.392	0.391	24.606	62.742	[10]
Morey - X.5.10	2.538	2.577	0.394	0.388	23.994	60.904	[10]
Morey - X.5.100	2.454	2.459	0.408	0.407	25.390	62.306	[10]
Morey - X.5.101	2.453	2.458	0.408	0.407	25.292	62.052	[10]
Morey - X.5.102	2.461	2.473	0.406	0.404	24.735	60.878	[10]
Morey - X.5.103	2.457	2.467	0.407	0.405	24.876	61.126	[10]
Morey - X.5.104	2.445	2.452	0.409	0.408	25.281	61.801	[10]
Morey - X.5.105	2.443	2.449	0.409	0.408	25.302	61.809	[10]
Morey - X.5.106	2.451	2.458	0.408	0.407	25.014	61.307	[10]
Morey - X.5.107	2.434	2.440	0.411	0.410	25.546	62.187	[10]
Morey - X.5.108	2.421	2.426	0.413	0.412	25.971	62.885	[10]
Morey - X.5.109	2.440	2.450	0.410	0.408	24.930	60.820	[10]
Morey - X.5.11	2.532	2.570	0.395	0.389	24.049	60.887	[10]
Morey - X.5.110	2.418	2.428	0.414	0.412	25.512	61.691	[10]
Morey - X.5.111	2.428	2.439	0.412	0.410	25.040	60.790	[10]
Morey - X.5.112	2.416	2.429	0.414	0.412	25.356	61.265	[10]
Morey - X.5.113	2.423	2.437	0.413	0.410	25.092	60.807	[10]
Morey - X.5.114	2.419	2.433	0.413	0.411	25.232	61.026	[10]
Morey - X.5.115	2.403	2.417	0.416	0.414	25.710	61.768	[10]
Morey - X.5.116	2.402	2.416	0.416	0.414	25.681	61.690	[10]
Morey - X.5.117	2.402	2.425	0.416	0.412	25.483	61.215	[10]
Morey - X.5.118	2.401	2.419	0.416	0.413	25.287	60.722	[10]
Morey - X.5.12	2.527	2.558	0.396	0.391	24.087	60.858	[10]

Glass ID	ρ_{measured} (g/cm ³)	$\rho_{\text{predicted}}$ (g/cm ³)	$1/\rho_{\text{measured}}$ (cm ³ /g)	$\Sigma V_i/M_g$ (cm ³ /g)	V_{glass} (cm ³ /mol)	M_g	Reference
Morey - X.5.13	2.524	2.553	0.396	0.392	24.106	60.845	[10]
Morey - X.5.14	2.523	2.553	0.396	0.392	24.118	60.844	[10]
Morey - X.5.15	2.521	2.551	0.397	0.392	24.135	60.839	[10]
Morey - X.5.16	2.507	2.530	0.399	0.395	24.246	60.786	[10]
Morey - X.5.17	2.504	2.529	0.399	0.395	24.271	60.785	[10]
Morey - X.5.18	2.504	2.528	0.399	0.396	24.275	60.781	[10]
Morey - X.5.19	2.489	2.511	0.402	0.398	24.403	60.739	[10]
Morey - X.5.2	2.566	2.627	0.390	0.381	23.785	61.024	[10]
Morey - X.5.20	2.492	2.511	0.401	0.398	24.369	60.738	[10]
Morey - X.5.21	2.487	2.502	0.402	0.400	24.418	60.716	[10]
Morey - X.5.22	2.481	2.498	0.403	0.400	24.471	60.704	[10]
Morey - X.5.23	2.464	2.480	0.406	0.403	24.613	60.657	[10]
Morey - X.5.24	2.461	2.443	0.406	0.409	24.606	60.560	[10]
Morey - X.5.25	2.460	2.474	0.406	0.404	24.648	60.642	[10]
Morey - X.5.26	2.449	2.462	0.408	0.406	24.751	60.610	[10]
Morey - X.5.27	2.448	2.461	0.409	0.406	24.759	60.606	[10]
Morey - X.5.28	2.434	2.448	0.411	0.409	24.883	60.572	[10]
Morey - X.5.29	2.431	2.444	0.411	0.409	24.918	60.562	[10]
Morey - X.5.3	2.564	2.624	0.390	0.381	23.798	61.019	[10]
Morey - X.5.30	2.426	2.440	0.412	0.410	24.959	60.551	[10]
Morey - X.5.31	2.414	2.431	0.414	0.411	25.073	60.526	[10]
Morey - X.5.32	2.413	2.430	0.414	0.411	25.080	60.525	[10]
Morey - X.5.33	2.413	2.430	0.414	0.412	25.087	60.524	[10]
Morey - X.5.34	2.401	2.422	0.417	0.413	25.202	60.503	[10]
Morey - X.5.35	2.394	2.417	0.418	0.414	25.272	60.489	[10]
Morey - X.5.36	2.381	2.409	0.420	0.415	25.393	60.468	[10]
Morey - X.5.39	2.355	2.389	0.425	0.419	25.658	60.411	[10]
Morey - X.5.40	2.354	2.388	0.425	0.419	25.667	60.409	[10]
Morey - X.5.41	2.331	2.373	0.429	0.421	25.900	60.366	[10]
Morey - X.5.42	2.320	2.365	0.431	0.423	26.005	60.343	[10]
Morey - X.5.43	2.641	2.683	0.379	0.373	22.819	60.271	[10]
Morey - X.5.44	2.608	2.657	0.383	0.376	23.241	60.602	[10]
Morey - X.5.46	2.624	2.652	0.381	0.377	22.925	60.146	[10]
Morey - X.5.47	2.598	2.624	0.385	0.381	23.212	60.297	[10]
Morey - X.5.49	2.572	2.587	0.389	0.387	23.520	60.492	[10]
Morey - X.5.5	2.561	2.615	0.391	0.382	23.821	60.998	[10]
Morey - X.5.50	2.547	2.576	0.393	0.388	23.819	60.677	[10]
Morey - X.5.52	2.607	2.615	0.384	0.382	22.969	59.889	[10]
Morey - X.5.54	2.576	2.579	0.388	0.388	23.299	60.012	[10]

Glass ID	ρ_{measured} (g/cm ³)	$\rho_{\text{predicted}}$ (g/cm ³)	$1/\rho_{\text{measured}}$ (cm ³ /g)	$\Sigma V_i/M_g$ (cm ³ /g)	V_{glass} (cm ³ /mol)	M_g	Reference
Morey - X.5.55	2.585	2.583	0.387	0.387	23.153	59.852	[10]
Morey - X.5.56	2.546	2.552	0.393	0.392	23.653	60.222	[10]
Morey - X.5.57	2.523	2.531	0.396	0.395	23.935	60.387	[10]
Morey - X.5.60	2.556	2.553	0.391	0.392	23.464	59.984	[10]
Morey - X.5.62	2.500	2.510	0.400	0.398	24.200	60.496	[10]
Morey - X.5.63	2.533	2.531	0.395	0.395	23.724	60.095	[10]
Morey - X.5.65	2.498	2.500	0.400	0.400	24.113	60.235	[10]
Morey - X.5.67	2.528	2.519	0.396	0.397	23.644	59.763	[10]
Morey - X.5.68	2.464	2.471	0.406	0.405	24.514	60.404	[10]
Morey - X.5.69	2.494	2.492	0.401	0.401	24.027	59.911	[10]
Morey - X.5.7	2.554	2.608	0.392	0.383	23.879	60.979	[10]
Morey - X.5.70	2.496	2.497	0.401	0.400	23.940	59.757	[10]
Morey - X.5.71	2.473	2.476	0.404	0.404	24.247	59.973	[10]
Morey - X.5.73	2.419	2.435	0.413	0.411	24.878	60.181	[10]
Morey - X.5.74	2.389	2.416	0.419	0.414	25.224	60.250	[10]
Morey - X.5.75	2.561	2.611	0.391	0.383	24.099	61.705	[10]
Morey - X.5.76	2.550	2.587	0.392	0.387	24.599	62.715	[10]
Morey - X.5.77	2.548	2.586	0.392	0.387	24.579	62.637	[10]
Morey - X.5.78	2.541	2.571	0.394	0.389	24.934	63.356	[10]
Morey - X.5.79	2.553	2.595	0.392	0.385	24.354	62.184	[10]
Morey - X.5.8	2.552	2.600	0.392	0.385	23.892	60.960	[10]
Morey - X.5.80	2.518	2.537	0.397	0.394	25.151	63.334	[10]
Morey - X.5.81	2.526	2.549	0.396	0.392	24.784	62.601	[10]
Morey - X.5.82	2.516	2.535	0.397	0.395	25.151	63.288	[10]
Morey - X.5.83	2.530	2.557	0.395	0.391	24.546	62.111	[10]
Morey - X.5.84	2.530	2.557	0.395	0.391	24.540	62.095	[10]
Morey - X.5.85	2.490	2.498	0.402	0.400	25.397	63.231	[10]
Morey - X.5.86	2.503	2.521	0.399	0.397	24.764	61.988	[10]
Morey - X.5.87	2.511	2.531	0.398	0.395	24.489	61.493	[10]
Morey - X.5.88	2.517	2.539	0.397	0.394	24.269	61.081	[10]
Morey - X.5.89	2.489	2.497	0.402	0.401	25.374	63.159	[10]
Morey - X.5.90	2.498	2.511	0.400	0.398	24.984	62.402	[10]
Morey - X.5.91	2.492	2.510	0.401	0.398	24.478	60.988	[10]
Morey - X.5.92	2.462	2.465	0.406	0.406	25.662	63.167	[10]
Morey - X.5.93	2.475	2.485	0.404	0.402	24.996	61.863	[10]
Morey - X.5.94	2.458	2.462	0.407	0.406	25.638	63.018	[10]
Morey - X.5.95	2.483	2.493	0.403	0.401	24.731	61.406	[10]
Morey - X.5.96	2.481	2.495	0.403	0.401	24.702	61.296	[10]
Morey - X.5.97	2.481	2.493	0.403	0.401	24.671	61.197	[10]

Glass ID	ρ_{measured} (g/cm ³)	$\rho_{\text{predicted}}$ (g/cm ³)	$1/\rho_{\text{measured}}$ (cm ³ /g)	$\Sigma V_i/M_g$ (cm ³ /g)	V_{glass} (cm ³ /mol)	M_g	Reference
Morey - X.5.98	2.465	2.475	0.406	0.404	25.030	61.707	[10]
Morey - X.5.99	2.468	2.479	0.405	0.403	24.871	61.390	[10]
Morey - X3.1	2.435	2.449	0.411	0.408	24.912	60.668	[10]
Morey - X3.10	2.476	2.480	0.404	0.403	24.253	60.043	[10]
Morey - X3.100	2.498	2.499	0.400	0.400	26.634	66.531	[10]
Morey - X3.101	2.596	2.601	0.385	0.384	25.453	66.076	[10]
Morey - X3.102	2.635	2.648	0.380	0.378	25.253	66.543	[10]
Morey - X3.103	2.502	2.503	0.400	0.399	26.865	67.217	[10]
Morey - X3.104	2.519	2.526	0.397	0.396	26.725	67.321	[10]
Morey - X3.105	2.500	2.505	0.400	0.399	27.062	67.656	[10]
Morey - X3.106	2.481	2.481	0.403	0.403	27.366	67.895	[10]
Morey - X3.107	2.672	2.711	0.374	0.369	25.049	66.930	[10]
Morey - X3.108	2.606	2.616	0.384	0.382	25.974	67.689	[10]
Morey - X3.109	2.509	2.516	0.399	0.397	27.199	68.241	[10]
Morey - X3.11	2.484	2.487	0.403	0.402	24.157	60.007	[10]
Morey - X3.110	2.658	2.684	0.376	0.373	25.412	67.546	[10]
Morey - X3.111	2.505	2.508	0.399	0.399	27.756	69.530	[10]
Morey - X3.112	2.542	2.561	0.393	0.390	28.238	71.780	[10]
Morey - X3.113	2.481	2.481	0.403	0.403	24.816	61.561	[10]
Morey - X3.114	2.515	2.506	0.398	0.399	24.920	62.662	[10]
Morey - X3.115	2.540	2.542	0.394	0.393	24.963	63.417	[10]
Morey - X3.116	2.546	2.561	0.393	0.390	25.468	64.835	[10]
Morey - X3.117	2.565	2.577	0.390	0.388	25.365	65.070	[10]
Morey - X3.118	2.580	2.646	0.388	0.378	26.085	67.294	[10]
Morey - X3.119	2.599	2.676	0.385	0.374	25.903	67.328	[10]
Morey - X3.12	2.490	2.492	0.402	0.401	24.050	59.895	[10]
Morey - X3.120	2.620	2.705	0.382	0.370	26.145	68.506	[10]
Morey - X3.121	2.633	2.733	0.380	0.366	26.569	69.956	[10]
Morey - X3.122	2.644	2.762	0.378	0.362	26.706	70.615	[10]
Morey - X3.13	2.587	2.576	0.387	0.388	23.103	59.758	[10]
Morey - X3.14	2.555	2.551	0.391	0.392	23.331	59.605	[10]
Morey - X3.15	2.429	2.434	0.412	0.411	25.203	61.229	[10]
Morey - X3.16	2.425	2.433	0.412	0.411	25.405	61.600	[10]
Morey - X3.17	2.418	2.431	0.414	0.411	25.760	62.291	[10]
Morey - X3.18	2.410	2.421	0.415	0.413	26.054	62.798	[10]
Morey - X3.2	2.375	2.408	0.421	0.415	25.544	60.662	[10]
Morey - X3.20	2.401	2.408	0.416	0.415	26.556	63.762	[10]
Morey - X3.21	2.517	2.486	0.397	0.402	24.808	62.449	[10]
Morey - X3.22	2.519	2.491	0.397	0.401	24.788	62.428	[10]

Glass ID	ρ_{measured} (g/cm ³)	$\rho_{\text{predicted}}$ (g/cm ³)	$1/\rho_{\text{measured}}$ (cm ³ /g)	$\Sigma V_i/M_g$ (cm ³ /g)	V_{glass} (cm ³ /mol)	M_g	Reference
Morey - X3.23	2.526	2.499	0.396	0.400	24.764	62.543	[10]
Morey - X3.24	2.525	2.508	0.396	0.399	24.845	62.743	[10]
Morey - X3.25	2.529	2.520	0.395	0.397	24.928	63.031	[10]
Morey - X3.26	2.523	2.549	0.396	0.392	25.149	63.452	[10]
Morey - X3.27	2.522	2.569	0.397	0.389	25.283	63.752	[10]
Morey - X3.28	2.513	2.590	0.398	0.386	25.500	64.075	[10]
Morey - X3.29	2.487	2.598	0.402	0.385	26.063	64.810	[10]
Morey - X3.3	2.438	2.453	0.410	0.408	24.842	60.574	[10]
Morey - X3.30	2.472	2.626	0.405	0.381	26.329	65.087	[10]
Morey - X3.31	2.394	2.656	0.418	0.377	27.199	65.103	[10]
Morey - X3.32	2.436	2.449	0.411	0.408	25.087	61.100	[10]
Morey - X3.33	2.438	2.447	0.410	0.409	25.104	61.203	[10]
Morey - X3.34	2.447	2.447	0.409	0.409	25.100	61.407	[10]
Morey - X3.35	2.466	2.465	0.405	0.406	24.998	61.649	[10]
Morey - X3.36	2.467	2.479	0.405	0.403	25.119	61.974	[10]
Morey - X3.37	2.483	2.492	0.403	0.401	25.055	62.219	[10]
Morey - X3.38	2.440	2.457	0.410	0.407	25.002	60.997	[10]
Morey - X3.39	2.456	2.468	0.407	0.405	25.060	61.556	[10]
Morey - X3.4	2.442	2.459	0.410	0.407	24.785	60.514	[10]
Morey - X3.40	2.466	2.481	0.406	0.403	25.157	62.024	[10]
Morey - X3.41	2.478	2.489	0.404	0.402	25.184	62.407	[10]
Morey - X3.42	2.488	2.496	0.402	0.401	25.164	62.618	[10]
Morey - X3.43	2.505	2.516	0.399	0.397	25.248	63.232	[10]
Morey - X3.44	2.521	2.531	0.397	0.395	25.159	63.417	[10]
Morey - X3.45	2.505	2.549	0.399	0.392	25.578	64.064	[10]
Morey - X3.46	2.496	2.513	0.401	0.398	25.028	62.478	[10]
Morey - X3.47	2.585	2.603	0.387	0.384	24.988	64.600	[10]
Morey - X3.48	2.670	2.676	0.375	0.374	24.777	66.150	[10]
Morey - X3.49	2.753	2.772	0.363	0.361	24.770	68.184	[10]
Morey - X3.5	2.446	2.461	0.409	0.406	24.710	60.447	[10]
Morey - X3.50	2.462	2.489	0.406	0.402	25.363	62.455	[10]
Morey - X3.51	2.555	2.582	0.391	0.387	25.249	64.520	[10]
Morey - X3.52	2.626	2.641	0.381	0.379	25.057	65.809	[10]
Morey - X3.53	2.449	2.444	0.408	0.409	24.394	59.751	[10]
Morey - X3.54	2.453	2.472	0.408	0.405	24.514	60.137	[10]
Morey - X3.55	2.471	2.485	0.405	0.402	24.656	60.914	[10]
Morey - X3.56	2.484	2.510	0.403	0.398	24.944	61.947	[10]
Morey - X3.57	2.507	2.529	0.399	0.395	25.288	63.404	[10]
Morey - X3.58	2.420	2.434	0.413	0.411	24.669	59.706	[10]

Glass ID	ρ_{measured} (g/cm ³)	$\rho_{\text{predicted}}$ (g/cm ³)	$1/\rho_{\text{measured}}$ (cm ³ /g)	$\Sigma V_i/M_g$ (cm ³ /g)	V_{glass} (cm ³ /mol)	M_g	Reference
Morey - X3.59	2.452	2.464	0.408	0.406	24.699	60.571	[10]
Morey - X3.6	2.451	2.467	0.408	0.405	24.648	60.404	[10]
Morey - X3.60	2.476	2.482	0.404	0.403	24.726	61.210	[10]
Morey - X3.69	2.659	2.633	0.376	0.380	22.427	59.633	[10]
Morey - X3.7	2.460	2.483	0.406	0.403	24.588	60.491	[10]
Morey - X3.70	2.360	2.401	0.424	0.417	25.758	60.790	[10]
Morey - X3.71	2.783	2.767	0.359	0.361	21.391	59.531	[10]
Morey - X3.72	2.546	2.543	0.393	0.393	23.686	60.303	[10]
Morey - X3.73	2.528	2.528	0.396	0.396	24.164	61.087	[10]
Morey - X3.75	2.793	2.804	0.358	0.357	21.638	60.436	[10]
Morey - X3.76	2.501	2.505	0.400	0.399	24.669	61.696	[10]
Morey - X3.77	2.593	2.595	0.386	0.385	23.662	61.356	[10]
Morey - X3.78	2.412	2.424	0.415	0.412	25.834	62.312	[10]
Morey - X3.79	2.492	2.494	0.401	0.401	24.989	62.272	[10]
Morey - X3.8	2.465	2.477	0.406	0.404	24.438	60.240	[10]
Morey - X3.80	2.584	2.585	0.387	0.387	23.972	61.944	[10]
Morey - X3.81	2.371	2.397	0.422	0.417	26.705	63.317	[10]
Morey - X3.82	2.683	2.689	0.373	0.372	23.182	62.198	[10]
Morey - X3.83	2.800	2.861	0.357	0.350	22.129	61.961	[10]
Morey - X3.84	2.569	2.572	0.389	0.389	24.521	62.994	[10]
Morey - X3.85	2.448	2.464	0.408	0.406	25.991	63.626	[10]
Morey - X3.86	2.473	2.478	0.404	0.404	25.812	63.832	[10]
Morey - X3.87	2.412	2.420	0.415	0.413	26.742	64.503	[10]
Morey - X3.88	2.613	2.621	0.383	0.382	24.377	63.698	[10]
Morey - X3.89	2.473	2.476	0.404	0.404	26.045	64.409	[10]
Morey - X3.9	2.468	2.472	0.405	0.404	24.337	60.068	[10]
Morey - X3.90	2.544	2.548	0.393	0.392	25.378	64.561	[10]
Morey - X3.91	2.461	2.466	0.406	0.406	26.414	65.005	[10]
Morey - X3.92	2.470	2.470	0.405	0.405	26.526	65.520	[10]
Morey - X3.93	2.701	2.734	0.370	0.366	23.855	64.433	[10]
Morey - X3.94	2.554	2.562	0.392	0.390	25.537	65.222	[10]
Morey - X3.95	2.686	2.705	0.372	0.370	24.110	64.760	[10]
Morey - X3.96	2.546	2.550	0.393	0.392	25.715	65.469	[10]
Morey - X3.97	2.405	2.413	0.416	0.414	27.717	66.659	[10]
Morey - X3.98	2.560	2.569	0.391	0.389	25.798	66.044	[10]
Morey - X3.99	2.665	2.690	0.375	0.372	24.594	65.544	[10]
Na05	2.377	2.381	0.421	0.420	27.107	64.422	[28]
Na10	2.397	2.402	0.417	0.416	26.742	64.106	[28]
Na20	2.491	2.472	0.401	0.405	25.701	64.019	[28]

Glass ID	ρ_{measured} (g/cm ³)	$\rho_{\text{predicted}}$ (g/cm ³)	$1/\rho_{\text{measured}}$ (cm ³ /g)	$\Sigma V_i/M_g$ (cm ³ /g)	V_{glass} (cm ³ /mol)	M_g	Reference
NEW-SHUM-1	2.699	2.826	0.370	0.354	26.276	70.926	[9, 26, 27]
NEW-SHUM-10	2.661	2.741	0.376	0.365	25.497	67.840	[9, 26, 27]
NEW-SHUM-11	2.628	2.689	0.381	0.372	25.186	66.187	[9, 26, 27]
NEW-SHUM-12	2.613	2.639	0.383	0.379	24.723	64.611	[9, 26, 27]
NEW-SHUM-13	2.560	2.592	0.391	0.386	24.652	63.110	[9, 26, 27]
NEW-SHUM-14	2.525	2.545	0.396	0.393	24.429	61.677	[9, 26, 27]
NEW-SHUM-14	2.526	2.545	0.396	0.393	24.418	61.677	[9, 26, 27]
NEW-SHUM-14	2.527	2.545	0.396	0.393	24.403	61.677	[9, 26, 27]
NEW-SHUM-15	2.493	2.501	0.401	0.400	24.195	60.307	[9, 26, 27]
NEW-SHUM-16	2.463	2.458	0.406	0.407	23.954	58.998	[9, 26, 27]
NEW-SHUM-17	2.687	2.762	0.372	0.362	25.403	68.256	[9, 26, 27]
NEW-SHUM-18	2.654	2.710	0.377	0.369	25.089	66.585	[9, 26, 27]
NEW-SHUM-19	2.595	2.659	0.385	0.376	25.045	64.992	[9, 26, 27]
NEW-SHUM-2	2.669	2.771	0.375	0.361	25.897	69.114	[9, 26, 27]
NEW-SHUM-20	2.581	2.611	0.387	0.383	24.589	63.475	[9, 26, 27]
NEW-SHUM-21	2.556	2.564	0.391	0.390	24.270	62.027	[9, 26, 27]
NEW-SHUM-22	2.510	2.519	0.398	0.397	24.163	60.643	[9, 26, 27]
NEW-SHUM-23	2.478	2.475	0.404	0.404	23.937	59.320	[9, 26, 27]
NEW-SHUM-24	2.439	2.433	0.410	0.411	23.798	58.054	[9, 26, 27]
NEW-SHUM-25	2.675	2.729	0.374	0.366	25.027	66.957	[9, 26, 27]
NEW-SHUM-26	2.639	2.678	0.379	0.373	24.764	65.347	[9, 26, 27]
NEW-SHUM-27	2.613	2.628	0.383	0.380	24.424	63.814	[9, 26, 27]
NEW-SHUM-28	2.564	2.581	0.390	0.387	24.319	62.351	[9, 26, 27]
NEW-SHUM-29	2.526	2.535	0.396	0.394	24.127	60.952	[9, 26, 27]
NEW-SHUM-3	2.641	2.718	0.379	0.368	25.517	67.394	[9, 26, 27]
NEW-SHUM-30	2.486	2.491	0.402	0.402	23.983	59.616	[9, 26, 27]
NEW-SHUM-31	2.449	2.448	0.408	0.409	23.825	58.338	[9, 26, 27]
NEW-SHUM-32	2.377	2.394	0.421	0.418	23.831	56.653	[9, 26, 27]
NEW-SHUM-4	2.605	2.667	0.384	0.375	25.243	65.757	[9, 26, 27]
NEW-SHUM-5	2.571	2.617	0.389	0.382	24.971	64.197	[9, 26, 27]
NEW-SHUM-6	2.533	2.570	0.395	0.389	24.758	62.711	[9, 26, 27]
NEW-SHUM-7	2.512	2.525	0.398	0.396	24.397	61.292	[9, 26, 27]
NEW-SHUM-8	2.499	2.480	0.400	0.403	23.984	59.934	[9, 26, 27]
NEW-SHUM-9	2.692	2.795	0.372	0.358	25.851	69.578	[9, 26, 27]
NEW-SHUM-T	2.636	2.693	0.379	0.371	25.063	66.063	[9, 26, 27]
NEW-SHUM-T	2.637	2.693	0.379	0.371	25.053	66.063	[9, 26, 27]
NEW-SHUM-T	2.640	2.693	0.379	0.371	25.026	66.063	[9, 26, 27]
NIST 1830	2.490	2.489	0.402	0.402	23.695	59.000	[21]
NP2-23	2.660	2.672	0.376	0.374	24.287	64.602	[29]

Glass ID	ρ_{measured} (g/cm ³)	$\rho_{\text{predicted}}$ (g/cm ³)	$1/\rho_{\text{measured}}$ (cm ³ /g)	$\Sigma V_i/M_g$ (cm ³ /g)	V_{glass} (cm ³ /mol)	M_g	Reference
NP2-Low Li	2.450	2.627	0.408	0.381	28.627	70.137	[29]
NP-MC-BNa-1	2.510	2.637	0.398	0.379	27.468	68.945	[29]
Parkinson - et al - 2005 HLW - 1	2.320	2.473	0.431	0.404	25.409	58.949	[31]
Parkinson - et al - 2005 HLW - 2	2.400	2.596	0.417	0.385	26.808	64.339	[31]
Parkinson - et al - 2005 HLW - 3	2.520	2.653	0.397	0.377	26.592	67.012	[31]
Parkinson - et al - 2005 HLW - 4	2.470	2.709	0.405	0.369	28.221	69.707	[31]
Parkinson - et al - 2005 HLW - 5	2.620	2.815	0.382	0.355	28.663	75.097	[31]
Parkinson - et al - 2005 HLW - 6	2.650	2.913	0.377	0.343	30.364	80.465	[31]
PYREX	2.224	2.366	0.450	0.423	27.780	61.774	[25]
Rao-1	2.382	2.391	0.420	0.418	27.737	66.070	[32]
Rao-10	2.585	2.605	0.387	0.384	27.403	70.846	[32]
Rao-11	2.644	2.666	0.378	0.375	27.191	71.897	[32]
Rao-12	2.700	2.730	0.370	0.366	27.028	72.980	[32]
Rao-13	2.747	2.797	0.364	0.357	26.975	74.095	[32]
Rao-14	2.783	2.868	0.359	0.349	27.040	75.246	[32]
Rao-15	2.844	2.942	0.352	0.340	26.877	76.432	[32]
Rao-16	2.897	3.020	0.345	0.331	26.811	77.657	[32]
Rao-17	2.958	3.102	0.338	0.322	26.681	78.922	[32]
Rao-19	2.583	2.601	0.387	0.384	27.817	71.841	[32]
Rao-2	2.480	2.495	0.403	0.401	27.393	67.921	[32]
Rao-20	2.679	2.726	0.373	0.367	27.640	74.036	[32]
Rao-21	2.708	2.793	0.369	0.358	27.762	75.184	[32]
Rao-22	2.807	2.863	0.356	0.349	27.205	76.369	[32]
Rao-23	2.854	3.014	0.350	0.332	27.630	78.854	[32]
Rao-24	2.967	3.183	0.337	0.314	27.473	81.507	[32]
Rao-25	2.981	2.853	0.335	0.351	26.409	78.718	[32]
Rao-26	3.183	3.003	0.314	0.333	25.559	81.361	[32]
Rao-27	3.212	3.170	0.311	0.315	26.208	84.188	[32]
Rao-28	3.280	3.357	0.305	0.298	26.590	87.219	[32]
Rao-29	3.531	3.536	0.283	0.283	27.569	97.357	[32]
Rao-3	2.583	2.610	0.387	0.383	27.055	69.879	[32]
Rao-30	3.571	3.649	0.280	0.274	27.826	99.354	[32]
Rao-31	3.615	3.770	0.277	0.265	28.063	101.435	[32]
Rao-32	3.708	4.037	0.270	0.248	28.554	105.870	[32]
Rao-4	2.670	2.735	0.375	0.366	26.950	71.953	[32]
Rao-5	2.782	2.873	0.359	0.348	26.651	74.155	[32]
Rao-6	2.834	2.947	0.353	0.339	26.569	75.307	[32]
Rao-7	2.914	3.108	0.343	0.322	26.674	77.723	[32]
Rao-8	2.470	2.492	0.405	0.401	27.869	68.835	[32]

Glass ID	ρ_{measured} (g/cm ³)	$\rho_{\text{predicted}}$ (g/cm ³)	$1/\rho_{\text{measured}}$ (cm ³ /g)	$\Sigma V_i/M_g$ (cm ³ /g)	V_{glass} (cm ³ /mol)	M_g	Reference
Rao-9	2.533	2.547	0.395	0.393	27.570	69.826	[32]
Rb05	2.393	2.411	0.418	0.415	28.001	67.010	[28, 32]
Rb10	2.442	2.450	0.410	0.408	28.143	68.722	[28, 32]
Rb20	2.613	2.567	0.383	0.390	28.219	73.724	[28, 32]
SB6VS-01	2.646	2.647	0.378	0.378	24.544	64.941	[6, 18]
SB6VS-02	2.644	2.660	0.378	0.376	24.579	64.990	[6, 18]
SB6VS-03	2.640	2.632	0.379	0.380	24.458	64.578	[6, 18]
SB6VS-04	2.656	2.651	0.377	0.377	24.353	64.682	[6, 18]
SB6VS-06	2.640	2.622	0.379	0.381	24.359	64.308	[6, 18]
SB6VS-07	2.627	2.620	0.381	0.382	24.465	64.276	[6, 18]
SB6VS-08	2.655	2.654	0.377	0.377	24.362	64.679	[6, 18]
SB6VS-09	2.665	2.651	0.375	0.377	24.239	64.585	[6, 18]
SB6VS-11	2.623	2.621	0.381	0.382	24.380	63.944	[6, 18]
SB6VS-12	2.662	2.643	0.376	0.378	24.061	64.046	[6, 18]
SB6VS-13	2.617	2.622	0.382	0.381	24.644	64.496	[6, 18]
SB6VS-14	2.632	2.617	0.380	0.382	24.298	63.960	[6, 18]
SB6VS-15	2.639	2.654	0.379	0.377	24.472	64.578	[6, 18]
SB6VS-16	2.659	2.649	0.376	0.377	24.485	65.094	[6, 18]
SB6VS-17	2.666	2.669	0.375	0.375	24.603	65.601	[6, 18]
SB6VS-18	2.646	2.601	0.378	0.384	24.169	63.948	[6, 18]
SB6VS-19	2.656	2.619	0.377	0.382	24.259	64.423	[6, 18]
SB6VS-20	2.673	2.631	0.374	0.380	24.325	65.027	[6, 18]
SB6VS-21	2.685	2.653	0.372	0.377	24.416	65.549	[6, 18]
SB6VS-22	2.701	2.663	0.370	0.375	24.486	66.128	[6, 18]
SB7a-702-01	2.651	2.617	0.377	0.382	23.914	63.395	[5, 17]
SB7a-702-02	2.663	2.625	0.376	0.381	23.981	63.862	[5, 17]
SB7a-702-03	2.673	2.644	0.374	0.378	24.035	64.246	[5, 17]
SB7a-702-04	2.691	2.663	0.372	0.375	24.073	64.782	[5, 17]
SB7a-702-05	2.709	2.676	0.369	0.374	24.097	65.278	[5, 17]
SB7aVS-01	2.663	2.652	0.376	0.377	24.217	64.489	[5, 17]
SB7aVS-02	2.665	2.626	0.375	0.381	23.987	63.926	[5, 17]
SB7aVS-03	2.665	2.640	0.375	0.379	24.392	65.004	[5, 17]
SB7aVS-04	2.666	2.633	0.375	0.380	24.124	64.315	[5, 17]
SB7aVS-05	2.691	2.651	0.372	0.377	24.257	65.276	[5, 17]
SB7aVS-06	2.670	2.637	0.375	0.379	23.998	64.075	[5, 17]
SB7aVS-07	2.646	2.612	0.378	0.383	24.387	64.529	[5, 17]
SB7aVS-08	2.660	2.634	0.376	0.380	24.501	65.174	[5, 17]
SB7aVS-09	2.643	2.613	0.378	0.383	24.425	64.556	[5, 17]
SB7aVS-10	2.660	2.621	0.376	0.382	24.460	65.065	[5, 17]

Glass ID	ρ_{measured} (g/cm ³)	$\rho_{\text{predicted}}$ (g/cm ³)	$1/\rho_{\text{measured}}$ (cm ³ /g)	$\Sigma V_i/M_g$ (cm ³ /g)	V_{glass} (cm ³ /mol)	M_g	Reference
SB7aVS-11	2.657	2.629	0.376	0.380	24.368	64.747	[5, 17]
SB7aVS-12	2.648	2.632	0.378	0.380	24.511	64.904	[5, 17]
SB7aVS-13	2.658	2.625	0.376	0.381	24.399	64.851	[5, 17]
SB7aVS-14	2.639	2.621	0.379	0.382	24.387	64.357	[5, 17]
SB7aVS-15	2.645	2.617	0.378	0.382	24.175	63.943	[5, 17]
SB7aVS-16	2.660	2.637	0.376	0.379	24.312	64.669	[5, 17]
SB7aVS-17	2.664	2.632	0.375	0.380	24.204	64.478	[5, 17]
SB7aVS-18	2.670	2.651	0.375	0.377	24.450	65.281	[5, 17]
SB7aVS-19	2.671	2.645	0.374	0.378	24.391	65.149	[5, 17]
SB7aVS-20	2.686	2.657	0.372	0.376	24.546	65.930	[5, 17]
SB7aVS-21	2.693	2.666	0.371	0.375	24.344	65.559	[5, 17]
SB7aVS-22	2.695	2.678	0.371	0.373	24.569	66.215	[5, 17]
SB7aVS-23	2.696	2.676	0.371	0.374	24.483	66.007	[5, 17]
SB7b-01	2.717	2.681	0.368	0.373	24.188	65.719	[4, 16]
SB7b-02	2.750	2.730	0.364	0.366	23.997	65.992	[4, 16]
SB7b-03	2.694	2.662	0.371	0.376	23.489	63.278	[4, 16]
SB7b-04	2.647	2.598	0.378	0.385	24.539	64.954	[4, 16]
SB7b-05	2.671	2.623	0.374	0.381	23.865	63.745	[4, 16]
SB7b-06	2.701	2.671	0.370	0.374	24.032	64.911	[4, 16]
SB7b-07	2.645	2.626	0.378	0.381	23.838	63.050	[4, 16]
SB7b-08	2.729	2.702	0.366	0.370	23.485	64.092	[4, 16]
SB7b-09	2.724	2.672	0.367	0.374	23.887	65.069	[4, 16]
SB7b-10	2.703	2.643	0.370	0.378	24.045	64.994	[4, 16]
SB7b-11	2.706	2.696	0.370	0.371	24.619	66.620	[4, 16]
SB7b-12	2.698	2.660	0.371	0.376	24.190	65.266	[4, 16]
SB7b-13	2.691	2.627	0.372	0.381	23.433	63.058	[4, 16]
SB7b-14	2.663	2.623	0.376	0.381	23.469	62.497	[4, 16]
SB7b-15	2.687	2.647	0.372	0.378	23.914	64.257	[4, 16]
SB7b-16	2.745	2.663	0.364	0.376	23.603	64.790	[4, 16]
SB7b-17	2.677	2.624	0.374	0.381	23.671	63.369	[4, 16]
SB7b-18	2.722	2.691	0.367	0.372	23.948	65.187	[4, 16]
SB7b-19	2.671	2.649	0.374	0.378	24.192	64.617	[4, 16]
SB7b-20	2.662	2.617	0.376	0.382	24.264	64.590	[4, 16]
SB7b-21	2.694	2.653	0.371	0.377	23.617	63.625	[4, 16]
SB7b-22	2.672	2.645	0.374	0.378	23.908	63.883	[4, 16]
SB7b-23	2.684	2.633	0.373	0.380	23.815	63.919	[4, 16]
SB7b-24	2.677	2.653	0.374	0.377	23.839	63.817	[4, 16]
SB7b-25	2.712	2.670	0.369	0.375	23.553	63.876	[4, 16]
SB7b-26	2.700	2.661	0.370	0.376	24.230	65.420	[4, 16]

Glass ID	ρ_{measured} (g/cm ³)	$\rho_{\text{predicted}}$ (g/cm ³)	$1/\rho_{\text{measured}}$ (cm ³ /g)	$\Sigma V_i/M_g$ (cm ³ /g)	V_{glass} (cm ³ /mol)	M_g	Reference
SB7b-27	2.707	2.674	0.369	0.374	23.849	64.558	[4, 16]
SB7b-28	2.707	2.668	0.369	0.375	24.043	65.085	[4, 16]
SB7b-29	2.659	2.624	0.376	0.381	23.974	63.746	[4, 16]
SB7b-30	2.691	2.645	0.372	0.378	24.070	64.773	[4, 16]
SB7b-31	2.709	2.664	0.369	0.375	24.199	65.554	[4, 16]
SB7b-32	2.667	2.628	0.375	0.380	23.732	63.294	[4, 16]
SB7b-33	2.691	2.655	0.372	0.377	23.814	64.085	[4, 16]
SB7b-34	2.723	2.678	0.367	0.373	23.927	65.154	[4, 16]
SB8VS-01	2.675	2.661	0.374	0.376	24.291	64.966	[3, 15]
SB8VS-02	2.673	2.660	0.374	0.376	24.235	64.781	[3, 15]
SB8VS-03	2.692	2.684	0.371	0.373	24.357	65.569	[3, 15]
SB8VS-04	2.687	2.675	0.372	0.374	24.252	65.165	[3, 15]
SB8VS-05	2.706	2.702	0.370	0.370	24.440	66.135	[3, 15]
SB8VS-06	2.705	2.700	0.370	0.370	24.302	65.724	[3, 15]
SB8VS-07	2.722	2.719	0.367	0.368	24.463	66.587	[3, 15]
SB8VS-08	2.719	2.711	0.368	0.369	24.356	66.211	[3, 15]
SB8VS-09	2.740	2.743	0.365	0.365	24.560	67.295	[3, 15]
SB8VS-10	2.734	2.741	0.366	0.365	24.466	66.889	[3, 15]
SB8VS-11	2.704	2.689	0.370	0.372	24.344	65.815	[3, 15]
SB8VS-12	2.720	2.725	0.368	0.367	24.439	66.462	[3, 15]
SB8VS-13	2.699	2.688	0.371	0.372	24.338	65.689	[3, 15]
SB8VS-14	2.711	2.696	0.369	0.371	24.153	65.466	[3, 15]
SB8VS-15	2.681	2.685	0.373	0.372	24.505	65.685	[3, 15]
SB8VS-16	2.707	2.707	0.369	0.369	24.434	66.143	[3, 15]
SB8VS-17	2.702	2.701	0.370	0.370	24.632	66.543	[3, 15]
SB8VS-18	2.701	2.695	0.370	0.371	24.392	65.870	[3, 15]
SB8VS-19	2.703	2.699	0.370	0.370	24.213	65.435	[3, 15]
SB8VS-20	2.723	2.712	0.367	0.369	24.401	66.431	[3, 15]
SB8VS-21	2.709	2.708	0.369	0.369	24.503	66.378	[3, 15]
SB8VS-22	2.700	2.702	0.370	0.370	24.259	65.486	[3, 15]
SB9VS01	2.665	2.653	0.375	0.377	24.309	64.782	[7, 14]
SB9VS02	2.678	2.681	0.373	0.373	24.432	65.429	[7, 14]
SB9VS03	2.696	2.702	0.371	0.370	24.454	65.927	[7, 14]
SB9VS04	2.709	2.720	0.369	0.368	24.568	66.555	[7, 14]
SB9VS05	2.731	2.738	0.366	0.365	24.499	66.908	[7, 14]
SB9VS06	2.669	2.662	0.375	0.376	24.375	65.057	[7, 14]
SB9VS07	2.667	2.656	0.375	0.376	24.199	64.538	[7, 14]
SB9VS08	2.676	2.675	0.374	0.374	24.330	65.107	[7, 14]
SB9D01	2.700	2.698	0.370	0.371	24.434	65.971	[7, 14]

Glass ID	ρ_{measured} (g/cm ³)	$\rho_{\text{predicted}}$ (g/cm ³)	$1/\rho_{\text{measured}}$ (cm ³ /g)	$\Sigma V_i/M_g$ (cm ³ /g)	V_{glass} (cm ³ /mol)	M_g	Reference
SB9D02	2.684	2.694	0.373	0.371	24.463	65.659	[7, 14]
SB9D03	2.715	2.718	0.368	0.368	24.518	66.565	[7, 14]
SB9D04	2.731	2.733	0.366	0.366	24.503	66.917	[7, 14]
SB9D05	2.725	2.741	0.367	0.365	24.509	66.787	[7, 14]
Shchavelev - 1	2.528	2.565	0.396	0.390	26.239	66.331	[24]
Shchavelev - 10	2.699	2.743	0.371	0.365	26.341	71.095	[24]
Shchavelev - 11	3.139	3.148	0.319	0.318	24.762	77.727	[24]
Shchavelev - 12	2.558	2.599	0.391	0.385	26.926	68.876	[24]
Shchavelev - 13	3.052	3.048	0.328	0.328	25.021	76.364	[24]
Shchavelev - 14	2.464	2.478	0.406	0.404	27.148	66.893	[24]
Shchavelev - 15	2.482	2.483	0.403	0.403	27.038	67.107	[24]
Shchavelev - 16	2.824	2.845	0.354	0.351	26.035	73.522	[24]
Shchavelev - 17	2.660	2.673	0.376	0.374	26.677	70.960	[24]
Shchavelev - 18	3.136	3.163	0.319	0.316	25.155	78.886	[24]
Shchavelev - 19	3.057	3.070	0.327	0.326	25.410	77.678	[24]
Shchavelev - 2	2.510	2.528	0.398	0.396	26.318	66.059	[24]
Shchavelev - 20	2.521	2.527	0.397	0.396	27.238	68.668	[24]
Shchavelev - 21	2.947	2.960	0.339	0.338	25.854	76.190	[24]
Shchavelev - 22	2.831	2.856	0.353	0.350	26.403	74.746	[24]
Shchavelev - 23	2.758	2.759	0.363	0.362	26.597	73.354	[24]
Shchavelev - 24	3.065	3.082	0.326	0.324	25.727	78.853	[24]
Shchavelev - 25	2.646	2.668	0.378	0.375	27.213	72.006	[24]
Shchavelev - 26	2.580	2.583	0.388	0.387	27.403	70.701	[24]
Shchavelev - 27	2.481	2.503	0.403	0.399	27.992	69.449	[24]
Shchavelev - 28	2.831	2.849	0.353	0.351	26.763	75.767	[24]
Shchavelev - 29	2.640	2.644	0.379	0.378	27.587	72.830	[24]
Shchavelev - 3	2.675	2.684	0.374	0.373	25.745	68.868	[24]
Shchavelev - 30	2.727	2.743	0.367	0.365	28.100	76.629	[24]
Shchavelev - 4	2.487	2.484	0.402	0.403	26.423	65.714	[24]
Shchavelev - 5	2.821	2.816	0.354	0.355	25.385	71.612	[24]
Shchavelev - 6	2.524	2.529	0.396	0.395	26.544	66.997	[24]
Shchavelev - 7	3.053	3.053	0.328	0.328	24.766	75.611	[24]
Shchavelev - 8	2.435	2.440	0.411	0.410	26.946	65.614	[24]
Shchavelev - 9	2.896	2.917	0.345	0.343	25.439	73.672	[24]
Shelby - Day - LiKSi - 1	2.410	2.435	0.415	0.411	28.438	68.536	[24]
Shelby - Day - LiKSi - 10	2.310	2.334	0.433	0.428	22.880	52.853	[24]
Shelby - Day - LiKSi - 2	2.411	2.433	0.415	0.411	28.326	68.294	[24]
Shelby - Day - LiKSi - 3	2.414	2.431	0.414	0.411	28.091	67.812	[24]
Shelby - Day - LiKSi - 4	2.420	2.422	0.413	0.413	27.357	66.203	[24]

Glass ID	ρ_{measured} (g/cm ³)	$\rho_{\text{predicted}}$ (g/cm ³)	$1/\rho_{\text{measured}}$ (cm ³ /g)	$\Sigma V_i/M_g$ (cm ³ /g)	V_{glass} (cm ³ /mol)	M_g	Reference
Shelby - Day - LiKSi - 5	2.405	2.404	0.416	0.416	26.189	62.986	[24]
Shelby - Day - LiKSi - 6	2.387	2.389	0.419	0.419	25.376	60.573	[24]
Shelby - Day - LiKSi - 7	2.366	2.373	0.423	0.421	24.582	58.160	[24]
Shelby - Day - LiKSi - 8	2.331	2.350	0.429	0.426	23.571	54.944	[24]
Shelby - Day - LiKSi - 9	2.318	2.338	0.431	0.428	23.009	53.336	[24]
Shelby - Day - LiNaSi - 1	2.430	2.443	0.412	0.409	24.858	60.404	[24]
Shelby - Day - LiNaSi - 10	2.309	2.332	0.433	0.429	22.768	52.572	[24]
Shelby - Day - LiNaSi - 2	2.431	2.440	0.411	0.410	24.748	60.163	[24]
Shelby - Day - LiNaSi - 3	2.423	2.429	0.413	0.412	24.499	59.360	[24]
Shelby - Day - LiNaSi - 4	2.409	2.408	0.415	0.415	23.974	57.753	[24]
Shelby - Day - LiNaSi - 5	2.391	2.391	0.418	0.418	23.650	56.548	[24]
Shelby - Day - LiNaSi - 6	2.367	2.374	0.422	0.421	23.381	55.343	[24]
Shelby - Day - LiNaSi - 7	2.337	2.350	0.428	0.426	22.994	53.737	[24]
Shelby - Day - LiNaSi - 8	2.316	2.337	0.432	0.428	22.856	52.933	[24]
Shelby - Day - LiNaSi - 9	2.313	2.334	0.432	0.429	22.781	52.692	[24]
Shelby-Day-1	2.748	2.703	0.364	0.370	29.194	80.226	[24]
Shelby-Day-2	2.523	2.518	0.396	0.397	28.578	72.103	[24]
Shelby-Day-3	2.446	2.463	0.409	0.406	28.529	69.782	[24]
Shelby-Day-4	2.441	2.446	0.410	0.409	28.302	69.086	[24]
Shelby-Day-LiCsSi - 1969 - 1	2.762	2.894	0.362	0.346	30.414	84.002	[24]
Shelby-Day-LiCsSi - 1969 - 2	2.461	2.402	0.406	0.416	22.624	55.679	[24]
Shelby-Day-LiCsSi - 1969 - 3	2.440	2.360	0.410	0.424	22.045	53.791	[24]
Shelby-Day-NaKSi-1	2.417	2.435	0.414	0.411	28.322	68.455	[24]
Shelby-Day-NaKSi-10	2.432	2.445	0.411	0.409	25.069	60.968	[24]
Shelby-Day-NaKSi-11	2.432	2.445	0.411	0.409	24.970	60.726	[24]
Shelby-Day-NaKSi-12	2.432	2.445	0.411	0.409	24.920	60.605	[24]
Shelby-Day-NaKSi-2	2.419	2.435	0.413	0.411	28.199	68.214	[24]
Shelby-Day-NaKSi-3	2.420	2.436	0.413	0.411	28.021	67.811	[24]
Shelby-Day-NaKSi-4	2.433	2.437	0.411	0.410	27.540	67.006	[24]
Shelby-Day-NaKSi-5	2.435	2.439	0.411	0.410	26.856	65.395	[24]
Shelby-Day-NaKSi-6	2.439	2.440	0.410	0.410	26.482	64.590	[24]
Shelby-Day-NaKSi-7	2.443	2.441	0.409	0.410	26.109	63.785	[24]
Shelby-Day-NaKSi-8	2.436	2.443	0.411	0.409	25.523	62.175	[24]
Shelby-Day-NaKSi-9	2.432	2.444	0.411	0.409	25.234	61.370	[24]
Sr05	2.409	2.424	0.415	0.413	27.270	65.684	[28]
Sr10	2.498	2.490	0.400	0.402	26.745	66.811	[28]
Sr20	2.686	2.678	0.372	0.373	26.008	69.847	[28]
SRM 1826a	2.549	2.529	0.392	0.395	24.818	63.259	[22]
SRM 1827a	3.594	3.605	0.278	0.277	25.872	92.984	[23]

Glass ID	ρ_{measured} (g/cm ³)	$\rho_{\text{predicted}}$ (g/cm ³)	$1/\rho_{\text{measured}}$ (cm ³ /g)	$\Sigma V_i/M_g$ (cm ³ /g)	V_{glass} (cm ³ /mol)	M_g	Reference
SRS 0/100 (8-8)	2.857	2.926	0.350	0.342	25.610	73.168	[34]
SRS 100/0 (8-8)	2.692	2.764	0.371	0.362	24.539	66.060	[34]
SRS 20/80 (8-8)	2.828	2.892	0.354	0.346	25.332	71.640	[34]
SRS 40/60 (8-8)	2.793	2.858	0.358	0.350	25.134	70.198	[34]
SRS 60/40 (8-8)	2.728	2.825	0.367	0.354	25.217	68.791	[34]
SRS 80/20 (8-8)	2.724	2.793	0.367	0.358	24.758	67.442	[34]
SWPF-01	2.682	2.696	0.373	0.371	23.863	64.002	[19]
SWPF-02	2.761	2.636	0.362	0.379	22.279	61.513	[19]
SWPF-03	2.688	2.677	0.372	0.374	22.734	61.108	[19]
SWPF-04	2.717	2.636	0.368	0.379	22.853	62.091	[19]
SWPF-05	2.867	2.814	0.349	0.355	23.681	67.893	[19]
SWPF-06	2.658	2.605	0.376	0.384	23.266	61.841	[19]
SWPF-07	2.686	2.650	0.372	0.377	23.168	62.230	[19]
SWPF-08	2.818	2.838	0.355	0.352	25.477	71.796	[19]
SWPF-09	2.760	2.666	0.362	0.375	22.377	61.761	[19]
SWPF-10	2.884	2.920	0.347	0.343	25.133	72.483	[19]
SWPF-11	2.592	2.588	0.386	0.386	25.355	65.720	[19]
SWPF-12	2.813	2.777	0.355	0.360	24.257	68.236	[19]
SWPF-13	2.750	2.692	0.364	0.372	23.402	64.356	[19]
SWPF-14	2.570	2.607	0.389	0.384	24.462	62.868	[19]
SWPF-15	2.706	2.744	0.370	0.364	24.234	65.577	[19]
SWPF-16	2.717	2.689	0.368	0.372	23.682	64.344	[19]
SWPF-17	2.679	2.680	0.373	0.373	24.516	65.679	[19]
SWPF-18	2.698	2.675	0.371	0.374	23.674	63.873	[19]
SWPF-19	2.704	2.694	0.370	0.371	24.361	65.872	[19]
SWPF-20	2.780	2.784	0.360	0.359	23.796	66.152	[19]
SWPF-21	2.825	2.781	0.354	0.360	23.952	67.664	[19]
SWPF-22	2.767	2.805	0.361	0.357	24.771	68.541	[19]
SWPF-23	2.771	2.757	0.361	0.363	24.257	67.217	[19]
SWPF-24	2.753	2.765	0.363	0.362	25.240	69.487	[19]
SWPF-25	2.782	2.747	0.359	0.364	23.306	64.838	[19]
SWPF-26	2.779	2.726	0.360	0.367	23.121	64.254	[19]
SWPF-27	2.769	2.717	0.361	0.368	23.788	65.869	[19]
SWPF-28	2.759	2.736	0.362	0.365	23.910	65.967	[19]
SWPF-29	2.757	2.725	0.363	0.367	24.095	66.429	[19]
SWPF-30	2.707	2.741	0.369	0.365	25.358	68.645	[19]
SWPF-31	2.693	2.702	0.371	0.370	25.020	67.378	[19]
SWPF-32	2.719	2.676	0.368	0.374	23.726	64.512	[19]
SWPF-33	2.777	2.733	0.360	0.366	23.786	66.055	[19]

Glass ID	ρ_{measured} (g/cm ³)	$\rho_{\text{predicted}}$ (g/cm ³)	$1/\rho_{\text{measured}}$ (cm ³ /g)	$\Sigma V_i/M_g$ (cm ³ /g)	V_{glass} (cm ³ /mol)	M_g	Reference
SWPF-34	2.690	2.694	0.372	0.371	24.677	66.382	[19]
SWPF-35	2.754	2.761	0.363	0.362	24.026	66.167	[19]
SWPF-36	2.688	2.681	0.372	0.373	24.273	65.247	[19]
SWPF-37	2.737	2.712	0.365	0.369	23.918	65.463	[19]
SWPF-38	2.790	2.784	0.358	0.359	24.555	68.510	[19]
SWPF-39	2.707	2.685	0.369	0.372	23.644	64.005	[19]
SWPF-40	2.736	2.757	0.365	0.363	24.486	66.994	[19]
SWPF-41	2.705	2.687	0.370	0.372	23.399	63.293	[19]
SWPF-42	2.707	2.679	0.369	0.373	24.363	65.951	[19]
SWPF-43	2.773	2.757	0.361	0.363	23.732	65.809	[19]
SWPF-44	2.760	2.704	0.362	0.370	23.465	64.762	[19]
SWPF-45	2.721	2.725	0.368	0.367	24.776	67.416	[19]
SWPF-46	2.770	2.722	0.361	0.367	23.769	65.841	[19]
SWPF-47	2.746	2.736	0.364	0.366	23.923	65.702	[19]
SWPF-48	2.702	2.701	0.370	0.370	24.463	66.100	[19]
SWPF-49	2.712	2.707	0.369	0.369	24.109	65.384	[19]
SWPF-50	2.759	2.723	0.362	0.367	23.737	65.490	[19]
Ta05	2.390	2.443	0.418	0.409	28.193	67.388	[28]
Ta10	2.472	2.537	0.404	0.394	28.549	70.579	[28]
Ti05	2.326	2.396	0.430	0.417	27.933	64.963	[28]
TV 00	2.820	2.743	0.355	0.365	24.894	70.202	[33]
TV 01	2.724	2.674	0.367	0.374	25.344	69.037	[33]
TV 02	2.529	2.520	0.395	0.397	26.050	65.880	[33]
TV 03	2.517	2.519	0.397	0.397	25.519	64.232	[33]
TV 04	2.498	2.481	0.400	0.403	25.558	63.843	[33]
TV 05	2.699	2.660	0.371	0.376	24.815	66.976	[33]
TV 06	2.978	2.910	0.336	0.344	23.943	71.303	[33]
TV 07	3.004	2.900	0.333	0.345	23.204	69.706	[33]
TV 09	2.909	2.877	0.344	0.348	24.540	71.387	[33]
TV 10	2.735	2.677	0.366	0.374	24.719	67.605	[33]
TV 11	2.654	2.612	0.377	0.383	25.031	66.432	[33]
TV 12	2.807	2.731	0.356	0.366	24.127	67.723	[33]
TV 13	2.789	2.740	0.359	0.365	24.626	68.681	[33]
TV 15	2.857	2.778	0.350	0.360	24.948	71.277	[33]
TV 16	2.645	2.617	0.378	0.382	24.675	65.266	[33]
TV 17	2.786	2.718	0.359	0.368	24.120	67.197	[33]
TV 18	2.945	2.868	0.340	0.349	24.742	72.865	[33]
TV 19	2.748	2.674	0.364	0.374	24.515	67.369	[33]
TV 20	2.577	2.521	0.388	0.397	24.628	63.467	[33]

Glass ID	ρ_{measured} (g/cm ³)	$\rho_{\text{predicted}}$ (g/cm ³)	$1/\rho_{\text{measured}}$ (cm ³ /g)	$\Sigma V_i/M_g$ (cm ³ /g)	V_{glass} (cm ³ /mol)	M_g	Reference
TV 21	2.753	2.712	0.363	0.369	24.612	67.758	[33]
TV 22	2.798	2.774	0.357	0.360	25.297	70.781	[33]
TV 23	2.598	2.564	0.385	0.390	24.836	64.523	[33]
TV 24	2.366	2.401	0.423	0.416	26.699	63.170	[33]
WCP BATCH 1	2.647	2.701	0.378	0.370	24.815	65.694	[24, 25]
WCP BATCH 2	2.638	2.669	0.379	0.375	24.611	64.921	[24, 25]
WCP BATCH 3	2.651	2.673	0.377	0.374	24.447	64.809	[24, 25]
WCP BATCH 4	2.672	2.710	0.374	0.369	24.536	65.561	[24, 25]
WCP BLEND 1	2.641	2.673	0.379	0.374	24.577	64.907	[24, 25]
WCP HM	2.588	2.611	0.386	0.383	24.659	63.818	[24, 25]
WCP PUREX	2.683	2.740	0.373	0.365	24.820	66.593	[24, 25]
Wo 00	2.550	2.534	0.392	0.395	23.860	60.843	[33]
Wo 01	2.435	2.435	0.411	0.411	24.668	60.067	[33]
Wo 02	2.476	2.464	0.404	0.406	23.679	58.629	[33]
Wo 03	2.589	2.564	0.386	0.390	22.484	58.210	[33]
Wo 04	2.483	2.472	0.403	0.405	24.622	61.135	[33]
Wo 05	2.560	2.564	0.391	0.390	24.165	61.862	[33]
Wo 06	2.599	2.604	0.385	0.384	23.472	61.003	[33]
Wo 07	2.531	2.515	0.395	0.398	24.271	61.430	[33]
Wo 08	2.563	2.553	0.390	0.392	23.522	60.288	[33]
Wo 09	2.569	2.596	0.389	0.385	23.067	59.260	[33]
Wo 10	2.558	2.574	0.391	0.389	23.776	60.820	[33]
Wo 11	2.533	2.541	0.395	0.394	23.923	60.598	[33]
Wo 12	2.481	2.522	0.403	0.397	24.629	61.105	[33]
Wo 13	2.507	2.483	0.399	0.403	23.961	60.069	[33]
Wo 14	2.524	2.508	0.396	0.399	23.807	60.090	[33]
Wo 15	2.512	2.516	0.398	0.398	23.735	59.622	[33]
Wo 16	2.463	2.456	0.406	0.407	24.952	61.457	[33]
Wo 17	2.502	2.516	0.400	0.397	24.274	60.733	[33]
Wo 18	2.562	2.544	0.390	0.393	23.213	59.471	[33]
Wo 19	2.515	2.481	0.398	0.403	23.800	59.857	[33]
Wo 20	2.500	2.493	0.400	0.401	23.560	58.901	[33]
Wo 21	2.496	2.496	0.401	0.401	24.479	61.100	[33]
Wo 22	2.487	2.486	0.402	0.402	25.184	62.633	[33]
Wo 23	2.583	2.588	0.387	0.386	24.060	62.147	[33]
Wo 24	2.598	2.621	0.385	0.382	23.333	60.619	[33]
SHUM-1	2.592	2.677	0.386	0.374	24.967	64.716	[8, 26, 27]
SHUM-10A	2.557	2.548	0.391	0.392	23.603	60.353	[8, 26, 27]
SHUM-10B	2.560	2.551	0.391	0.392	23.661	60.573	[8, 26, 27]

Glass ID	ρ_{measured} (g/cm ³)	$\rho_{\text{predicted}}$ (g/cm ³)	$1/\rho_{\text{measured}}$ (cm ³ /g)	$\Sigma V_i/M_g$ (cm ³ /g)	V_{glass} (cm ³ /mol)	M_g	Reference
SHUM-10C	2.558	2.550	0.391	0.392	23.596	60.358	[8, 26, 27]
SHUM-11	2.805	2.829	0.357	0.354	24.102	67.606	[8, 26, 27]
SHUM-13	2.671	2.655	0.374	0.377	23.557	62.921	[8, 26, 27]
SHUM-14	2.598	2.582	0.385	0.387	23.604	61.323	[8, 26, 27]
SHUM-15	2.527	2.513	0.396	0.398	23.633	59.721	[8, 26, 27]
SHUM-2	2.650	2.714	0.377	0.369	24.690	65.429	[8, 26, 27]
SHUM-3	2.592	2.632	0.386	0.380	24.510	63.531	[8, 26, 27]
SHUM-4	2.693	2.751	0.371	0.363	24.576	66.183	[8, 26, 27]
SHUM-5	2.642	2.668	0.379	0.375	24.226	64.004	[8, 26, 27]
SHUM-6	2.581	2.589	0.387	0.386	23.990	61.918	[8, 26, 27]
SHUM-7	2.740	2.788	0.365	0.359	24.499	67.127	[8, 26, 27]
SHUM-8	2.690	2.704	0.372	0.370	24.005	64.574	[8, 26, 27]
SHUM-9	2.627	2.620	0.381	0.382	23.729	62.335	[8, 26, 27]
SHUM-T1	2.707	2.704	0.369	0.370	23.998	64.963	[8, 26, 27]
SHUM-T2	2.685	2.704	0.372	0.370	24.195	64.963	[8, 26, 27]
SHUM-T4	2.705	2.704	0.370	0.370	24.016	64.963	[8, 26, 27]

Appendix B

Developing Upper Tolerance Limits for Predicted Densities

Initially, a lower tolerance limit for the inverse of the glass density may be computed using

$$LTL_{\rho_i}^{\frac{1}{\rho_i}} = b + m \cdot x_i + s \left\{ \sqrt{pF_{\alpha}(p, n-p)} \sqrt{\underline{c}_0 (\mathbf{X}^T \mathbf{X})^{-1} \underline{c}_0^T} + z_{1-\alpha_0} \sqrt{\frac{n-p}{\chi_{\alpha/2, n-p}^2}} \right\} \quad (2)$$

where

- $LTL_{\rho_i}^{\frac{1}{\rho_i}}$ equals the lower tolerance limit for the inverse of the glass density, ρ_i , for a glass yielding a [Sum of Vols]/[g/mol_glass] value of x_i (the unit of $LTL_{\rho_i}^{\frac{1}{\rho_i}}$ is cm^3/g),
- the estimated slope and intercept of the fitted model are m and b , respectively, (where $m = 1.0004692 \text{ cm}^3/\text{g}$ per unit of [Sum of Vols]/[g/mol_glass] and $b = 0.0010279 \text{ cm}^3/\text{g}$),
- s is the RMSE for the fitted model for $1/\rho$ (the value is given by $0.006755 \text{ cm}^3/\text{g}$),
- $F_{\alpha}(p, n-p)$ is the $100(1-\alpha)\%$ quantile of the F distribution, which depends on $n=1104$ (i.e., the number of data points on which this p -parameter ($p=2$) model is based), and the desired confidence level for bounding the estimated mean of $1/\rho$ (when the glass of interest yields a value of [Sum of Vols]/[g/mol_glass] equal to x_i) is represented by $100(1-\alpha)\%$,
- the inverse product-moment matrix is represented by $(\mathbf{X}^T \mathbf{X})^{-1}$ where the product moment matrix contains information describing the data for the independent variable (i.e., the values of [Sum of Vols]/[g/mol_glass]) used to generate the regression equation (the values of the $\mathbf{X}^T \mathbf{X}$ and $(\mathbf{X}^T \mathbf{X})^{-1}$ matrices are given in Figure B-1 below),
- \underline{c}_0 is the vector, $[1 \ x_i]$, containing the x_i ,
- $Z_{1-\alpha_0}$ represents the one-sided $100(1-\alpha_0)\%$ percentile point from the standard normal distribution representing the $1-\alpha_0$ fraction of the model predictions to be covered, and
- $\chi_{\alpha/2, n-p}^2$ represents the lower (i.e., $100(\alpha/2)\%$) percentile point of the χ^2 distribution with $(n-p)$ degrees of freedom, used to establish a lower bound for the variance of the inverse densities around the fitted line.

LTLs were determined using the approach provided on page 124 of Miller [52]. The notation $(1-\alpha)100\%/(1-\alpha_0)100\%$ LTL, such as $99\%/99\%$ LTL, will be used to represent these LTLs. The notation refers to a tolerance limit that provides $(1-\alpha)100\%$ confidence that $(1-\alpha_0)100\%$ of the inverse densities are greater than the LTL. The approach is based on a normal distribution. The $99\%/99\%$ LTLs are inverted to provide upper tolerance limits with 99% confidence for 99% of the densities themselves, with each limit for a specific glass associated with the corresponding value of [Sum of Vols]/[g/mol_glass] for that glass.

Figure B-2 shows the UTL generated via this statistical approach compared to the UTL derived from the k -value approach discussed in Section 3.2. In the region of interest for HLW glass density (approximately 2.6 - 2.8 g/cm^3), the two approaches provide upper bounds that are nearly identical, which lends more confidence to the approach outlined in this report. Furthermore, this approach has a similar applicability in terms of bounding a specific ratio of $M_g/\sum x_i v_i$. That is to say, infinitely many compositions with a given $M_g/\sum x_i v_i$ ratio are bounded by the UTLs provided in this document.

$$X'X = \begin{pmatrix} 1104 & 423.9738422 \\ 423.9738422 & 163.6456452 \end{pmatrix}$$

$$(X'X)^{-1} = \begin{pmatrix} 0.179638222553 & -0.465407480505 \\ -0.465407480505 & 1.211890469020 \end{pmatrix}$$

Figure B-1: $X^T X$ and $(X^T X)^{-1}$ for the Density Model

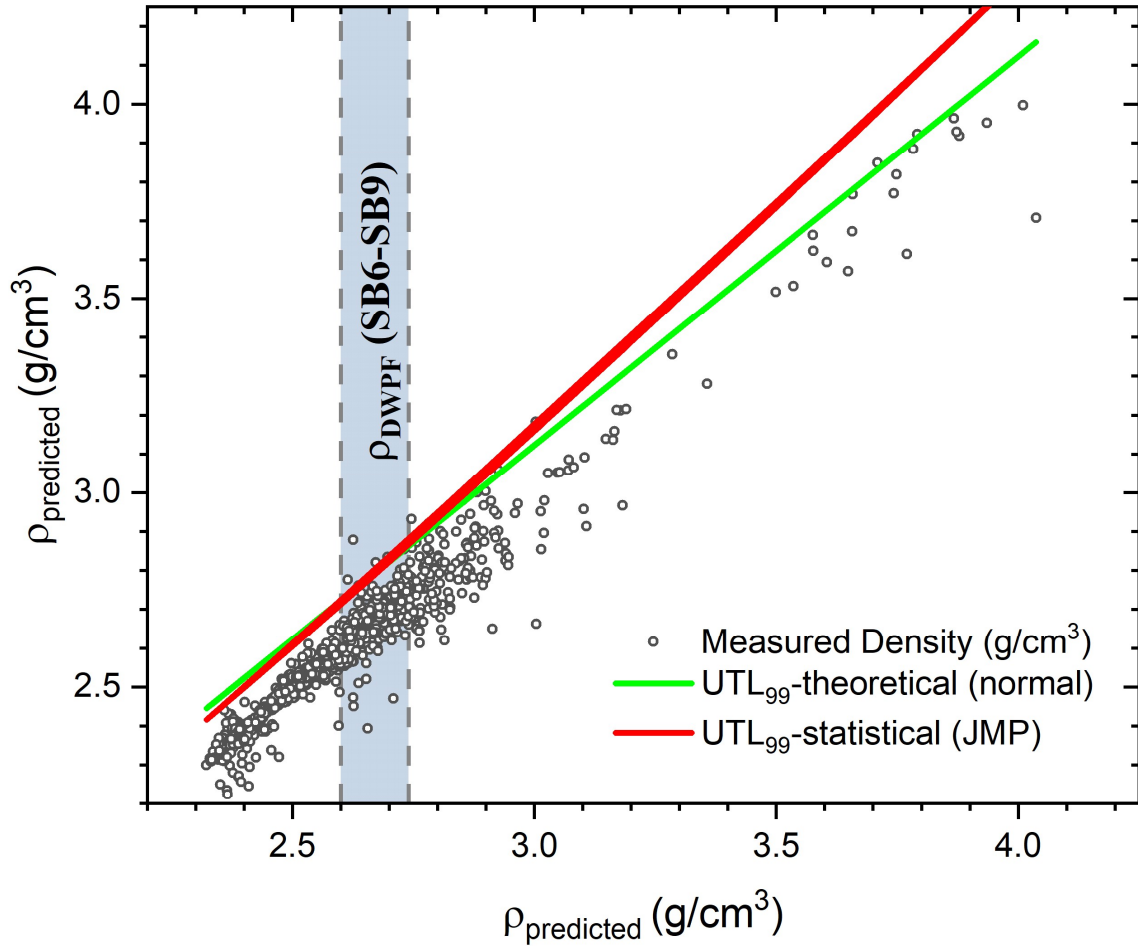


Figure B-2: A comparison of the UTLs derived from theory and statistical approaches. The two predicted UTLs are nearly identical in the region of interest for anticipated HLW glass densities.

Appendix C

Table 5: Partial molar volumes of the oxides used in the density predictions.

Oxide	Partial Molar Volume (cm ³ /mol)	Oxide	Partial Molar Volume (cm ³ /mol)	Oxide	Partial Molar Volume (cm ³ /mol)
Al ₂ O ₃ ⁱ	40.78	Fe ₂ O ₃ ⁱⁱ	31.20	SO ₃ , SO ₄ (as Na ₂ SO ₄) ⁱⁱⁱ	52.61
As ₂ O ₃ ⁱⁱ	52.89	Gd ₂ O ₃ ⁱⁱⁱ	48.92	Sb ₂ O ₃ ⁱ	47.02
B ₂ O ₃ ⁱ	24.87	K ₂ O ⁱ	33.64	Se (as SeO ₃ ²⁻) ⁱⁱⁱ	36.91
BaO ⁱ	21.91	La ₂ O ₃ ⁱⁱⁱ	50.05	SiO ₂ ⁱ	26.36
Bi ₂ O ₃ ⁱ	45.24	Li ₂ O ⁱ	11.07	Sm ₂ O ₃ ⁱⁱⁱ	45.88
CaO ⁱ	14.38	MgO ⁱ	12.22	SrO ⁱ	17.56
CdO ⁱ	17.83	MnO ⁱⁱ	13.70	Ta ₂ O ₅ ⁱⁱⁱ	53.62
CeO ₂ ⁱⁱ	23.60	MnO ₂ ⁱⁱⁱ	17.11	TeO ₂ ⁱⁱⁱ	27.05
Ce ₂ O ₃ ⁱⁱ	46.90	MoO ₃ ⁱⁱⁱ	30.63	ThO ₂ ⁱ	31.81
CoO ⁱⁱ	13.20	Na ₂ O ⁱ	20.00	TiO ₂ ⁱ	21.02
CrO ₃ ⁱⁱ	37.00	Nd ₂ O ₃ ⁱⁱⁱ	46.48	Tl ₂ O ⁱ	63.40
Cr ₂ O ₃ ⁱⁱ	29.20	NiO ⁱⁱ	33.50	U ₃ O ₈ ⁱⁱⁱ	100.48
Cs ₂ O ⁱⁱ	63.00	P ₂ O ₅ ⁱⁱ	59.50	UO ₂ ⁱⁱ	24.80
CuO ⁱⁱ	12.40	PbO ⁱ	22.32	UO ₃ ⁱⁱ	39.20
Cu ₂ O ⁱⁱ	23.80	Pr ₂ O ₃ ⁱⁱⁱ	47.80	Y ₂ O ₃ ⁱⁱ	46.70
F (loose bond with Si and Al) ^{iv}	14.20	Rb ₂ O ⁱ	45.59	ZnO ⁱ	14.53
FeO ⁱⁱ	12.60	RuO ₂ ⁱⁱⁱ	18.87	ZrO ₂ ⁱ	23.25

The partial molar volume of any oxide can be determined by dividing the molar mass of the oxide (or compound) by the physical density according to Equation C-1 below:

$$v_i = \frac{M_i}{\rho_i} , \left\{ \frac{cm^3}{mol} \right\} \quad C-1$$

where, M_i is the molar mass of oxide or compound “ i ” and ρ_i is the physical density of oxide or compound “ i .”

ⁱ Ref [11]

ⁱⁱ Ref [12]

ⁱⁱⁱ Ref [13]

^{iv} Ref [42]

Appendix D

Effects of Reduction/Oxidation (REDOX) Chemistry on Density

The control of glass REDOX is important for many aspects of HLW glass processing including: extending melter lifetime by lessening refractory corrosion, mitigating metal precipitation in the melt, limiting the volatilization of certain chemical species, and melter cold-cap integrity [53]. As a result, an operational window has been defined in which DWPF strives to maintain the REDOX of any sludge batch – glass system. The window is defined by the $\text{Fe}^{2+}/\Sigma\text{Fe}$ ratio. Given that all the DWPF-type glasses contained in the database were from variability studies, which are fully oxidized glasses, an exercise was undertaken to determine the effects of varying the $\text{Fe}^{2+}/\Sigma\text{Fe}$ ratio on glass density. The results are presented in this appendix.

To determine the effects of varying the REDOX ratio on predicted density related to the measured density, the $\text{Fe}^{2+}/\Sigma\text{Fe}$ ratio was artificially and incrementally varied from fully oxidized ($\text{Fe}^{2+}/\Sigma\text{Fe} = 0$) to fully reduced ($\text{Fe}^{2+}/\Sigma\text{Fe} = 1$). The resulting predicted densities were recorded. Figure D-1 shows the results of this exercise for the entire HLW glass subset, where the variation in the predicted density caused by changing REDOX potential is given by the error bars in the x-axis values.

The maximum density variation for a single glass composition caused by changing the REDOX state of the Fe species was 0.006 g/cm^3 for the composition HLP-42, a glass composition that contains almost 16 wt % Fe oxides. The average variation across the entire HLW dataset including the VS and “other” glass compositions was 0.0005 g/cm^3 , which is an order of magnitude less than the best possible analytical precision achievable with density measurement techniques.

Based on these results, the effect of REDOX variation during HLW glass fabrication is negligible.

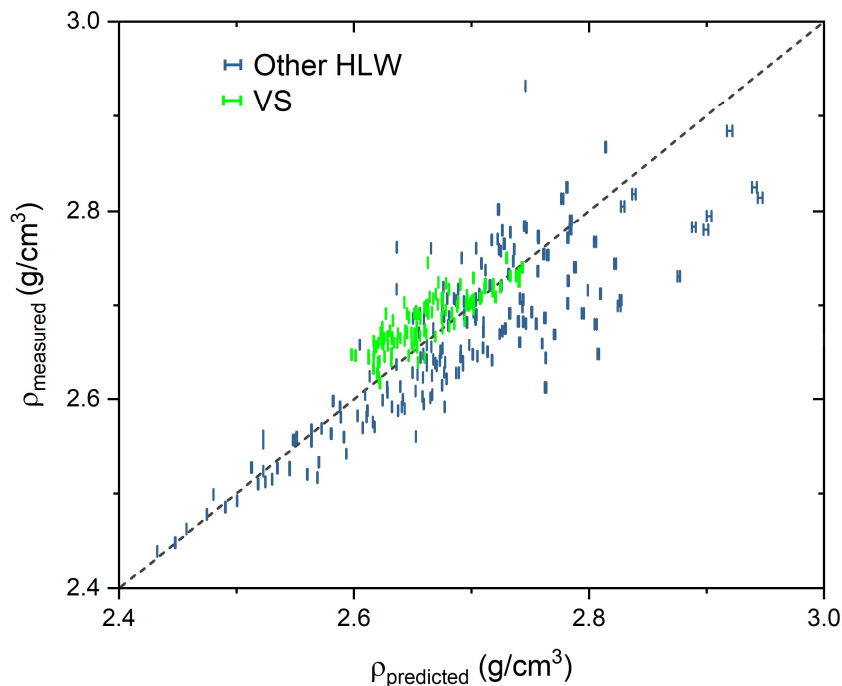


Figure D-1: The effect of varying $\text{Fe}^{2+}/\text{Fe}^{3+}$ ratio on the HLW glass compositions listed in the database. The range of the variation for an individual composition is given by the “error” bars. The dashed line represents the ideal theoretical density (measurement = prediction).

Appendix E

Including Density Predictions as Part of MAR Assessments at SRNL and SME Evaluations at DWPF

As stated earlier, the density of the glass produced by DWPF is of interest as fissile loading evaluations are conducted during SME acceptability decisions. In this appendix, two ways that the density model presented in this report are to be used in support of the fissile loading evaluations are discussed.

Density Predictions as Part of MAR Assessments

As part of its frit development efforts for DWPF, SRNL conducts Measurement Acceptance Region (MAR) assessments of candidate sludge/frit glass systems. These assessments rely on projections of representative compositions from these glass systems. These glass compositions are evaluated against criteria of DWPF's Product Composition Control System (PCCS) for Slurry Mix Evaporator (SME) acceptability decisions to provide a projected operating window in waste loading (WL) space for the sludge/frit system.

The glass compositions and projected operating windows are developed in the following manner. Oxide intervals representing compositions for sludge-only or coupled operations are developed and used to generate extreme vertices (EVs) of the corresponding sludge region. The EVs are the corner-points of the sludge compositional region defined by the set of the sludge oxide intervals for each operational projection of interest.

Each EV is combined with a candidate frit at WLs in the range of interest for DWPF operation, and each of the resulting glass compositions is evaluated against the PCCS MAR criteria to determine whether the composition would pass the SME acceptability process. A projected operating window for a sludge/frit glass system is a WL interval over which all EVs for that system are MAR acceptable. The objective of these evaluations is to identify a frit that provides a projected operating window of at least 9 WL points centered around an acceptably high WL.

By utilizing the density model developed in this report, SRNL can add a density prediction to the results generated for each glass composition evaluated during MAR assessments. The density predictions may then be summarized as part of the information associated with a projected operating window for a sludge/frit glass system. To demonstrate this approach, a portion of the MAR evaluations supporting frit selection for the SB9/SWPF operation are repeated in Table 6, which includes a summary of density predictions.

Table 6: Frit 625 and SB9 Coupled with SWPF

(5,700 gal from Tank 40 to the SRAT; 12,800 gals of Strip Effluent with BobCalixC6; and 2,400 gals of Sludge Solids Receipt Tank as the Baseline Case)

% WL	MAR Status	Number of EVs	Max(Density) g/cm ³
24		3410	2.589
24	highv	1282	2.586
25		4483	2.598
25	highv	209	2.588
26		4692	2.608
27		4692	2.618
28		4692	2.627
29		4692	2.637
30		4692	2.647
31		4692	2.657
32		4692	2.667
33		4692	2.678
34		4692	2.688
35		4692	2.698
36		4692	2.709
37		4692	2.719
38		4692	2.730
39		4692	2.740
40		4692	2.751
41		4692	2.762
42		4344	2.773
42	lowv	348	2.765

The table indicates that there are 4,692 EVs for this sludge projection; that Frit 625 was used for the MAR assessment, which covered WLs from 24% to 42%; that high and low viscosity (abbreviated as highv and lowv, respectively) constraints restricted the operating region; and that the projected operating window for this glass system was 26 to 41% WL. For each WL, the last column provides the maximum projected density for the glasses evaluated at that WL. For the operating window, the maximum of the maximum predicted densities for acceptable glasses is 2.762 g/cm³.

Table 7 provides a higher-level summary of information, including the predicted densities, for both frit 625 and 803 for SB9 coupled with other possible options for SWPF streams^f. This table tracks the projected operating windows for various options for DWPF/SWPF coupled operations for both Frit 625 and Frit 803. For example, the first row of data in the table shows a projected operating window for Frit 625 of 26 to 41% WL as SB9 is processed coupled with 12,800 gallons of SE with BobCalixC6 (BC) solvent and 2400 gallons of SSRT. The projected glass compositions representing that region have a maximum predicted density of 2.762 g/cm³. A review of Table 7 shows that the largest projected density for the results over both frits is 2.772 g/cm³. As part of future frit recommendation efforts, SRNL plans to include information such as that provided in Table 7 for glass compositions determined to be in the projected operating window of the glass system of interest.

^f See Table 5-4 of SRNL-STI-2019-00004, Revision 0 [54], for a more complete description of the options that were evaluated as part of the frit recommendation efforts for SB9/SWPF operations.

Table 7: Operating Windows for Frits 625 and 803 with SB9 Coupled with Options from SWPF Additions

Frit	Sludge Type	Operating Window Size	Min(% WL)	Max(% WL)	Maximum Predicted Density (g/cm ³)
Frit 625	SB9 Table 1 BC: 12,800; SSRT: 2,400; Cs2O: 1.60; Na2O: 27.26; TiO2: 6.37 EV	16	26	41	2.762
Frit 625	SB9 Table 1 BC: 12,800; SSRT: 2,800; Cs2O: 1.56; Na2O: 27.67; TiO2: 7.26 EV	15	26	40	2.750
Frit 625	SB9 Table 1 BC: 12,800; SSRT: 3,200; Cs2O: 1.53; Na2O: 28.06; TiO2: 8.12 EV	16	25	40	2.749
Frit 625	SB9 Table 1 BC: 12,800; SSRT: 3,600; Cs2O: 1.50; Na2O: 28.43; TiO2: 8.94 EV	14	26	39	2.738
Frit 625	SB9 Table 2 BC: 12,800; SSRT: 2,400; Cs2O: 1.61; Na2O: 27.43; TiO2: 6.41 EV	15	26	40	2.753
Frit 625	SB9 Table 2 BC: 12,800; SSRT: 2,800; Cs2O: 1.58; Na2O: 27.87; TiO2: 7.31 EV	15	26	40	2.753
Frit 625	SB9 Table 2 BC: 12,800; SSRT: 3,200; Cs2O: 1.54; Na2O: 28.28; TiO2: 8.19 EV	13	27	39	2.741
Frit 625	SB9 Table 2 BC: 12,800; SSRT: 3,600; Cs2O: 1.51; Na2O: 28.69; TiO2: 9.02 EV	13	27	39	2.741
Frit 625	SB9 Table 3 600SS BC: 12,800; SSRT: 2,400; Cs2O: 1.40; Na2O: 23.92; TiO2: 5.59 EV	11	29	39	2.744
Frit 625	SB9 Table 3 600SS BC: 12,800; SSRT: 2,800; Cs2O: 1.35; Na2O: 23.86; TiO2: 6.26 EV	11	29	39	2.744
Frit 625	SB9 Table 3 600SS BC: 12,800; SSRT: 3,200; Cs2O: 1.30; Na2O: 23.81; TiO2: 6.89 EV	10	29	38	2.733
Frit 625	SB9 Table 3 600SS BC: 12,800; SSRT: 3,600; Cs2O: 1.25; Na2O: 23.76; TiO2: 7.47 EV	10	29	38	2.733
Frit 625	SB9 Table 4 BC: 12,800; SSRT: 3,800; Cs2O: 1.44; Na2O: 27.78; TiO2: 12.08 EV	13	27	39	2.740
Frit 625	SB9 Table 4 BC: 12,800; SSRT: 4,200; Cs2O: 1.41; Na2O: 28.05; TiO2: 13.05 EV	12	27	38	2.729
Frit 625	SB9 Table 5 BC: 12,800; SSRT: 3,800; Cs2O: 1.45; Na2O: 28.01; TiO2: 12.18 EV	11	28	38	2.732
Frit 625	SB9 Table 5 BC: 12,800; SSRT: 4,200; Cs2O: 1.42; Na2O: 28.30; TiO2: 13.16 EV	10	29	38	2.731
Frit 803	SB9 Table 1 BC: 12,800; SSRT: 2,400; Cs2O: 1.60; Na2O: 27.26; TiO2: 6.37 EV	11	30	40	2.757
Frit 803	SB9 Table 1 BC: 12,800; SSRT: 2,800; Cs2O: 1.56; Na2O: 27.67; TiO2: 7.26 EV	10	30	39	2.745
Frit 803	SB9 Table 1 BC: 12,800; SSRT: 3,200; Cs2O: 1.53; Na2O: 28.06; TiO2: 8.12 EV	9	31	39	2.745
Frit 803	SB9 Table 1 BC: 12,800; SSRT: 3,600; Cs2O: 1.50; Na2O: 28.43; TiO2: 8.94 EV	9	31	39	2.744
Frit 803	SB9 Table 2 BC: 12,800; SSRT: 2,400; Cs2O: 1.61; Na2O: 27.43; TiO2: 6.41 EV	10	31	40	2.759
Frit 803	SB9 Table 2 BC: 12,800; SSRT: 2,800; Cs2O: 1.58; Na2O: 27.87; TiO2: 7.31 EV	9	31	39	2.748
Frit 803	SB9 Table 3 600SS BC: 12,800; SSRT: 2,400; Cs2O: 1.40; Na2O: 23.92; TiO2: 5.59 EV	14	28	41	2.772
Frit 803	SB9 Table 3 600SS BC: 12,800; SSRT: 2,800; Cs2O: 1.35; Na2O: 23.86; TiO2: 6.26 EV	13	28	40	2.761
Frit 803	SB9 Table 3 600SS BC: 12,800; SSRT: 3,200; Cs2O: 1.30; Na2O: 23.81; TiO2: 6.89 EV	13	28	40	2.760
Frit 803	SB9 Table 3 600SS BC: 12,800; SSRT: 3,600; Cs2O: 1.25; Na2O: 23.76; TiO2: 7.47 EV	13	28	40	2.760

As a final step, the 99%/99% uncertainty of these predictions, as discussed in Section 3.2, should be applied to provide an upper bound on the expected densities for glasses over the projected operating windows of the sludge/frit system. For example, with the largest predicted density of 2.772 g/cm^3 , applying uncertainty yields $2.772 + 0.123 = 2.895 \text{ g/cm}^3$. This would be the bounding density for the glass system as compared to the 2.846 g/cm^3 value developed in reference [7].

This section of the appendix demonstrates how SRNL plans to provide predicted densities as part of the information generated during frit development and MAR assessment efforts. Such information is expected to be of value as DWPF develops preliminary estimates of the fissile mass in the glass anticipated to be produced by upcoming sludge/frit systems as done for earlier sludge batches including for SB8 [55] and the earlier processing of SB9 [56].

Density Predictions as Part of SME Acceptability Evaluations at DWPF

Another purpose served by these SB8 [55] and SB9 [56] documents was to provide specific details of how DWPF was to monitor fissile loading during the processing of these sludge batches. This section of the appendix is used to illustrate a method, that is being recommended, for utilizing the density model developed in this report along with information available for each SME batch to monitor the fissile loading in future processing at DWPF.

Figure E1 provides an overview of the calculations that demonstrate the use of compositional and calcine solids measurements from PCCS to provide a density prediction for the glass product from the SME batch. The data presented in this example were taken from SME 565 of SB6.

- Column A provides a list of the analytes whose measurements, determined from samples of the SME batch, are PCCS inputs.
- Column B provides the averages of the measurements from these samples. These are values directly available from PCCS, which may be used to provide a density prediction.
- Column C provides the oxides corresponding to the elemental data.
- Column D provides the molecular weight of the oxide.
- Column E provides the gravimetric factor that may be used to convert the elemental wt % to an oxide, as shown in Column F, wt % (i.e., the oxide wt % = [elemental wt %] × [gravimetric factor]).
- Column G, the molar oxide fraction for each oxide, is determined by dividing the mass fraction of the oxide by the molecular weight of the oxide.
- Column H provides the normalized molar fraction (NMF) (i.e., each value of Column G divided by the sum in Cell G32).
- The rows of Column I are the partial molar volume (PMV) values for the oxides; these values were provided earlier in Table 5 of Appendix C. Please note that per the assumptions provided in Section 2.3, the PMV value for sulfur corresponds to the PMV for Na_2SO_4 and the PMV value for uranium is a weighted average of the PMV values for UO_2 and UO_3 (i.e., it is equal to $0.33 \times 24.8 + 0.67 \times 39.2$).
- Each row of Column K is the product of the NMF and PMV values for the corresponding oxide. The sum of these values (provided in row 32 of Column K) is the denominator term in the density predictor.
- Each row of Column N is the contribution of the corresponding oxide to the grams/mole of glass (i.e., [oxide molecular weight] × [NMF]). Please note that the value for sulfur utilizes the molecular weight of SO_4 and that the value for uranium utilizes a weighted average of the molecular weights for UO_2 and UO_3 (i.e., it is equal to $0.33 \times 270.0278 + 0.67 \times 286.0272$).
- The sum of Column N (provided in row 32 of Column N) is the numerator term in the density predictor.

- With numerator and denominator terms of the density predictor model determined, the resulting ratio of these terms (i.e., the density prediction, is provided in row 35 of Column N).
- The value in row 34 of Column O provides the uncertainty (for 99% coverage at 99% confidence) described in Section 3.2.
- The value in row 34 of Column P applies the uncertainty to determine the bound on the density for the glass produced by this SME batch.

Calculations in the block of Cells J36 through P42 demonstrate the completion of the evaluation of the fissile loading for the glass produced by the SME batch against the 897 g fissile equivalent/cm³ of glass (already part of the fissile loading evaluation process conducted by DWPF, see for example references [55] and [56]). This evaluation utilizes an estimate of the fissile to iron ratio, on a mass basis, for the Tank 40 sludge, the iron concentration in the SME batch (the average Fe content plus 2 times the standard deviation of the sample results for iron), and the bounding density determined in Cell P32. The sample average and standard deviation of the iron content are readily available since these values may be computed from the entries to PCCS. The formulas used to complete these calculations are documented in Figure E-1.

Currently, a fissile loading decision is conducted by DWPF for each SME batch. Figure E-1 demonstrates how this process may be modified to include determining a bounding density value for the SME batch that may be utilized in the calculations supporting this decision. SRNL recommends that DWPF implement this modification into their fissile loading decisions in future SME processing.

	A	B	C	D	E	F	G	H	I	J	K	L	M	N	O	P	Q		
1	Element	Measured wt%	Oxide	Molecular Wt	Gravimetric Factor	Mass wt%	Molar Oxide	Normalized Molar Fraction (NMF)	Partial Molar Volume (PMV)		NMF *			Contribution to (g/mol) in glass					
2	Al	5.07700	Al2O3	101.9612	1.8895	9.5930	0.09408	0.063596	40.7800		2.5934			6.4843					
3	B	1.41800	B2O3	69.6202	3.2199	4.5658	0.06558	0.044329	24.8700		1.1025			3.0862					
4	Ba	0.00000	BaO	153.3394	1.1165	0.0000	0.00000	0.000000	21.9100		0.0000			0.0000					
5	Ca	0.39100	CaO	56.0794	1.3992	0.5471	0.00976	0.006594	14.3800		0.0948			0.3698					
6	Ca	0.00000	Ca2O3	328.2382	1.1713	0.0000	0.00000	0.000000	46.9000		0.0000			0.0000					
7	Cr	0.02950	Cr2O3	151.9902	1.4616	0.0431	0.00028	0.000192	29.2000		0.0056			0.0291					
8	Cs	0.00000	Cs2O	281.8094	1.0602	0.0000	0.00000	0.000000	63.0000		0.0000			0.0000					
9	Cu	0.02750	CuO	79.5394	1.2520	0.0344	0.00043	0.000293	12.4000		0.0036			0.0233					
10	Fe	6.42850	Fe2O3	159.6922	1.4297	9.1908	0.05755	0.038903	31.2000		1.2138			6.2125					
11	K	0.04400	K2O	94.2034	1.2046	0.0530	0.00056	0.000380	33.6400		0.0128			0.0358					
12	La	0.00000	La2O3	325.8182	1.1728	0.0000	0.00000	0.000000	50.0500		0.0000			0.0000					
13	Li	2.11700	Li2O	29.8814	2.1529	4.5577	0.15253	0.103099	11.0700		1.1413			3.0807					
14	Mg	0.23350	MgO	40.3114	1.6581	0.3872	0.00960	0.006492	12.2200		0.0793			0.2617					
15	Mn	1.96400	MnO	70.9374	1.2912	2.5359	0.03575	0.024164	13.7000		0.3310			1.7141					
16	Mo	0.00000	MoO3	143.9382	1.5003	0.0000	0.00000	0.000000	30.6300		0.0000			0.0000					
17	Na	11.08480	Na2O	61.9790	1.3480	14.9423	0.24109	0.162960	20.0000		3.2592			10.1001					
18			SO4	96.0616	2.9959	0.3275	0.00341	0.002304	52.6100	for Na2SO4	0.1212			0.2214					
19	Nd	0	Nd2O3	336.4782	1.1664	0.0000	0.00000	0.000000	46.4800		0.0000			0.0000					
20	Ni	0.8348	NiO	74.7094	1.2725	1.0623	0.01422	0.009611	33.5000		0.3220			0.7180					
21			P2O5	141.9446	2.2914	0.1068	0.00075	0.000509	59.5000		0.0303			0.0722					
22	Pb	0	PbO	223.1894	1.0772	0.0000	0.00000	0.000000	22.3200		0.0000			0.0000					
23	Si	22.0688	SiO2	60.0843	2.1393	47.2118	0.78576	0.531127	26.3600		14.0005			31.9124					
24	Th	0	ThO2	264.0368	1.1379	0.0000	0.00000	0.000000	31.8100		0.0000			0.0000					
25	Ti	0.217	TiO2	79.8988	1.6680	0.3620	0.00453	0.003062	21.0200		0.0644			0.2447					
26	U	1.5293	U3O8	842.0840	1.1792	1.8034	0.00214	0.001448	34.4150	0.33*24.8 + 0.67*39.2	0.0498			0.4064					
27		1.5293	UO2&UO3	280.7474	U ₂ O ₇ value is used in normalization; but in the remaining calculations the uranium value is a weighted combination of UO ₂ and UO ₃ values.														
28	Y	0	Y2O3	225.8082	1.2699	0.0000	0.00000	0.000000	46.7000		0.0000			0.0000					
29	Zn	0	ZnO	81.3694	1.2448	0.0000	0.00000	0.000000	14.5300		0.0000			0.0000					
30	Zr	0.1265	ZrO2	123.2188	1.3508	0.1709	0.00139	0.000937	23.2500		0.0218			0.1155					
31	Measured ppm														Uncertainty				
32	PO4	526		94.9714	3.0662	sum	1.47942	1.00000		Sum of Vol	24.4474		g/mol glass	65.0883	Buffer	Density			
33	SO4	1205		96.0616	2.9959									(99%/99%)	Bound				
34	Measured wt%														Predicted Density				
35	Calcine solids	36.795												2.662384	0.123	2.785	g/cm ³		
36	The U3O8 molecular wt uses														Tank 40 Information				
37			UO2	270.0278							0.004		g fissile/g iron						
38			UO3	286.0272							average	Std Dev	Fe Bound						
39			as follows														SME Fe Information		
40			0.33*270.0278+0.67*286.0272														Fe conc (wt%)		
41																	Conclusion		
42																	fissile conc		
																	733.2 g fissile/m ³ (= cell K37*cell M39*cell P34*10000)		
																	Constrain Met		
																	yes (i.e., fissile conc less than 897 g fissile/m ³)		

Figure E-1: Illustration of Use of PCCS Information to Determine a Bounding Density for the SME Glass Product and the Corresponding Fissile Loading (SB6 SME 565)